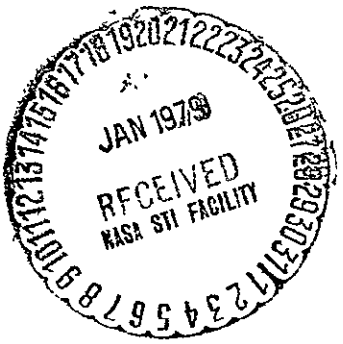

THE UNIVERSITY OF CHICAGO

ESTIMATION OF VENUS WIND VELOCITIES FROM HIGH-RESOLUTION INFRARED SPECTRA

A DISSERTATION SUBMITTED TO
THE FACULTY OF THE DIVISION OF THE PHYSICAL SCIENCES
IN CANDIDACY FOR THE DEGREE OF
DOCTOR OF PHILOSOPHY

DEPARTMENT OF THE GEOPHYSICAL SCIENCES

BY

MARY ANN HRIVNAK SMITH

CHICAGO, ILLINOIS
DECEMBER 1978

ACKNOWLEDGEMENTS

The author would like to express her sincere thanks to Professor Lewis D. Kaplan for his guidance, encouragement and support for the work leading to this dissertation.

Special words of appreciation are also necessary for Dr. Pierre Connes and Dr. Janine Connes, of the Centre National de la Recherche Scientifique, Orsay, who measured and processed the planetary spectra and supplied the computer program and other data necessary for the detailed study of these spectra. Thanks are also due to Dr. Guy Guelachvili of the Laboratoire d'Infrarouge, University of Paris, Orsay, who on request made laboratory measurements of the pressure-induced lineshifts of HCl and HF. Without these data this dissertation could not exist.

The author also thanks C. Boulet of the Laboratoire d'Infrarouge for providing his calculations of the lineshifts for HCl perturbed by HF and for his helpful comments on the work discussed in Chapter II. She is also grateful to Professor Gilbert Amat of the Laboratoire de Physique Moleculaire et d'Optique Atmospherique, C.N.R.S., Orsay, for his helpful discussions concerning this work, and to Professor Dave Fultz of the University of Chicago for his comments on the results presented in Chapter IV.

Acknowledgement is also due to Mrs. Mary Adlyn Evans for her typing of this dissertation.

This research was supported by the U.S. National Aeronautics and Space Administration, under grant NGR 14-001-194.

Finally, the author would like to express her deep appreciation to

her husband, Charles, and to her mother, brothers and her late father for their past and continued support and encouragement.

TABLE OF CONTENTS

TABLE OF CONTENTS--Continued

LIST OF TABLES

LIST OF ILLUSTRATIONS

LIST OF ILLUSTRATIONS--Continued

LIST OF ILLUSTRATIONS--Continued

ABSTRACT

Zonal velocity profiles in the Venus atmosphere above the clouds can be estimated from measured asymmetries of HCℓ and HF infrared absorption lines in high-resolution Fourier interferometer spectra of the planet. These asymmetries are caused by both pressure-induced shifts in the positions of the hydrogen-halide lines perturbed by CO_2 and Doppler shifts due to atmospheric motions. Particularly in the case of the HCℓ 2-0 band, the effects of the two types of lineshifts can be easily isolated, making it possible to estimate a profile of average Venus equatorial zonal velocity as a function of pressure in the region roughly 60 to 70 km above the surface of the planet. Although there are large uncertainties in the resulting wind profiles, the mean magnitudes of the winds appear to be realistic and are not inconsistent with those measured by other investigators. The mean profiles obtained show strong vertical shear in the Venus zonal winds near the cloud-top level, and both the magnitude and direction of winds at all levels in this region appear to vary greatly with longitude relative to the sub-solar point.

CHAPTER I

INTRODUCTION

The development of a high-resolution Fourier-transform infrared interferometer in 1966 by J. and P. Connes has been a significant contribution to the study of planetary atmospheres. The resolving power of the Fourier-transform interferometer in the infrared spectrum of Venus was about one hundred times greater than that of the best scanning grating spectrometers in use at the time (Connes and Connes, 1966). A major advantage of Fourier spectroscopy is that line positions can be measured with great accuracy, so that positions determined in planetary spectra often approach the accuracy of laboratory measurements. Details of the design of the Connes instrument and the Fourier-transform scheme used to produce the final spectrum can be found in several of their papers (Connes and Connes, 1966; Connes et al., 1967).

The earlier Connes planetary spectra, published in their Atlas in 1969, had a resolution of 0.08 cm^{-1}, which was far superior to that of previous planetary spectra. Line positions in the HCℓ 2-0 band in the Venus spectra were measured with an accuracy better than 0.01 cm^{-1}. From these planetary spectra the Connes and their associates were able to identify and measure for the first time the presence of CO, HCℓ and HF in the Venus atmosphere (Connes et al., 1967, 1968) and CO in the Martian atmosphere (Kaplan et al., 1969).

During October and November of 1973, using an improved version of the interferometer, Dr. P. Connes took interferograms of Venus and Mars

through the Hale 5m (200in) telescope at Mt. Palomar. A second set of interferograms of Venus were taken at the same site in June 1974. In addition a lunar spectrum was measured during the 1973 observation period, for comparison and to aid in identifying telluric absorption features in the planetary spectra. The resolution of all the spectra is about 0.01 cm^{-1}, and line positions can be determined to the nearest 0.001 cm^{-1} in the 1.7 μm region. The Mars spectra measured in 1973 have been used to provide a pre-Viking estimate of the amount of inert gases present in the Martian atmosphere (Kaplan et al., 1975).

The accuracy of line positions measured in these new planetary spectra is sufficient to allow detection of pressure-induced shifts of HCℓ and HF infrared absorption lines due to the CO_2 in the Venus atmosphere. In addition to shifts measured at the peaks of the absorption lines, there were found asymmetries in the line shapes apparently arising from both the pressure-induced lineshifts and Doppler shifts due to Venus atmospheric motions. It is possible to invert these measured line asymmetries for a given absorption band to obtain an estimated profile of the average equatorial zonal velocity as a function of pressure for the Venus atmosphere above the main cloud deck.

Before the estimation of Venus wind profiles from absorption line asymmetries is described, it is very helpful to discuss in more detail the phenomenon of pressure-induced lineshifts.

CHAPTER II

PRESSURE-INDUCED SHIFTS OF INFRARED ABSORPTION LINES

A detailed and precise understanding of the vibration-rotation bands of the hydrogen halides is important for high-resolution infrared spectroscopic studies of the atmospheres of both Earth and Venus. Since these halogen compounds, primarily HCℓ and HF, are at most minor constituents of the planetary atmospheres, their absorption spectra are very likely to be affected by other atmospheric gases. The most common effect is Lorentz, or pressure-induced, broadening of the absorption line. However, in addition to the broadening of the line profile, the line center is displaced by a small amount proportional to the pressure of the perturbing gas.

Laboratory measurements of pressure-induced lineshifts for hydrogen halides were first made in the late 1950s (Kuipers, 1958; Kimel et al., 1959; Rank et al., 1960a,b). The original intent of these early experiments was to measure foreign-gas broadening and self-broadening in the HCℓ and HF 1-0 and 2-0 bands, using gas pressures from several cmHg to 5 atm. Specific measurements of pressure-induced lineshifts, as well as theoretical studies, have continued to the present time. The most commonly studied lineshifts have been those of HF or HCℓ perturbed by the noble gases (Boulet et al., 1972a,b; Jarecki and Herman, 1975). More recently theoretical studies have appeared dealing with pressure-induced lineshifts due to more polar perturbers (Boulet et al., 1976).

2.1 Characteristics of the Shifts

The most important characteristic of pressure-induced lineshifts in terms of their usefulness in the study of planetary atmospheres is that the magnitude of the shift for a given spectral line varies linearly with the pressure of the perturbing gas. This linear relationship became obvious in experiments by Kimel et al. (1959), where self-induced lineshifts in the HCl 2-0 band were measured at several gas pressures between 20 and 700 torr, and the linearity was verified for other molecules by later investigators (Rank et al., 1960a; Shaw and Lovell, 1968). If a set of pressure-induced lineshifts for a specific pair of absorbing and perturbing gases is measured in a planetary spectrum, the atmospheric pressure at which the maximum absorption occurs could be easily determined from the linear dependence of the lineshifts on pressure.

When the pressure-induced lineshifts in the same vibration-rotation band are examined together, it becomes apparent that the lineshifts are strongly dependent on the rotational quantum number (J) of the absorbing molecule. For example, in Figure 1(a) for the HF 1-0 band perturbed by Ar, the shifts become increasingly negative for larger values of J, reaching a maximum magnitude for J values of 6 or 7, then slightly decreasing. Pressure-induced lineshifts also show some dependence on the vibrational quantum number of the absorbing molecule. This fact can also be seen in Figure 1(b), where the lineshifts for the HF 2-0 band perturbed by Ar appear to be approximately twice as large as corresponding lineshifts in the HF 1-0 band.

The J-dependent pattern of the lineshifts is specifically tied to the particular absorber-perturber pair. Rank et al. (1960b) have shown empirically for HCl absorption lines that the magnitude of the lineshift

depends largely on the polarizability and molecular mass of the perturbing gas. In addition it has been observed that nonpolar molecules such as N_2 and the noble gases produce smooth, rather symmetrical patterns when perturbing strongly polar molecules such as HF and HCℓ (Figures 1 and 2). However, the pattern of lineshifts becomes increasingly complex for more polar perturbing gases (Figures 3-5,7,8) due to stronger electrostatic interactions between the absorbing and perturbing molecules.

2.2 Theoretical Discussion

Broadening effects in the absorption spectra of diatomic polar molecules have long been a subject of theoretical investigation, but only recently has similar attention been focused on the corresponding pressure-induced lineshifts. Most theoretical studies of lineshifts have dealt with interactions of diatomic polar molecules with the noble gases (Herman and Tipping, 1970; Boulet et al., 1973a,b; Jarecki and Herman, 1975). Very recently Boulet et al. (1976) have published a theoretical analysis of pressure-induced lineshifts due to the interaction of several species of diatomic polar molecules with each other. The theory of pressure-induced lineshifts will be qualitatively summarized here, following the model and notation used by the several authors mentioned above.

The foreign-gas-induced shift of any vibration-rotation line may be considered as the difference of the shifts of the two energy levels involved in the transition, that is,

$$\delta_{line} = \delta_f - \delta_i \tag{2.1}$$

where the subscripts i and f denote the initial and final levels, respectively. Each level shift has both a first-order and a second-order contribution,

$$\delta_i = \delta_i^{(1)}(v_i, J_i) - \sum_{v_i', J_i'} \delta_i^{(2)}(v_i, J_i, v_i', J_i') \qquad (2.2)$$

where v_i and J_i are the vibrational and rotational quantum numbers for the level in the absorbing molecule, and v_i' and J_i' are the corresponding quantum numbers describing the rotation-vibration state of the perturbing molecule. Of course v_i' and J_i' are not applicable to monatomic perturbers.

The two terms in the level shift arise from the expansion of the binary intermolecular potential V using the impact approximation developed by Foley (1946) and later applied specifically to the theory of pressure-induced lineshifts by Herman and Tipping (1970), Boulet et al. (1972a,b); Jarecki and Herman (1975); and Boulet et al. (1976). The first-order term in the expansion of V is imaginary and contributes only to shifts of spectral lines. There are a number of second-order terms which are complex; the real part of each of these terms contributes to line broadening and the imaginary part to the lineshifts.

In the calculation of lineshifts, each term in the expansion of the binary intermolecular potential must be averaged over all possible directions of the initial relative velocity of the colliding molecules in order to obtain the net perturbation of the level in the absorbing molecule. As a result of this averaging, the first-order term vanishes when the absorbing molecule is in the ground vibrational state, i.e., $\delta_i^{(1)} = 0$ for $v_i = 0$. For higher vibrational states, the first-order level shift is always negative and less important than the second-order shift except for very large values of v_i and J_i. The magnitude of the first-order level shift increases directly with v_i, so that always $|\delta_f^{(1)}| \geq |\delta_i^{(1)}|$, producing a negative (or zero for purely rotational lines) first-order

contribution to the line shift.

The imaginary parts of the second-order terms in the collision Hamiltonian (derived from the expansion of the binary intermolecular potential V) provide the most significant contribution to the pressure-induced lineshifts. The predominant shifting mechanisms vary according to the impact parameter b, which represents the effective collision cross-section of the absorbing molecule relative to the perturber. Below a certain critical "cutoff value" b_o, short-range interactions predominate, as is the case for diatomic polar molecules perturbed by noble gases (Herman and Tipping, 1970; Jarecki and Herman, 1975). Among the important short-range shifting mechanisms are anisotropic repulsion forces which contribute mainly to the shifts for low J values by causing bending of the particle trajectories. Both elastic and inelastic collisions produce phase shifts in the vibration-rotation mode of the absorbing molecule. Long-range electrostatic interactions may be safely neglected.

For values of the impact parameter much greater than b_o, as is the case for diatomic polar molecules as perturbers, the interactions between the absorbing and perturbing molecules are primarily long-range and electrostatic. The variety of short-range forces which were important for noble-gas perturbers may be ignored in this case. Long-range dipole-dipole interactions cause the colliding molecules to induce rotational transitions in each other. These induced transitions occur for all combinations of absorbing and perturbing polar molecules, but in cases where the rotational constant for the perturber is approximately twice that for the absorber (as for HCl-HF, DCl-HCl and DF-HF), near-resonant induced transitions occur which are particularly efficient in causing level shifts. As illustrated in Figure 6 for HCl perturbed by HF, there are two types of these near-

resonant interactions.

(i) In the first type (I) of near-resonant interaction, the transitions in resonance differ in energy by approximately integral multiples of B_{OHF}, the ground-state rotational constant for HF. Since for HF the upper vibration-rotation states have populations that are at most 10^{-7} the population of the ground state at normal atmospheric temperatures, only the ground-state rotational transitions in HF may be considered as effectively producing level shifts in HCℓ molecules. Several of these Type I resonances for both even and odd J_i levels are denoted by the dashed arrows, e.g., A1<-->A2, B1<-->B2, in Figure 6. The most effective of these resonances in producing HCℓ level shifts are those whose energy difference $\Delta\omega$ is least. For a first approximation contributions from resonances with energy differences larger than $\pm B_{OHF}$ can be neglected.

The largest part of the Type I contribution to the HCℓ level shift is represented by the difference of two terms corresponding to the A1<-->A2 resonance and the B1<-->B2 resonance. Each term contains a Boltzmann factor expressing the population of the initial level J_i' of the perturbing HF transition: $\exp[(-hc/kT) * B_{OHF} * J_i'(J_i'+1)]$, where $J_i' = f(J_i)$ is a relationship defined by the two transitions in resonance. In each term this Boltzmann population factor is also multiplied by an "interruption function" $IF1(\Delta\omega)$, where the energy difference $\Delta\omega = B_{OHF} \pm \Delta B_v(J_i+1)$ for even J_i, or $\Delta\omega = B_{OHF} \pm \Delta B_v J_i$ for odd J_i, with $\Delta B_v = 2B_{vHC\ell} - B_{OHF}$. The function IF1 describes the effectiveness of a given pair of transitions in producing level shifts in the absorbing molecule. For HCℓ and HF at typical atmospheric temperatures, $IF1(\Delta\omega)$ has a maximum at $\Delta\omega \doteq 5.7$ cm^{-1} and is linear for smaller values of $\Delta\omega$ and inversely proportional for larger values. Thus the sign and magnitude of the Type I contribution to the HCℓ level shift depend on the signs and magnitudes of the ΔB_v and the magnitude of

B_{OHF} [through IF1($\Delta\omega$)], as well as on the relative populations of the HF states involved in the two primary pairs of near-resonant transitions.

(ii) The second type (II) of shift-producing resonance involves transitions which have approximately the same energy, i.e., $\Delta\omega = \Delta B_v J_i$ for even J_i and $\Delta\omega = \Delta B_v(J_i+1)$ for odd J_i. The Type II resonances are denoted by small letters, e.g., a, b, c, in Figure 6. As is obvious from the figure, in the ground state of HCℓ the resonances cause the odd-J levels to be perturbed downward and the even-J levels to be perturbed upward. In the same manner as for the Type I resonances, the Type II contribution to the level shift is proportional to the population of the lower HF state involved in the resonant transition and to the interruption function IF1($\Delta\omega$), although for the Type II level shift there is only one pair of resonant transitions being considered. Since in this case $\Delta\omega$ is directly proportional to ΔB_v, the sign of ΔB_v is particularly important. The level shifts will be positive for even J_i and negative for odd J_i if ΔB_v is positive (as it is for the ground state of HCℓ), but if ΔB_v is negative (as in the second vibrational state of HCℓ) the phase of the shift oscillations will be reversed.

As illustrated by Boulet et al. (1976), the magnitudes of ΔB_v and B_o for the perturber determine the relative influence of Type I and Type II contributions to the shifts for a given vibrational state of the absorbing molecule. In the case of DCℓ perturbed by HCℓ, the relative influence of Types I and II resonances is approximately the same in the first and second vibrational states, while in the ground state the Type II resonances clearly predominate. Moreover, the magnitudes of the ground-state level shifts are generally larger than those in the upper states. When line shifts for the DCℓ 2-0 band are calculated, the predominance of the Type II

ground-state shifts results in a strongly oscillating pattern of line shifts, corresponding to those observed in the laboratory by Jaffe et al. (1964).

For HCℓ perturbed by HF, the ΔB_v values for all the lower vibrational states are large enough relative to B_{OHF} so that the Type II resonances are the predominant shifting mechanism in all these states. The magnitude of ΔB_2 is about three times as large as that of ΔB_o, making the shifts in the second vibrational state generally larger than those in the ground state; however, since ΔB_o is positive and ΔB_2 negative, the shift oscillations in the two states are out of phase. The resulting line shifts for the 2-0 band of HCℓ, both calculated (Boulet, 1977) and observed (Guelachvili and Smith, 1978), are shown in Figure 7.

The near-resonant interactions of HCℓ and HF can also be used to predict lineshifts for HF vibration-rotation transitions perturbed by HCℓ. The calculation of lineshifts becomes more complex since each HF rotational transition is involved in four major Type I near-resonant interactions with ground-state HCℓ rotational transitions and in two opposing (but not equal) Type II resonances (Figure 6). In addition, both isotopic species $H^{35}Cℓ$ and $H^{37}Cℓ$ are interacting with HF molecules in proportion to their relative abundance. Thus the number of second-order terms in this calculation is quadruple the number necessary for the calculation of HCℓ shifts due to HF. A partial calculation of the net relative second-order contribution to the HF lineshifts by HCℓ seems to correctly predict the behavior for low J values of the HCℓ-induced lineshifts observed in the HF 2-0 band by Guelachvili and Smith (1978), shown in Figure 8. However, more detailed theoretical calculations of these lineshifts are necessary. Nevertheless, it can be observed from Figures 7 and 8 that shifts of HCℓ lines perturbed by HF possess a strongly oscillating character, while for HF perturbed by

HCℓ there is no real obvious oscillation.

The observed pressure-induced lineshifts of HCℓ and HF shown in Figures 4, 5, 7 and 8 were deduced from experiments which were not performed for that purpose. The gas pressures used (not more than 10 torr) are not high enough to get very accurate measurements of the shifts. The results are nevertheless significant, since they contain the only HCℓ-HF lineshift measurements in existence at the present time. Obviously more theoretical and experimental study of this problem is necessary.

2.3 Pressure-induced Lineshifts for Infrared-absorbing Molecules in Planetary Atmospheres

For application to the study of planetary atmospheres, we are primarily interested in pressure-induced lineshifts of trace-constituent infrared-absorbing gases perturbed by the major atmospheric constituents. For the earth's atmosphere, measurements of CO, CO_2, H_2O, O_3, N_2O, CH_4, SO_2, NO, NO_2, NH_3, HCℓ, HF or HNO_3 perturbed by N_2, O_2 and Ar would all be important. Unfortunately, none of these shifts have been measured in the laboratory with the exception of CO perturbed by Ar (Rank et al., 1963; Bouanich, 1972) and HCℓ and HF perturbed by N_2 and by Ar (Rank et al., 1960a; Rank et al., 1963; Hirshfeld et al., 1960; Jaffe et al., 1965; Oksengorn, 1963; Wiggins et al., 1970; Guelachvili and Smith, 1978). In Figure 9 measurements by Guelachvili and Smith (1978) for the HCℓ 2-0 band perturbed by N_2 are compared with measurements by Kimel et al. (1959) for the same band perturbed by 1 atm dry air. Since dry air contains 78 percent N_2 by volume, it is not unexpected that the two sets of lineshifts are quite similar. Note also that the nitrogen curves are similar in form and magnitude to the ones for argon (Figure 2); this is not surprising since both molecules are nonpolar and have roughly similar molecular weights. The differences

between the shifts by air and by nitrogen can probably be accounted for by the effects of the 21 percent O_2 and 0.9 percent Ar also present in dry air. Unfortunately, there exists only a single measurement of a line-shift in the HCℓ 2-0 band perturbed by O_2; Rank et al. (1960a) have measured that the R10 line of $H^{35}C\ell$ is shifted -22.0×10^{-3} cm^{-1} per atm O_2. With so little information available, meaningful quantitative comparisons for the earth's atmosphere cannot yet be made.

For the Venus atmosphere the primary interest is measured shifts of HCℓ and HF perturbed by CO_2, although measurements of CO perturbed by CO_2 would be helpful if they existed. It is interesting to note that the pressure-induced shift patterns for HCℓ and HF perturbed by CO_2 (Figures 3 and 10) contain more "kinks" and are distinctly different from the corresponding shift patterns for these bands perturbed by Ar (Figures 1 and 2). In terms of the theoretical model discussed in the preceding section, the shifts by Ar represent mainly the weak first-order contribution plus stronger second-order contributions arising from short-range anisotropic repulsion forces. For the shifts by CO_2, the first-order and short-range second-order contributions remain, but there are additional long-range second-order terms arising from dipole-dipole interactions between the hydrogen halide molecule and CO_2 molecules in asymmetric vibrational states. Since CO_2 is at best a temporary dipole, the second-order long-range interactions are not nearly as strong as those between HF and HCℓ, and strongly oscillating shift patterns are not expected to occur. The interactions between HCℓ or HF and CO_2 have not yet been theoretically studied in detail, probably because of the complexity of calculations necessary in order to include both short- and long-range second-order effects.

CHAPTER III

THE VENUS ATMOSPHERE

Although scientific interest in the planet Venus began with telescopic observations by Galileo in 1609, the determination that Venus possesses an atmosphere was not made until nearly 200 years later. In the latter part of the eighteenth century several observers noted that the horns of the crescent of Venus extended far beyond the semicircle, which is not the case for an airless body such as the moon. There also was noted a considerable time difference between the predicted and actual occurrences of dichotomy, the point when exactly half the planetary disk is illuminated; this time difference could only be due to the presence of an atmosphere.

3.1 Composition and Structure

Information about the composition of the Venus atmosphere was not obtained until the early twentieth century, when spectroscopic observations became possible. At that time Venus and Earth were considered to be identically twins, and the Venus atmosphere was expected to be quite similar to the terrestrial one. The early Venus spectra revealed that the major optically active constituent of that planet's atmosphere is carbon dioxide, not oxygen as had been expected for a terrestrial-type atmosphere.

Until the recent successful missions carried out by the Soviet probes in the Venera series, studies of the composition and structure of the Venus atmosphere were limited to the region above the optically thick,

unbroken cloud deck. Nevertheless, more recent spectroscopic measurements made at much higher resolution than those at the turn of the century have fairly well established the composition of the Venus atmosphere. The atmosphere is composed almost entirely of CO_2, with CO appearing as a uniformly mixed minor constituent. The Venus atmosphere also contains small but spectroscopically measurable amounts of HCℓ and HF (Connes et al., 1967), and these two hydrogen halides also appear to be uniformly mixed in the atmosphere above the clouds. Despite difficulties due to strong telluric water vapor absorption features, the amount of H_2O in the Venus upper atmosphere has also been spectroscopically measured. The most recent of these measurements estimate the amount of water vapor to be roughly equivalent to 1 μm precipitable water in the atmosphere above the clouds (Gull et al., 1974). Only the five constituents mentioned above have actually been detected from spectra of Venus. However, several investigators have also calculated upper limits for many other geochemically plausible minor constituents such as NH_3, H_2S, COS, SO_2 and O_3, based on the non-appearance of their absorption features in Venus spectra. One of the most comprehensive works of this type is that of Owen and Sagan (1972), who made use of ultraviolet spectra from the Orbiting Astronomical Observatory. L. Young (1974) has compiled a table summarizing observations and calculated upper limits for the various molecules in the Venus atmosphere; the table is reproduced here as Table 2(a) and (b), with several more recent observations added.

Even though infrared, visible and ultraviolet spectroscopic studies were reasonably accurate in estimating amounts of atmospheric constituents, estimates of the surface pressure and temperature on Venus varied over a very broad range. In the late 1960s and early 1960s radio and microwave

astronomy experiments showed that Venus had an unexpectedly high radio-brightness temperature in excess of 400°C. Radar experiments also allowed investigators to at last determine the true rotation rate of the planet. Venus rotates in a retrograde direction, thus differing radically from most other planets in the solar system, with a period of about 243 days. Since the orbital period of Venus is somewhat shorter (225 days), the net length of a "day" from one sunrise to the next is about 117 Earth days. Also, the axis of rotation of Venus is nearly perpendicular to the planet's orbital plane, causing a virtual absence of seasons.

Although earth-based microwave measurements had narrowed down the wide range of previously estimated temperature and pressure profiles for the Venus atmosphere, it remained for the Soviet probes in the Venera series to provide accurate measurements of temperatures and pressures below the cloud deck. The earlier landers, Veneras 4 through 8, established the following facts: the surface pressure and temperature are 90-95 atm and 740-750 K; the principal atmospheric constituent is CO_2; the temperature lapse rate in the troposphere (0-50 km) corresponds to adiabatic equilibrium. Veneras 9 and 10 verified the results from the earlier landers. In addition, since Veneras 4 through 8 had landed near the morning terminator and Veneras 9 and 10 landed near the subsolar point, comparison of the two sets of temperature measurements reveals that daytime temperatures are 20 to 25°C higher than those at night above the 40-50 km level.

Direct measurements of Venus atmospheric temperatures and pressures were made by the Veneras only between the surface and maximum heights of 50 to 63 km. Above this region it is necessary to rely on indirect measurements such as those from the Mariner 5 and 10 flyby missions and from earth-based spectroscopic experiments. Figure 11 presents a temperature

profile for the Venus atmosphere which is a composite of several of the most recent measurements (Marov and Ryabov, 1972; Ainsworth and Herman, 1975; Taylor, 1975; Dierenfeldt et al., 1977; Keldysh, 1977).

When Venus is viewed from Earth or from space, the visible "surface" of the planet is formed by an optically thick, unbroken cloud cover. In recent years the structure and composition of these clouds has been the subject of considerable study and speculation by planetary scientists. However, much of the observational evidence relating to the cloud structure and composition is uncertain and sometimes contradictory, and no single model consistent with all the observations has yet appeared.

Significant information about the Venus clouds was obtained by Hansen and Hovenier (1974) in their careful analysis of infrared polarization measurements of reflected light from the planet made by at least eight different investigators between 1929 and 1971. From these measurements they deduced that the Venus cloud particles near the top of the infrared-reflecting layer are spherical in shape (probably liquid droplets), having a remarkably narrow size distribution about the mean particle radius of 1.1 μm. Hansen and Hovenier also used these scattering measurements to estimate that the cloud-top atmospheric pressure is about 50 mb, which corresponds to a height of about 70 km above the surface. This figure correlates well with pressure of line formation calculated from infrared absorption spectra for HCl (Connes et al., 1967) and CO_2 (L. Young, 1972; Dierenfeldt et al., 1977).

Photographs of Venus made in the visible and infrared portions of the spectrum show a rather uniform, yellowish-white cloud "surface." However, ultraviolet pictures taken through earth-based telescopes and by space probes such as Mariner 10 clearly reveal light and dark cloud features.

According to Keldysh (1977), these light and dark features correspond with high and low areas at the diffuse upper boundary of the clouds. The most notable of the ultraviolet cloud features include a large quasi-permanent Y-shaped dark marking which appears to travel around the planet's equator with a four-day rotation period, smaller rapidly-moving cloud formations, and brightening and darkening of the polar regions (Dollfus, 1975; Limaye, 1977). Since the apparent height of the ultraviolet features was generally greater than that estimated for the infrared-scattering cloud, it was speculated that there might be one or more UV-scattering haze layers above the main cloud deck.

The Soviet probe Venera 8 provided the information that the lower boundary of the cloudy region was about 35 km above the planetary surface, but gave few clues about the structure or composition of the clouds. A very surprising result from this mission was that a considerable amount of visible-wavelength sunlight reached the surface of Venus. This encouraged Soviet scientists to include television cameras in the instrument packages on Veneras 9 and 10, from which were transmitted the first photographs taken at the surface of Venus (Keldysh, 1977). These last two Veneras also carried a large series of experiments to investigate the optical characteristics of the atmosphere and clouds. These experiments revealed an apparent multilayered cloud structure. The main cloud deck, consisting of a layer of particles with radii from 0.5 to 2.5 μm, lies between 49 and 68 km. Below 49 km there are a few very tenuous haze layers, with no scattering aerosols detectable below 18 km. The upper boundary of the main cloud layer is rather diffuse, with considerable variations in particle concentration. As mentioned earlier, the light and dark cloud features appearing in UV photographs seem to be associated with high and low areas in this diffuse cloud top.

Although since the Venera 9 and 10 missions the structure of the clouds is more certain, their composition remains a subject of some debate. Literally dozens of chemical compounds have been suggested at one time or another as the substance of the Venus clouds. It was once assumed that the clouds were composed of water droplets, just as terrestrial clouds are, until spectroscopic studies revealed that the atmosphere of Venus contains very little water vapor. Spectroscopic data on the relative abundances of CO_2, CO, $HC\ell$, HF and H_2O in the atmosphere, as well as upper limits estimated for other proposed cloud constituents, have narrowed down the field of possible Venus cloud substances to several strongly hygroscopic materials such as carbon suboxide (C_3O_2), an aqueous solution of hydrochloric acid ($HC\ell.nH_2O$) or an aqueous solution of sulfuric acid ($H_2SO_4.nH_2O$). According to Hansen and Hovenier (1974), the best fit among these three proposed constituents to their cloud-droplet refractive indices deduced from polarization measurements is that given by a 75 to 83 percent solution of sulfuric acid, although within their given error limits a strong (about 30 percent) solution of $HC\ell$ cannot be completely ruled out. As A. Young (1975a) has pointed out, experimental information about strong sulfuric acid or hydrochloric acid aqueous solutions, possibly contaminated by HF, at conditions similar to those in the Venus clouds, is sketchy or nonexistent. Therefore the cloud-composition problem may not be completely settled for a number of years.

3.2 Atmospheric Motions

Measurements of Venus winds have been made directly only by the Soviet probes Venera 4 and Veneras 7 through 10 during their descents through the atmosphere. Unfortunately these measurements were made only up to heights of 50 to 60 km above the surface. Above this region there exist two main

types of wind measurements: (1) tracking of light and dark features apparent in ultraviolet photographs taken at low resolution from Earth or at high resolution from Mariner 10, (2) estimation of wind velocities from Doppler shifts of spectral lines. Figure 12 shows the results of all types of observations of Venus atmospheric motions to date.

Veneras 4 and 7 landed on the dark side of Venus near the morning terminator, while Venera 8 landed on the sunlit side of the same terminator. Velocity profiles obtained by these three probes are quite similar, with near-zero zonal winds near the surface, gradually increasing with height up to 35-40 km, then strongly increasing to maxima of -110 to -150 m sec^{-1} at a height of 50 km, where the measurements end. [A negative zonal wind velocity for Venus indicates retrograde motion, i.e., in the same direction as the planet's rotation.]

In Figure 12 the regions of strong turbulence represented by shaded areas were found in radio occulation experiments performed with Mariners 5 and 10 (Woo, 1975). In both these experiments the path of the radio beam passed through the local late-night and early morning regions of the Venus atmosphere. This orientation corresponded quite well with the landing sites of Veneras 4 through 8. The lower turbulent region coincides with the strong wind shear measured by the Veneras; this suggests that the strong wind shear near 50 km is the cause of the turbulence in this lower layer.

It is interesting to note that the wind profiles measured by Veneras 9 and 10, whose landing sites were nearer to the subsolar region, do not show evidence of the high velocities and strong wind shears measured by Veneras 4 through 8 near the morning terminator.

The earliest evidence for Venus atmospheric motions came from earth-based telescopic observations in ultraviolet light (Boyer and Camichel,

1961; Boyer and Guerin, 1969; Dollfus, 1975). The prominent large, dark Y-shaped feature at the planet's equator appeared to have a remarkably consistent rotation period of about 4 days in a retrograde direction. Before radar observations established the true rotation period of Venus as 243 days, this 4-day period had been assumed to represent the actual rotation of the planet. Since this was not the case, the only other possible conclusion was that the whole Venus atmosphere at the cloud-top level near the equator was moving with an average velocity of -110 m sec^{-1}. The range of wind velocities which have been estimated from earth-based UV photographs of Venus is indicated by the bracketed area in Figure 12. The double arrow labeled "4-day rotation" indicates the average velocity of the Y-shaped dark feature.

Taking into account these apparent high wind velocities in the upper part of the Venus atmosphere, Ainsworth and Herman (1977) have extrapolated the Venera 7 in situ measurements into two possible upper-atmosphere wind profiles, indicated by the dot-dashed curves in Figure 12. Profile (1) would be consistent with the suggestion by A. Young (1975b) that the estimated -100 m sec^{-1} winds in the Venus upper atmosphere are the result of observational bias and that the actual winds in this region are of the order of no more than 5 m sec^{-1}. Profile (2) assumes that the stratospheric wind velocities estimated from UV photographs and spectroscopic studies are not spurious results; in this profile the maximum velocity of -130 m sec^{-1} measured by Venera 7 at 50 km is expected to persist well into the stratospheric region.

High-resolution ultraviolet images from Mariner 10 support the general results of earth-based UV studies. Belton et al. (1976a,b) were able to identify many details in these images in addition to the large dark Y. These smaller features included bow-like waves, circumequatorial belts,

a polar ring, and cellular features with lifetimes smaller than 4 days. In his very thorough analysis of the Mariner 10 images Limaye(1977) tracked many of these UV features having spatial extents of the order of 100 km over a period of two and one-half days. He estimated that these features are located at altitudes of 65 to 78 km above the planet's surface, and that this is a region of great atmospheric stability, i.e., the stratosphere of Venus. From a large sample of wind vectors distributed over most of the planet's area, Limaye found a mean zonal velocity component of -96.0 ± 16.0 m sec^{-1} and a mean poleward meridional component of 3.1 ± 10.2 m sec^{-1}. He also found that the zonal winds generally slowly increase in magnitude away from the equator to about 30 degrees latitude, then decrease rapidly toward the poles. The meridional profile of the zonal component of velocity can be described by the equation

$$u(\phi) = U_o \{\sec \phi \ (1 - \sin^{\alpha}\phi) + \cos \phi \ \sin^{\alpha}\phi\} \qquad (3.1)$$

where $u(\phi)$ is the latitude-dependent zonal component of the wind, U_o is the equatorial zonal wind, ϕ is the latitude, and α is an empirical constant. When $\alpha = 0$, $u(\phi) = U_o \cos \phi$, indicating solid-body rotation of the atmosphere, which requires that the angular velocity be constant with latitude. At the other extreme, in the limit as α approaches infinity, $u(\phi) = U_o \sec \phi$ indicating that angular momentum is constant with latitude. Limaye has empirically determined that the value of α most consistent with his observations is 1.6, which means that the upper atmosphere of Venus is nearly in solid-body rotation. For this value of α, maximum zonal velocities of -101.1 m sec^{-1} occur at about 28° latitude, assuming a meridional distribution symmetric in latitude with an equatorial zonal velocity of -95.1 m sec^{-1}. The assumption of symmetry neglects the fact the zonal velocities measured for the southern

hemisphere were slightly higher than those for the northern hemisphere. However, the significance of these hemispheric differences was lost in the uncertainty of the data.

The result that the Venus stratosphere appears not to be exactly in solid-body rotation indicates that there must be a small non-zero meridional component of motion. The uncertainties involved in the tracking of the UV features, particularly regarding the true location of the poles, produce very large relative errors in the estimates of the meridional component of motion. The resulting standard deviation is several times larger than the average estimated meridional velocity, which is small and poleward-directed.

Limaye also analyzed the longitudinal variation of the zonal velocities, particularly in the neighborhood of the sub-solar region. He found a general trend that zonal velocities between the sunrise terminator and the sub-solar point (local "morning" on Venus) tended to have smaller than average magnitudes, while velocities measured for local "afternoon" regions were larger than the average. The velocity increase from morning to afternoon was of the order of 10 m sec^{-1}. Given the retrograde motion of the Venus atmosphere, it is obvious that features eastward (toward sunset) of the sub-solar point have been in the sunlit hemisphere of Venus longer than those nearer to the morning terminator; this extended opportunity for solar heating correlates with the increase of zonal velocities during the day.

An increase in average zonal velocity from morning to afternoon on Venus was also noted by Traub and Carleton (1975). These investigators made spectroscopic measurements of wind velocities using a CO_2 absorption line at 8708 Å and a Fraunhofer line at 6716 Å. The zonal wind velocities were determined by comparison of Doppler shifts of the same spectral line measured while viewing two different areas of the illuminated portion of

the planetary disk. The areas viewed were usually located on the equator at either the edge of the bright limb or near the terminator. Zonal velocities estimated in this manner for the CO_2 line varied from -2 to -125 m sec^{-1}, with an overall mean value of -83 m sec^{-1}. However, averaging local morning and afternoon measurements separately, they found generally smaller morning velocities (-73 m sec^{-1}) than afternoon velocities (-111 m sec^{-1}). These results are indicated by the points labeled Tcm and Tca in Figure 12. For the Fraunhofer line, the results represent an average of only four measurements made viewing the morning region of Venus. The average velocity obtained (-78 m sec^{-1}) refers to the motion of the opaque cloud deck from which the solar photons are reflected. The level of CO_2 line formation (for the narrow core of the line used for determining its precise position) appears to be somewhat above the main cloud, and the morning velocity determined from the CO_2 line is about 10 m sec^{-1} slower than that estimated for the main cloud. This appears to be a marginally significant result suggesting that in the morning hemisphere zonal velocities are increasing with depth into the Venus atmosphere.

Preliminary results from independent spectroscopic measurements of Venus zonal wind velocities have been very recently reported by Schorn and Young (1977). Their measurements of Venus spectra in the 7600 Å-8800 Å region have yielded a mean rotational velocity of 40 ± 47 m sec^{-1} retrograde, which is considerably smaller than the mean values reported by Traub and Carleton, but not outside the range of their individual measurements.

Theoretical models of the dynamics of the Venus atmosphere have had some difficulty explaining the observed temperature structure and motions of the entire atmosphere. Stone (1975) has examined the time scales characteristic of important atmospheric processes on Venus. His results,

together with observed wind velocities and temperatures, indicate that the Venus atmosphere contains two distinct regimes. The deep atmosphere, below 40 km, is characterized by a near-adiabatic temperature lapse rate, weak zonal, meridional and vertical velocities, and negligible diurnal effects. The more successful dynamical models assume that the greenhouse effect in this region is sufficient to cause the large observed surface temperatures and that the atmospheric motions up to about 40 km are due to a Hadley-type circulation (Sasamori, 1971; Kalnay de Rivas, 1975; Gierasch, 1975). These models can adequately explain the adiabatic, nonturbulent structure, the lack of strong horizontal gradients and the observed small horizontal velocities in the troposphere of Venus.

In the upper atmosphere, above about 70 km a different dynamic regime predominates; diurnal effects appear to be important, the temperature lapse rate is sub-adiabatic, and the zonal motions are quite strong. According to scaling of the equations of motion carried out by Leovy (1973) and others, the large-scale motions in the upper atmosphere appear to be in cyclostrophic balance. This can also be seen in mosaics of pictures from Mariner 10; the main circulation pattern in each hemisphere is a circumpolar vortex (Limaye, 1977). However, no mechanism yet proposed satisfactorily explains how this circumpolar vortex is formed in the Venus stratosphere. One likely possibility is the "moving flame" mechanism first studied in the laboratory by Fultz et al. (1959). The moving flame, which in the case of the Venus stratosphere would be strongly localized heating near the bottom of the layer due to CO_2 absorption in the sub-solar region, induces a thermal wave in the fluid. This wave lags behind the moving heat source by an amount which increases with height, because of the finite time required for conduction to transmit the heat into the fluid. There

soon arise convection cells which also have a tilt increasing with height from the bottom of the layer. Because of this tilt, horizontal momentum in a direction opposite to that of the motion of the heat source is transported upward. Thus the net motion at the top of the fluid layer has a direction opposite to that of the motion of the localized heat source, which in the case of Venus is the sun.

Numerical computations by Young and Schubert (1973) seem to indicate that the "moving flame" mechanism alone can account for both the magnitude and direction of the observed 4-day rotation of the Venus upper atmosphere. Essential to this result is the assumption that the atmosphere is stably stratified above altitudes of about 60 km, which is apparently the case in the real Venus stratosphere. However, as Stone (1975) points out, Young and Schubert were not able to obtain numerical results for the large values of the parameter Λ (the square of the inverse Froude number) appropriate for the real Venus atmosphere, since their iterative technique failed to converge for Λ values an order of magnitude smaller than that for Venus. Extrapolation of the results they did obtain for smaller values of Λ does produce zonal velocities within a factor of 2 of the observed wind speeds. Nevertheless, this extrapolation is by no means conclusive evidence that the "moving flame" is responsible for the Venus stratospheric circulation.

Another mechanism which may be partially responsible for the Venus upper atmospheric circulation has been discussed by Fels and Lindzen (1974). Internal gravity waves generated by diurnal heating will tend to transport prograde momentum upward out of the stratospheric layers where the absorption of solar radiation occurs, leaving these absorbing layers with net retrograde momentum. Prograde velocities supported by this mechanism cannot

exceed the apparent speed of the sun, about 4 m sec^{-1}. Retrograde velocities of the magnitudes observed, about 100 m sec^{-1}, can be supported only if a mean retrograde velocity of about 25 m sec^{-1} is produced independently by some other mechanism. Also, these strong retrograde velocities would exist only in a layer at most 5 km thick. The two-dimensional model of Ramanathan and Cess (1975), which neglected rotational effects, also showed that propagating internal gravity wave generated by diurnal heating could induce mean zonal velocities in the Venus stratosphere. Their analysis differs from that of Fels and Lindzen in that the diurnal heating occurs only in the upper part of this atmospheric region above altitudes of about 85 km. This diurnal heating and the associated gravity waves would induce mean zonal velocities in both the lower and upper parts of the stratosphere. This model results in retrograde mean zonal velocities of the order of those observed in the lower stratosphere, with these mean retrograde velocities increasing with height to about 300 m sec^{-1} near 100 km. However, the model results also include a diurnally fluctuating velocity component above 85 km which may have either prograde or retrograde direction and a magnitude exceeding that of the mean velocity. Thus, depending on the local time of day on Venus, the net velocities in the upper stratosphere can be prograde in direction.

More recently Young and Pollack (1977) have developed a three-dimensional model for the Venus atmospheric circulation from the planet's surface up to about 65 km. The principal physical mechanisms active in their model appear to be the mean meridional circulation, which initially transports net retrograde momentum upward from the slowly rotating planetary surface, and a nonlinear instability, which may be of finite amplitude, involving both the mean meridional circulation and planetary-scale eddies

arising from diurnal temperature variations in the upper atmosphere. The model was able to reproduce in direction and magnitude the observed mean zonal wind velocities of about -100 m sec^{-1} in the stratosphere, as well as other observed properties of the circulation such as small horizontal temperature gradients and meridional velocities of the order of 10 m sec^{-1} or less in low and mid-latitudes. Under certain conditions the model also produced planetary waves which exhibited vertical flow field contours in a horizontal Y-shaped configuration. However, although the agreement with the observed circulation appears to be good, the results of this model cannot be considered to be conclusive, particularly in regard to the variability of the Venus zonal winds with time and location, as observed by Traub and Carleton (1975) and Limaye (1977). The vertical profile of mean zonal velocity (averaged over all longitudes) determined from the model appears to be very similar to the Venera 8 profile (Figure 12). However, that profile refers only to a single region of the atmosphere near the morning terminator and is not necessarily representative of the veolcity profiles for other longitudes on the planet. For example, the Venera 9 and 10 velocity profiles, which refer to longitudes near the sub-solar point, appear to differ significantly from that measured by Venera 8, especially in the upper part of the atmosphere where diurnal effects appear to be more important. It is hoped that the planned modifications in the Young and Pollack model to include more realistic treatment of radiative heating and cooling and to extend the upper boundary to about 80 km will result in more realistic velocity profiles at all longitudes and will provide more insights into the general circulation in the atmosphere well above the clouds.

CHAPTER IV

ESTIMATION OF VENUS ZONAL VELOCITY PROFILES USING PRESSURE-INDUCED LINESHIFTS

4.1 Description of the Spectra

As mentioned in the introduction to this paper, the Venus spectra analyzed in this work were measured by Dr. P. Connes using an improved version of the Connes' interferometer at the coude' focus of the Hale 5 m (200 in) telescope at Mt. Palomar in October 1973 and June 1974. The best of these measured spectra were incorporated into two averaged spectra identified as Venus A and Venus 5.

Venus A is the average of four recordings made October 14, 15, 22 and 25 in 1973. Each recording was made over a two- to three-hour period beginning at about 2:00 P.M. local time. The planet appeared as an evening star with an average phase angle (defined as the Venus-centered angle between the sun and the earth) of 77.2°. During the period of the observations the disk of Venus had an average apparent semidiameter of 9.8 arc sec.

The spectrum identified as Venus 5 is the average of five recordings made on consecutive days from June 12 through 16 in 1974. Each of these spectra was also recorded over a two- to three-hour period, beginning at approximately 4:00 A.M. local time, since Venus was appearing as a morning star. Its average phase angle was 56.6°, and its average semidiameter was 6.9 arc sec. Specific parameters for all the individual recordings are given in Table 3. In each case the field of view was a circular area 12

arc sec in diameter centered on the midpoint of the illuminated limb. A more detailed discussion of the viewing geometry is given in Section 4.2.

For calibration purposes, during the measurement of the spectra making up Venus 5, an absorption cell containing a known amount of CO at low pressure was placed in the path of the interferometer. This caused sharp, unshifted CO absorption lines to appear in the Venus 5 spectrum along with the Doppler-shifted Venus CO lines. Lines in the 2-0 band of $C^{12}O^{16}$ due to the absorption cell were used to calibrate the Venus 5 spectrum, using as standards vacuum line positions for this same band measured with a similar interferometer in the laboratory by Guelachvili (1973). The positions of 23 telluric absorption lines due to (0-0) electronic transitions of O_2 near 7850 cm^{-1} were determined from the calibrated Venus 5 spectrum; the positions of these O_2 lines were then used as standards to calibrate the Venus A spectrum. After calibration, line positions for unblended telluric O_2 lines in this spectral region (7820-7900 cm^{-1}) measured in the two averaged spectra agreed within $\pm$ 0.4 x 10^{-3} cm^{-1}.

A preliminary survey of the spectra was carried out to determine whether pressure-induced lineshifts in the HF 1-0 and 2-0 bands and in the HCl 2-0 band due to the CO_2 in the Venus atmosphere could actually be detetected. Absolute wavenumbers for these three absorption bands measured by Guelachvili (1976) with a similar Fourier-transform interferometer were used as standards for comparison to the Connes planetary spectra. The standard line positions were corrected for Doppler shifts due to the relative motions of Venus and Earth and also due to the rotation of the earth. These corrected standard line positions were then compared with the HF and HCl line-center positions measured in the Venus A and Venus 5 spectra. The small residual lineshifts were then compared with laboratory measurements

of lineshifts due to CO_2 (Guelachvili and Smith, 1978); these results are shown in Figures 15 and 16.

In the two figures measurements belonging to poor-quality Venus spectral lines are indicated by open symbols, and "good" lines are denoted by solid symbols. All the HF and HCℓ lines identified in the two averaged spectra are listed in Table 4 along with their "quality factors"; a quality factor of 5 indicates that the spectral line is unblended and almost totally free of noise, while a line having a zero quality factor is identifiable in the spectrum but totally unusable for estimating pressure-induced lineshifts. The relatively large number of poor-quality lines is due to strong telluric absorption in some spectral regions such as the P-branch of the HF 1-0 band, and also to blending of several of the hydrogen halide absorption lines with some of the many Venus CO and CO_2 lines in the spectra. The net result is that both of the HF bands contain so few good lines that they cannot be used for the study of atmospheric-induced lineshifts; the P-branch of the HCℓ 2-0 band is also of poor general quality. However, in the R-branch of this band, nearly all the lines belonging to both isotopes are quite usable, having quality factors of 3 or greater. A portion of each spectrum containing several of the best-quality lines in the HCℓ band is shown in Figure 14.

Even the uncertain data points can provide some information, and comparison of all the measured residual lineshifts with the pressure-induced shifts by CO_2 measured in the laboratory indicates that pressure-induced lineshifts of HF and HCℓ perturbed by the CO_2 in the Venus atmosphere are large enough to be detected in these high-resolution planetary spectra. This is best seen in the R-branch of the HCℓ 2-0 band, where the Venus spectra show residual lineshifts increasing with J in the same manner as

the laboratory measurements of the pressure-induced lineshifts. Moreover, the entire Venus lineshift curves are apparently displaced by a constant amount from the laboratory curve; this indicates a small residual Doppler shift which is apparently due to motions in the Venus atmosphere, since the planet's true rotational velocity is nearly zero.

With the aid of a computer program called DERPTH developed by researchers at the Centre National de la Recherche Scientifique, Orsay, it is also possible to study in detail the symmetry of each absorption line. The program calculates the central positions of chords drawn across the line at five levels equally spaced from the base to the peak of the line (Figure 17). For the HCℓ lines studied in detail, it was found that the centers of these chords were increasingly displaced from the peak to the base of each line. Telluric lines in this same spectral region do not show the same asymmetric shape as the HCℓ lines. Considering these asymmetries together for the whole R-branch of the 2-0 band, the displacements of the chord centers appear to represent not only shifts due to increased CO_2 pressure at lower levels in the Venus atmosphere, but also a residual Doppler shift due to the variation of Venus wind velocities with height. The particular nature of the shift pattern for HCℓ makes it possible to calculate profiles of Venus zonal wind velocity as a function of atmospheric pressure, using the line asymmetries measured in the R-branch of the HCℓ 2-0 band. Details of the method of calculation and the resulting velocity profiles will be discussed in later sections of this chapter.

4.2 Geometry of the Problem

In order to estimate wind velocities on Venus from small residual lineshifts, it is first necessary to calculate as accurately as possible the contributions to the lineshifts which arise from the motions of Earth

and Venus in their respective revolutions about the Sun and from the rotation of the Earth. Also, since the spectra contain contributions from a rather large area of the illuminated portion of the Venus disk, we must take into account the variation of intensity of illumination of the planet and the latitudinal variation of zonal velocities on Venus in order to translate observed residual Doppler shifts of the spectral lines into zonal wind velocities in the planetary atmosphere.

4.2.1 Effect of translational and rotational Doppler shifts

The largest contribution to the shifts of the Venus spectral lines comes from the relative orbital motions of Earth and Venus. These translational Doppler shifts have been calculated and tabulated for convenient reference by Niehaus and Petrie (1961); Figure 18 is a graphical representation of their calculations for Venus for the period 1971 to 1977. It can be seen from the figure and Table 5 that the translational Doppler shift remained fairly constant throughout the 11-day period of observations for Venus A, while for the Venus 5 observations the shift factor decreased more rapidly in magnitude over a period of 5 days. The net change in the translational Doppler shift factor from the first to the last day of observations is about +1.2 percent for Venus A and about -2.1 percent for Venus 5. The larger variation in the translational Doppler shift causes the same lines in the Venus 5 averaged spectrum to be somewhat broader than those in the Venus A spectrum.

Since the Niehaus and Petrie (1961) calculations of the translational Doppler shift were intended to be a rough estimate for quick reference during observations and are accurate to only two significant figures, it is necessary for detailed study of the spectra to calculate the

translational shift more accurately. These calculations were made using listings from the American Ephemeris and Nautical Almanac (1973, 1974) giving the true distance between Earth and Venus at 0 h Universal Time for each day of the observations. The Doppler shift factors, listed in Table 5, were calculated for the midpoint of the two- to three-hour time period during which each interferogram was taken.

A smaller component of the Doppler shift, which arises from the Earth's rotation, depends on the specific location of the observatory and on the average position of Venus in the sky at the time of each observation. As listed in Table 1, the tangential speed of a point on the earth's surface at latitude ϕ in m sec^{-1} is 463.8 cos ϕ. Since Mt. Palomar is located at 33.18°N (geocentric latitude), its tangential velocity is about 387.9 m sec^{-1}. Thus the maximum possible rotational Doppler shift factor, if Venus were located at the horizon due east of the observatory, would be $+0.129 \times 10^{-5}$, which is an order of magnitude smaller than the translational Doppler shift.

The component of the earth's tangential velocity in the direction of Venus can be expressed as

$$v_T = -U_T \cos \bar{\alpha} \sin \bar{z} \qquad (4.1)$$

where U_T is the eastward tangential velocity of the observatory, and $\bar{\alpha}$ and $\bar{z}$ are respectively the average azimuth (from due north) and zenith angles of the planet Venus as seen from the observatory during the measurement of the interferograms. Using spherical trigonometry, $\bar{\alpha}$ and $\bar{z}$ can be calculated as functions of the latitude and longitude of the observatory, the time of day the observations were made, and the apparent position of Venus in the sky at 0 h Universal Time as given in the Ephemeris for each observation

date. The results of these calculations for the individual Venus spectra are listed in Table 5, along with the net Doppler shift factors combining both translation and rotational effects.

4.2.2 Scaling of residual Doppler shifts to obtain Venus equatorial zonal winds

In order to calculate Venus equatorial zonal wind velocities from the small residual Doppler shifts measured in the spectra, it is necessary to take into consideration the spherical shape of the planet, the variation of the zonal velocities with latitude, and the variation of brightness over the sampled portion of the planetary disk. The average areas viewed for each set of interferograms are shown in Figure 19. From the residual Doppler shifts determined from the spectra we can readily calculate a velocity v_s, which is the earthward component of the Venus atmosphere's apparent rotational velocity averaged over the observed circular area of the illuminated part of the planet's projected disk. Since at no time during the observations does Venus appear in full phase (when the sub-earth and sub-solar points on the planet coincide), and the viewing aperture is not centered on the sub-earth point, the usual air-mass parameterizations which describe the relative contribution of light reflected from each point on the planet to the spectrum (Moroz, 1967), are not very helpful in this case.

The average earthward velocity component v_s can be expressed as a function of the planetary geometry, zonal velocity distribution and brightness distribution by the equation

$$v_s = \frac{\iint_{\text{Aperture}} u(\phi)\ \sin\lambda\ I_R(\lambda,\phi)\ d\lambda\ d\phi}{\iint_{\text{Aperture}} I_R(\lambda,\phi)\ d\lambda\ d\phi} \qquad (4.2)$$

where $u(\phi)$ is the zonal velocity distribution as a function of latitude, $I_R(\lambda,\phi)$ is the brightness distribution relative to that at the sub-solar point, and the sin λ term arises from the projection of the spherical planet onto the plane of the apparent disk. The variables λ and ϕ are respectively longitude and latitude on Venus, with the origin defined as the sub-earth point, i.e., the center of the apparent disk.

The simplest velocity distribution which can be used in the above equation is that corresponding to uniform solid-body rotation of the atmosphere, i.e., $u(\phi) = U_o \cos\phi$, where U_o is the equatorial zonal velocity. However, since the integration of (4.2) is done numerically, it is not very difficult to use a more realistic expression for the velocity distribution such as that determined empirically by Limaye (1977), which is given in Equation (3.1). The zonal velocity can be expressed as the product of the constant equatorial velocity U_o with a zonal velocity distribution function $\bar{u}(\phi)$. The constant U_o can be taken out of the integral in the numerator, allowing the calculation of a convenient velocity scaling factor $F_v = U_o$. Velocities obtained from residual Doppler shifts in a spectrum can then be quickly divided by the appropriate scaling factor F_v to obtain the average equatorial zonal wind velocities.

Several distributions for the solar illumination of the disk of Venus were considered, but for the sake of simplicity of calculation, only Lambert's Law for diffuse reflection from a solid surface and the reflection

law for isotropic scattering seemed appropriate for use in the integration of (4.2). Exact calculations of the brightness distribution for Venus assuming a semi-infinite cloud with Mie scattering have been carried out using the method of spherical harmonics by Devaux et al. (1975) for wavelengths ranging from the visible orange (λ = 0.6 μm) to the ultraviolet (λ = 0.4 μm). However, Hapke (1976) has pointed out that calculations assuming isotropic scattering by the Venus clouds are in reasonable agreement with observations for this same wavelength region, particularly toward the orange wavelengths, where the single-scattering albedo of the clouds approaches 1.00. In the infrared region of interest in the present work (1.5 to 2.0 μm), the single-scattering albedo is also close to 1.00, and the isotropic-scattering regime is applicable. A mathematically simpler distribution, which may be a good first approximation to isotropic scattering, is that given by Lambert's Law for diffuse reflection, which assumes that the reflected light is isotropic and is independent of the state of polarization and the angle of incidence of the incident light. The brightness distributions due to both types of diffuse reflection laws will be compared here for the Earth-Venus-Sun configurations at the time of the measurements for Venus A and Venus 5.

Following the notation used by Chandrasekhar (1960), the intensity of illumination $I(\mu,\mu_o)$ of any point M on the planet's surface as seen from space is the function of the cosines of the zenith angles of the observer (μ) and the sun (μ_o) as seen from point M. These zenith angle cosines in turn can be expressed as functions of the Venus phase angle (V_i) and of the latitude and longitude of point M, that is,

$$\mu = \cos \lambda \cos \phi \tag{4.3a}$$

$$\mu_o = \cos (\lambda - V_i) \cos \phi \tag{4.3b}$$

where as before, longitude and latitude (λ,ϕ) are defined with the sub-earth point as the origin, and V_i is taken to be positive when Venus is an evening star and negative when it is a morning star. Lambert's Law for diffuse reflection can then be stated as

$$I(\mu,\mu_o) = \bar{\omega}_o \mu_o F \tag{4.4}$$

where $\bar{\omega}_o$ is the single-scattering albedo and F is the incident flux at the top of the atmosphere at the sub-solar point, where $\mu_o = 1$. Thus the brightness of any point on Venus relative to that of the sub-solar point is simply the cosine of the solar zenith angle at that point, i.e.,

$$I_R(\lambda,\phi) = \frac{I(\mu,\mu_o)}{I(\cos V_i, 1)} = \frac{\bar{\omega}_o \mu_o F}{\bar{\omega}_o F} = \mu_o \tag{4.5}$$

The diffuse reflection law for isotropic scattering, however, is more complex, and the brightness at any point on the planet depends on the positions of both the earth and the sun in relation to that point. The law is given by

$$I(\mu,\mu_o) = \frac{\bar{\omega}_o F}{4} \left(\frac{\mu}{\mu+\mu_o} \right) H(\mu)\ H(\mu_o) \tag{4.6}$$

where $H(\mu)$ and $H(\mu_o)$ are Chandrasekhar H-functions which also depend on the value of the single-scattering albedo $\bar{\omega}_o$. The values of the H-functions for given values of μ and $\bar{\omega}_o$ can be found by lengthy calculation or in already published tables (Chandrasekhar, 1960).

Using the tables of H-functions, the longitudinal distribution of relative brightness of the disk of Venus along the equator and at two other

latitudes, assuming isotropic scattering, was calculated for both the Venus A and Venus 5 viewing configurations. Figure 20 shows the calculated brightness distribution for isotropic scattering (dashed lines), as well as the corresponding calculated distribution assuming Lambert's Law reflection (solid lines). It is apparent in the figure that the results for the two laws of diffuse reflection are nearly identical, except near the extreme edge of the planetary disk in lower latitudes. Therefore it seems reasonable to use the mathematically simpler Lambert's Law to describe the brightness distribution of the planetary disk for the particular viewing configurations of the spectra studied in this work. Since most of the differences between the two distributions appear near the sub-solar region, it is expected that the more realistic isotropic-scattering distribution should be used when Venus appears at or near full phase.

It should also be noted that in Figure 20 the coordinates given for location on the planet are not latitude and longitude, but Cartesian coordinates in the plane of the apparent disk of Venus with the origin at the midpoint of the bright limb; horizontal and vertical coordinates (x,y) are scaled so that the planetary radius R = 1. The sub-earth point in this system then has the coordinates $(-x_o,0)$. This transformation to Cartesian coordinates facilitates the integration of the velocity scaling function over the illuminated portion of the circular field of view. Careful comparison of the Venus phase angle and semidiameter for each observation date reveals that for a number of the individual spectra the field of view, which is circular with a more or less constant diameter of 12 arc sec, overlaps both the terminator and the edge of the planetary disk (Figure 18b). Therefore the area over which integration of Equation (4.2) is performed may not be a circle, but a circle with arcs of larger radius cutting off its edges.

Figure 21 shows the distribution of the relative contribution to the spectroscopically observed earthward velocity component for both Venus A (a) and Venus 5 (b), isoplethed for the observed illuminated area of the disk. The quantity isoplethed in the figure represents the integrand in the numerator of the following equation, which was evaluated numerically

$$F_v = \frac{v_s}{U_0} = \frac{\iint \bar{u}(y)\ (x+x_0)\ I_R(x,y)\ dx\ dy}{\iint I_R(x,y)\ dx\ dy} \qquad (4.7)$$

in order to find the velocity scaling factor F_v for each of the individual spectra and for the averaged spectra. In the equation above $\bar{u}(y)$, $(x+x_o)$ and $I_R(x,y)$ are the Cartesian-coordinate equivalents of $\bar{u}(\phi)$, $\sin\lambda$ and $I_R(\lambda,\phi)$ used in Equation (4.2). The results of the numerical integrations show that the velocity scaling factor F_v is 1.147 for Venus A and -0.878 for Venus 5. The scaling factors for the individual spectra differ from these mean values by not more than ± 0.029.

4.3 The Direct Problem: Calculation of Expected Line Asymmetries for a Model Atmosphere

Direct calculation of expected line shapes in the R-branch of the $H^{35}Cl$ 2-0 band for given profiles of temperature, pressure and equatorial zonal wind velocity (U_o) in the Venus upper atmosphere aids in the understanding of the relationship of the pressure-induced and wind-induced line-shifts at specific atmospheric levels to the asymmetric profile of the entire absorption line. Such a calculation is relatively straightforward, using the standard formulas for the absorption coefficient and transmittance for a line having the Voigt profile in a plane-parallel, non-homogeneous

atmosphere (Goody, 1964). In this model it is assumed that no significant scattering of the infrared radiation occurs in the atmosphere above the clouds, and that the cloud tops act as an unbroken surface reflecting infrared radiation according to Lambert's Law.

The variation of intensity for an incident ray of intensity I_ν passing through a region in thermodynamic equilibrium containing an amount of absorber dm is given by

$$dI_\nu = k_\nu (I_\nu - B_\nu)\, dm \tag{4.8}$$

where k_ν is the coefficient of absorption and B_ν is the black-body intensity at the temperature of the medium. In the case of sunlight reflected from the Venus cloud tops, I_ν is at least 10 orders of magnitude greater than B_ν. Thus we can neglect B_ν in the transfer Equation (4.8) and integrate to obtain

$$I = I_{\nu_0}\, e^{-\int_{m_1}^{m_2} k_\nu\, dm} \tag{4.9}$$

where I_{ν_o} is the original intensity of the ray before it has passed through the medium. We can also define the transmittance as $\mathcal{T}_\nu = I_\nu / I_{\nu_o} = \exp\left(-\int k_\nu\, dm\right)$.

The absorption coefficient k_ν depends not only on frequency, but also on the pressure, temperature and molecular composition of the absorbing medium. At the conditions present in the Venus atmosphere 50 to 80 km above the surface, the HCℓ absorption lines are expected to have a Voigt profile. Calculation of expected magnitudes of both Doppler-broadened

and collision-broadened half-widths, as well as line intensities and mean amounts of HCℓ absorber for this region of the Venus atmosphere shows that the HCℓ absorption lines should fall in the linear and transition regions of the curve of growth (see Goody, 1964, p. 237). The Voigt line shape can be expressed as

$$k_\nu = \frac{S\ a}{\alpha_D \pi^{3/2}} \int_{-\infty}^{+\infty} \frac{\exp\ (-y^2)}{a^2 + (t-y)^2}\, dy \qquad (4.10)$$

where S is the line intensity, α_D is the Doppler half-width at 1/e height of the line, and $a = \alpha_L / \alpha_D$, where α_L is the Lorentz, or collision broadened half-width at half-height of the line. Under the integral y is a dummy variable of integration, while $t = (\nu - \nu_o)/\alpha_D$, where ν_o is the central frequency of the line.

The value of α_L depends on both pressure and temperature as follows

$$\alpha_L = \alpha_s \left(\frac{p}{p_s}\right) \left(\frac{T_s}{T}\right)^n \qquad (4.11)$$

where α_s is the Lorentz half-width measured at standard pressure p_s (usually 1 atm) and standard temperature T_s (usually about 300 K). The exponent n is generally taken to be 1/2, which is the value obtained assuming that molecular collisions occur with the frequency given by classical kinetic theory. Unfortunately, complete measurements of CO_2-broadened Lorentz half-widths in the HCℓ 2-0 band are for the R0 and R10 lines by Rank et al. (1960a).

However, reasonable estimates of CO_2-broadened halfwidths for the other lines in this band can be made using existing measurements of self-broadened halfwidths in this same band by Toth et al. (1970). By comparing measurements in the fundamental of HCℓ of self-broadened (Benedict et al., 1956) and CO_2-broadened (Varanasi et al., 1972) halfwidths, one can calculate broadening coefficients $\gamma(CO_2) = \alpha_s(CO_2)/\alpha_s(HC\ell)$ for each of the lines in this band. Careful examination of the results of Rank et al. (1963) for broadening by Kr and Xe in both the 1-0 and 2-0 bands of HCℓ shows that the ratio of broadening coefficients for lines having identical J values in the two bands, $\gamma(2\text{-}0)/\gamma(1\text{-}0)$ remains more or less constant for different perturbing molecules. Thus the CO_2-broadened halfwidths in the HCℓ 2-0 band can be calculated by multiplying the measured self-broadened halfwidth for the 2-0 band by the broadening coefficient for the 1-0 band determined from the Varanasi et al. (1972) measurements, and finally by the previously determined ratio of the broadening coefficient $\gamma(2\text{-}0)/\gamma(1\text{-}0)$. The results of such calculations were used along with the two direct measurements by Rank et al. (1960a) in Equation (4.11) in the model.

The Doppler halfwidth α_D is independent of pressure, depending only on the ambient temperature and the central frequency of the absorption line. It is calculated directly using the formula

$$\alpha_D = \frac{\omega_o}{c}\sqrt{\frac{2\,k\,T}{m}} \qquad (4.12)$$

where ω_o is the wavenumber of the line center in cm^{-1}, c is the velocity of light, k is Boltzmann's constant and m is the mass of a single HCℓ molecule.

The line intensity S also depends on temperature, which affects the population of the lower energy state involved in the absorption transition.

For a line in the HCℓ 2-0 band the intensity can be expressed as

$$S(T) = S(T_s) \frac{Q_R(T_s)}{Q_R(T)} \exp \left[\frac{hcB_{oHC\ell}\, J(J+1)}{k} \left(\frac{1}{T_s} - \frac{1}{T} \right) \right] \quad (4.13)$$

where again T_s is the standard temperature at which the reference line intensity $S(T_s)$ was measured. The function $Q_R(T)$ is the rotational partition function for the molecule; its exact values have been tabulated for a number of atmospheric molecules, but it can also be approximated by $Q_R(T) = kT/hcB$ for sufficiently large values of $B_{oHC\ell}$ and T. As pointed out by Herzberg (1950), this approximation appears reasonable for HCℓ at temperatures near 300 K. Under the approximation the ratio $Q_R(T_s)/ Q_R(T)$ appearing in Equation (4.13) would be replaced by T_s/T.

In Equation (4.10) the central frequency ν_o is usually taken to be constant for a given line. However, in this study of line asymmetries, the central frequency varies with pressure, through both the pressure-induced lineshifts and the Doppler shift due to the wind velocity at each pressure level, i.e.,

$$\nu_o(p) = (1 + f_D(p)) \nu_{s_o} + \delta_s \frac{p}{p_s} \quad (4.14)$$

where $f_D(p)$ is the Doppler shift factor $\Delta\nu/\nu$ arising from the wind velocity specified for each pressure level, ν_{s_o} is the standard vacuum wavenumber for the line center, and δ_s is the laboratory-measured pressure-induced shift per atm of the perturbing gas.

Since a number of terms in $k_\nu(p,T)$ are directly dependent on pressure, it is more convenient to express the incremental path length dm in Equation (4.9) also in terms of atmospheric pressure. In a plane-parallel Venus atmosphere, the amount of HCℓ in each increment of the path is

$$dm = q \frac{\rho}{\rho_s} \eta \, dz \tag{4.15}$$

where q is the volume mixing ratio of HCℓ to CO_2, ρ is the actual density of the atmosphere at height z, and ρ_s is the density of CO_2, which makes up 95-99 percent of the atmosphere, at STP. The effects of non-vertical paths of the beam through the atmosphere are taken into account by calculating an average airmass factor $\bar{\eta}$ for the viewing configuration. For a beam of sunlight reflected toward earth by a single point on the surface of Venus, $\eta = \sec\theta_o + \sec\theta$, where θ_o and θ are respectively the zenith angles of the sun and the earth at that point. For the whole field of view for each spectrum an average airmass factor, weighted according to the relative illumination of each point of the planet, is calculated by the following formula

$$\bar{\eta} = \frac{\iint \left(\frac{1}{\mu_o(x,y)} + \frac{1}{\mu_o(x,y)} \right) I_R(x,y) \, dx \, dy}{\iint I_R(x,y) \, dx \, dy} \tag{4.16}$$

where $\mu_o = \cos\theta_o$ and $\mu = \cos\theta$ and the Cartesian coordinates (x,y) as well as the integration limits, are the same as those defined in Section 4.2.2. In the airmass calculation for the Venus spectra a Lambert's Law brightness distribution [$I_R(x,y) = \mu_o$] was used, and the integrations were carried out

numerically in the same manner as for the calculation of the velocity scaling factor in Section 4.2.2. The results of these calculations give $\bar{\eta}$ = 3.427 for Venus A, and $\bar{\eta}$ = 4.804 for Venus 5.

Assuming that the atmosphere is generally in hydrostatic equilibrium, i.e., $dp = -\rho g dz$, then the above equation becomes

$$dm = \frac{\bar{q}}{\rho_s g} \bar{\eta}\, dp \qquad (4.17)$$

where g, of course, is the acceleration of gravity for Venus (885.2 cm sec^{-2}). Thus the transmittance of a given layer of the Venus atmosphere in the neighborhood of each HCℓ line becomes

$$\tau_\nu = \exp\left[-\int_{p_2}^{p_1} \frac{q\,\bar{\eta}}{\rho_s g} k_\nu (p,T)\, dp\right] \qquad (4.18)$$

Finally, in order to approximate as nearly as possible the actual shapes of the lines as they would appear in planetary spectra, the profiles τ_ν were convolved with the instrumental line shape (ILS) appropriate for the planetary spectra. Since all the Venus spectra were unapodized, the proper ILS is simply the classical Fourier Transform of the apodizing function $P(\delta) = 1$, where $P(\delta)$ is the weighting given to the interferogram as a function of the path difference δ. The ILS thus is of the form $(\sin x)/x$, where $x = 2\pi\sigma M$; σ is the distance in cm^{-1} from the center of the instrumental line profile, and M is the maximum path difference in cm. For the Venus spectra used in this study, the ILS is quite narrow, having a half-width at half-height

of 0.006 cm^{-1}, and convolution of this ILS with the theoretical profile does not significantly alter the line shape. An excellent discussion, along with graphical representations, of several types of apodizing functions used in Fourier spectrometry can be found in the work of Norton and Beer (1976).

In the model calculations, $S(T)$, $\alpha_D(T)$, $\alpha_L(p,T)$ and $\nu_o(p)$ for the R0 through R8 lines in the $H^{35}Cl$ 2-0 band were computed for 46 levels spaced 1 km apart between 50 and 95 km above the surface. The pressure and temperature profiles used (Figure 22) were from the Venus model atmosphere given by Marov and Ryabov (1972). Four wind velocity profiles were used and are shown in Figure 22. The profile designated "A-H(1)" in the figure is a linear representation of the extrapolation by Ainsworth and Herman (1977) of the Venera 7 data to allow small zonal velocities in the upper atmosphere (see also Figure 12). Likewise, the line "A-H(2)" is their other extrapolation of the Venera 7 results, specifying a constant zonal velocity of -130 m sec^{-1} throughout the upper atmosphere. The "Median" model velocity profile also shows a decrease to near-zero wind speeds at 90 km, but was drawn so as to include the measurements of Traub and Carleton (1975) and Limaye (1977), as well as those of Venera 7. A fourth model, called "A-H(2B)" has the same constant velocity profile as "A-H(2)", with the exception that the zonal velocity is zero in the layer between 70 and 72 km.

For each level in the model the absorption coefficient $k(\nu,p,T)$ was calculated at discrete frequencies spaced 0.002 cm^{-1} apart, extending over a region $\pm$ 0.100 cm^{-1} from the absolute central frequency of each line. The frequency spacing used here is the same as the spacing of data points (DELTAG in the DERPTH program) in the Venus A and Venus 5 planetary spectra, and the total width of the region over which the absorption is calculated is

large enough to include the most significant parts of the profiles of the HCℓ lines, whose half-widths in the planetary spectra lie between 0.01 and 0.02 cm^{-1}. FORTRAN routines written by Armstrong (1967) were used to evaluate numerically the integral in Equation (4.10). Then, after the calculation of the absorption coefficient for all levels, Equation (4.18) was integrated numerically using the trapezoidal rule to obtain the transmittance at each frequency for the atmospheric layer between 95 km and each level of interest. Since the Venus atmosphere is very thin above 95 km, with total pressures less than 0.01 mb, the contribution to the transmittance arising from layers above 95 km is negligible when compared with the contributions from lower layers. Thus the calculated values for the layer up to 95 km can be considered to represent the total transmittance from the level of interest to the top of the atmosphere. As the final step in the calculation of realistic HCℓ line profiles, the theoretical transmittances were convolved with the ILS for the unapodized spectra.

Figures 23 and 24 show a sample of the results for the median model, giving profiles of the absorption coefficient (Figure 23) and transmittance (Figure 24) in the region of the $H^{35}C\ell$ R4 line. In the four graphs the letters plotted refer to different significant levels in the model atmosphere, which are also indicated on the vertical axis in Figure 22. The absorption coefficient profiles for the different levels shown in Figure 23 indicate that near the peak of the line, the maximum contribution to the absorption comes from the upper layers of the atmosphere, while near the base of the line the maximum contribution is from lower atmospheric levels. Figure 24 illustrates the net transmittance between the top of the atmosphere and each of the significant levels. These significant levels can be viewed also as the locations of the reflecting surface at the top of the

cloud deck. The most realistic locations for this surface are between 60 and 69 km; absorption and transmittance for these layers are represented in the figures by curves B through E. Note that there is increasing asymmetry in the line shapes for the lower regions of the atmosphere (curves E, F, and G). This is due to the increasing negative displacement of the central peak of the absorption coefficient profile with depth into the atmosphere. Careful comparison of the line shapes calculated separately using the Venus A (Figure 24a) and Venus 5 (Figure 24b) velocity scaling factors reveals subtle differences in the two asymmetric line shapes for the same model atmosphere. This is because the identical profile of retrograde zonal velocities produces a positive Doppler shift for Venus A and a negative one for Venus 5; coupled with the pressure-induced lineshift, which is always negative for the R4 line, the difference in sign of the Doppler shifts causes the Venus 5 line profiles to be even more skewed toward smaller frequencies than would be expected for the Venus A profile.

In Figure 25 there is reproduced the $H^{35}C\ell$ R4 line profile for transmittance between 63 and 95 km in the Venus 5 median model atmosphere, which is the same as curve "D" in Figure 24b. The five equally-spaced chords were drawn across the line profile and their central positions calculated using the same algorithms as those in the DERPTH program. The heights in the model atmosphere to which these chord-center shifts correspond are given along the right-hand vertical scale of the figure. The details of calculation of these heights from the shifts are given in Section 4.4.1. The specific distribution of the chord-center shifts with height in a spectral line depends on the particular line, as well as on the pressure and wind velocity profiles. For the line shown in the figure, the shifts are all negative, and their magnitudes increase monotonically from the peak to the base of the line.

The question arises whether the correspondence between each equally spaced chord and a given atmospheric pressure level remains the same for all lines in the absorption band. Shifts of the five chord centers as shown in Figure 25 were calculated for each of the eight lines in the HCℓ R-branch, and the heights, pressures and wind velocities corresponding to these chords were compared. Results are given in Table 6 for the A-H(1) model velocity profile for both Venus A and Venus 5 synthetic line profiles. In the table are listed the heights in km in the model Venus atmosphere corresponding to each chord for the individual lines, along with mean values and standard deviations for the whole R-branch.

There appears to be more variation in the reference heights for chords c_1 and c_2 relative to the other chords. This variability is due to the fact that the spacing of data points in the line profile is 0.002 cm^{-1}, allowing calculation of the chord-center positions within only ± 0.002 cm^{-1}. For lower J values and near the peaks of the lines, the magnitudes of the pressure- and wind-induced lineshifts are generally less than about 0.001 cm^{-1}, so that the uncertainty in determining the positions of the chord centers is very significant. For chords c_3 and c_4, in the middle and lower portion of the absorption line, most of the expected lineshifts are considerably larger (from 0.001 to about 0.005 cm^{-1}), and the uncertainty is not so important. The reference heights for chord c_5 also show considerable variability due to noise in the line profile near the mean background level (FM in Figure 25) caused by the side lobes of the instrumental line shape for the unapodized spectra. The maximum amplitude of these side lobes is about 0.18, so that the noise introduced into the line profile by the side lobes will extend to a level of at most 0.82, which is less than the transmittance at the level of chord c_5 for all but the strongest lines in the band.

Also in Table 6 it appears that the reference heights for the chords

in lines having lower J numbers are somewhat greater than those determined for the other lines in the band. This effect is an artifact of the method by which the chords are drawn across the line profile. The DERPTH program studies the symmetry of each line over a constant interval of width 6*DS, where DS is a programmer-specified average half-width for all the lines of interest in the spectrum. As illustrated in Figure 17, the program finds the difference between the mean background and minimum intensities within this interval (DGMAX = FM - GGMIN), and takes 1/6 of this difference as the spacing for the chords. If the interval 6*DS is narrower than the width of the absorption line at its base, the mean background level will be drawn at a higher level in the line profile, and the five chords will be drawn only in the upper part of the line. In the model calculations given in Table 6, the width of the spectral interval 6*DS was 0.200 cm^{-1}, which caused the background level FM to be located at heights less than 0.99 in the "D" line profiles for the R0 through R3 lines. A survey of the actual halfwidth of the HCℓ lines in the planetary spectra shows that for Venus A the largest halfwidth is 0.0138 cm^{-1}, while the interval 6*DS is 0.1020 cm^{-1}, and for Venus 5 the largest halfwidth is 0.205 cm^{-1} and 6*DS = 0.3660 cm^{-1}. Thus we expect all the HCℓ line profiles in the planetary spectra to be completely contained in the interval 6*DS, and that the mean reference levels for the low-J lines calculated from these spectra will not differ significantly from the mean values for the whole band. Since the half-widths for the calculated "D" line profiles are close to those measured for the HCℓ lines in the spectra, the standard deviations given for the reference levels in Table 6 are probably not very different from those for the planetary spectra. Barring other sources of error, we would expect to be able to calculate reference heights within at least ±1.5 km, which corresponds to an error of at most 30 percent in atmospheric pressures in the region 60 to 70 km above the

planet's surface.

The model results for shifts of the central positions of the chords for all the HCℓ lines are presented graphically in Figures 26 through 28. In both the A-H(1) and median models, the velocity is increasing with depth into the atmosphere. Thus not only do the corresponding lineshift curves have increasing slopes, reflecting pressure-induced lineshifts increasing with depth, but also the entire curve for each level is displaced due to the wind-related Doppler shift. This Doppler shift can easily be found from the graphs, by measuring the displacement of the zero-crossing point for each curve, which is located between the R2 and R3 lines at approximately 5730 cm^{-1}. Note that for the A-H(2) model (Figure 28), which has a constant velocity at all levels, the displacements of the zero-crossing points are identical, and all the pressure-shift curves pass through the same point. Although this may also appear to be the case in Figures 26 and 27, close examination of the shifts shows that the curves do not intersect at exactly the same point for these two cases where the wind velocity is not constant with height in the atmosphere.

The zonal velocity profiles retrieved from the calculated line profiles in all four models are shown in Figure 29 along with the original wind profiles for each model. With the exception of model A-H(2B), which has sharp variations in zonal wind velocities within a few kilometers, the retrieved profiles appear to closely approximate the original ones. A more detailed discussion of the results and sources of error in these retrieved model profiles, along with the results for the planetary spectra, will be undertaken in Section 4.4.2.

4.4 The inverse problem: estimation of the velocity profile from measured line asymmetries in the HCℓ 2-0 band

In the previous section it was shown by direct calculation how pressure-induced lineshifts and wind-induced Doppler shifts can be responsible for detectable asymmetries in HCℓ spectral lines in high-resolution planetary spectra. It was also shown that the shifts in the central positions of chords equally spaced from the base to the peak of each line consistently represent the effects of wind velocity and pressure at distinct atmospheric levels for the R0 through R6 lines in the HCℓ 2-0 band. Thus the use of measured line asymmetries to calculate both atmospheric pressures and zonal wind velocities at specific levels seems to be a viable means of estimating vertical profiles of wind velocity in the Venus atmosphere above the clouds.

4.4.1 Procedure

The DERPTH program calculates and prints out for each spectral line the central position determined for chord c_1 (Figures 17 and 25) and the deviations of the central positions of the four succeeding chords from that of c_1. This program was used for the Venus 5 averaged spectrum and for all of the individual spectra. An earlier version of the same program called DERPTX was used for the Venus A averaged spectrum; in this case nine chords were drawn across each spectral line and had their central positions determined.

In each spectrum all the lines in the R-branch of the $H^{35}C\ell$ and $H^{37}C\ell$ 2-0 bands having quality factors of 3 or greater were used in the calculation of the pressures and zonal wind velocities. For each line there first was calculated a Doppler-corrected absolute position, i.e.,

$$\omega_D = \left(1 + \left(\frac{\Delta\nu}{\nu}\right)\right) \omega_0 \qquad (4.19)$$

where ω_o is the absolute vacuum wavenumber for the line measured by Guelachvili (1976) and $\Delta\nu/\nu$ is the combined translational and earth-rotational Doppler shift factor calculated from Ephemeris data for the spectrum. The Doppler-corrected absolute position was then subtracted from the central position determined by the program for chord c_1 (listed in Table 4) in order to obtain the lineshift for that chord, δ_1. Lineshifts for the succeeding chords were then found by adding the value of δ_1 to the chord-center displacements ($\delta_2 - \delta_1$, $\delta_3 - \delta_1$, etc.) which had been previously calculated by the DERPTH or DERPTX programs. The resulting lineshifts for all the chords are plotted for the whole R-branch in Figure 30 for the two averaged spectra Venus A and Venus 5. The points plotted in the figure are averages of the shifts for the $H^{35}Cl$ and $H^{37}Cl$ lines, weighted by their respective quality factors; this averaging produces a "good" data point for each J value. Chord-center shifts were also measured in individual spectra recorded on the first and last days of observations included in these averages. The patterns of the lineshifts for the individual spectra are quite similar to those for the averaged spectra.

An initial value of the wind-induced Doppler shift component (δ_{Di}) of the lineshift for each chord was estimated from the graphs. Pressure-shift factors r_i were then calculated for each line in the R-branch, using the formula

$$r_i = \frac{\delta_i - \delta_{Di}}{\delta_s} \qquad (4.20)$$

where δ_i is the net shift of the chord center, and δ_s is the laboratory measured lineshift averaged for both isotopic species, which refers to a standard CO_2 pressure of 122.2 mb.

Several iterations of this calculation of r_i for the R-branch lines were necessary in order to find the best value of δ_{Di}. If the estimated value for δ_{Di} is too large and negative, the calculated values of r_i will be small for the higher-J lines relative to those for the R0 and R1 lines; similarly, a too-large positive estimate for δ_{Di} will cause the R0 and R1 lines to have excessively high values of r_i. The iteration of the estimation of δ_{Di} and the calculation of r_i continues until the values of r_i obtained appear to be evenly distributed with respect to J. The final values of r_i are then averaged over J and multiplied by 122.2 to obtain the average pressure at level i in mb.

It is assumed that the wind-induced Doppler shift δ_{Di} refers to the displacement of the zero-crossing point of each pressure-shift curve, which occurs at about 5730 cm^{-1}. Thus v_{si}, the spectrally-determined earthward component of Venus zonal velocity can be found using the formula

$$v_{si} = \frac{\delta_{Di}}{5730\ cm^{-1}} * c \qquad (4.21)$$

where c is the velocity of light. The equatorial zonal velocity U_{oi} can then be found through dividing v_{si} by the velocity scaling factor F_v derived in section 4.2.2.

4.4.2 Results and error analysis

Velocity profiles retrieved from the calculated $H^{35}Cl$ model line profiles are shown in Figure 29, and the results obtained from the planetary spectra are given in Figure 31. The vertical error bars on the points plotted in Figure 29 represent the standard deviation from the mean reference pressure determined for each chord, averaged over the R0 through R8 lines of the

$H^{35}Cl$ 2-0 band. The standard deviation is about 18 percent for chord c_1, 15 percent for chords c_2 and c_3, and 20 to 25 percent for chords c_4 and c_5. This result is consistent with the variation of the reference heights for the chords in model A-H(1) presented in Table 6 and discussed in Section 4.3. In the results for the planetary spectra the standard deviations in the calculated pressure levels are approximately twice as large as those for the model line profiles. This additional uncertainty is most probably due to variations in the HCl line profiles in the planetary spectra resulting from overlapping of those lines with other absorption features arising in the atmospheres of both Venus and the earth. Such superimposition of absorption features was not accounted for when the model line profiles were calculated.

From the model calculations we can also estimate a minimum error limit on the zonal wind velocity determined for each pressure level. The displacement of the zero-crossing point (δ_{Di}) of the pattern of lineshifts for each chord can be estimated graphically within $\pm 0.05 \times 10^{-3}$ cm^{-1}, so that at best the corresponding zonal wind velocity can be determined within ± 3 m sec^{-1}. Since the displacement of the zero-crossing point affects the estimate of pressure for each chord-center shift, there exists a direct relationship between the uncertainty in the reference pressure and uncertainty in the wind velocity calculated for each chord. In both the model calculations and the planetary spectra results, it appears that for chords near the peaks of the HCl lines, a 1-percent error in estimation of the pressure corresponds to about a 2-percent error in the zonal wind velocity at that level. The range of possible wind velocities corresponding to a given pressure seems to increase with depth into the atmosphere; for chord c_5, near the base of the line and heavily influenced by background noise, a 1-percent error in calculated pressure can correspond to as much as 25 percent error in the

calculated wind velocity. In other words, for the profiles determined from the planetary spectra, the uncertainty in the estimated zonal wind velocity ranges from about 30 percent in the upper part of the profile to several hundred percent for some values estimated from chord c_5. Error bars showing the variability of the calculated wind velocities are shown in Figure 31; in the interest of clarity they are drawn only for the two profiles obtained from the averaged spectra.

One additional comment must be made concerning the model results. In model A-H(2B) the original velocity profile showed an abrupt decrease in wind speed from 130 m sec^{-1} to zero in a narrow layer about 2 km thick. However, the retrieved velocity profile shows a much more gradual change in wind velocity with height than was actually the case. This suggests that retrieval of wind velocity profiles from pressure-induced lineshifts is relatively insensitive to variations in the true velocity profile with vertical scales smaller than about 5 km. However, as can be seen from the results for the other three models presented in Figure 29, the mean shape of the velocity profile can be detected quite well. It may be a worthwhile future endeavor to calculate the shape of weighting functions for the retrieval of wind velocities from measured asymmetries in various parts of a spectral line profile.

Velocity profiles estimated from the two averaged planetary spectra (solid lines) and from four of the individual spectra (dashed lines) are shown in Figure 31. It is apparent in the figure that the profiles obtained using the individual spectra have generally the same shape as those obtained from the corresponding averaged spectra, but the magnitudes of the velocities vary greatly from one profile to the next. It was noted in the preceding section that the patterns of the chord shifts are similar for each averaged spectrum and its component spectra. Generally the wind velocities determined

from the individual spectra appear to fall within the range of velocities given by the error limits for the averaged spectra. However, careful comparison of the individual shift patterns also shows that the wind-induced Doppler displacements of the pressure-shift curves are generally more positive on the first day of observations and more negative on the last day. This suggests that there may be systematic errors in the calculation of the translational and/or earth-rotational Doppler shift factors, probably associated with the averaging of direction and distance of Venus from the observation site during the 2 to 3 hours necessary for each recording. An alternative explanation for these apparently uniform differences between velocity profiles from individual spectra is that they may actually represent real changes in the zonal velocity field during each period of observations (10 days for Venus A, 5 days for Venus 5).

An independent estimate of zonal wind velocities in the upper atmosphere of Venus was made from the same set of spectra, using lines in the $C^{12}O^{16}$ 2-0 band near 2.35 μm. Nearly all the lines in this band from P24 through R24 appeared in the planetary spectra, and a little more than half of these were sufficiently unblended with other absorption features to be useful in calculating the Doppler shift factor $\Delta\nu/\nu$ for the spectrum. In these calculations the absolute wavenumber measurements of Guelachvili (1973) were used as standards for the spectra in the Venus A series, while for the Venus 5 series the measured positions of lines arising from the CO cell which had been placed in the path of the interferometer were used whenever possible. According to the results of L. Young (1972) and Connes et al. (1968), the mean pressure of line formation for CO in the Venus atmosphere is 36 to 60 mb, corresponding to a height of 67 to 70 km above the surface. At these pressures the magnitudes of lineshifts induced in CO by CO_2 are likely to be no greater than 5×10^{-4} cm^{-1}, and can be neglected. The difference

between the Doppler shift factor calculated from the CO 2-0 band and that calculated from the Ephemeris data for each spectrum represents the Venus wind velocity at the mean level of CO line formation. The results are listed in Table 7. It can be seen that the velocities calculated from the CO band generally are consistent with those calculated from the upper parts of the HCℓ lines in the same spectra. Nevertheless there again appear the wide variations in velocities determined from different individual spectra in the same series, which adds to the evidence that these variations are caused either by averaging errors in the calculation of the Doppler shift factors from the Ephemeris data, or by actual changes in the zonal velocity field.

For comparison to the velocities estimated here from HCℓ lines in the infrared spectra, the maximum zonal winds measured by Veneras 4, 8, 9 and 10 between 40 and 60 km are also indicated in Figure 31. The shaded region in the figure represents the range of velocities estimated from UV photographs and other spectroscopic studies. It is noted that both of the velocity profiles estimated from HCℓ lines in the averaged spectra contain some values that lie in this shaded region, which indicates that the magnitudes and directions of these estimated velocities are more or less realistic.

Another estimate of the range of realistic wind velocities possible in the Venus upper atmosphere can be made by calculating the speed of sound waves for this region, using the relation $c(\text{sound}) = \sqrt{\gamma RT/m_{CO_2}}$. Zonal wind velocities would not be expected to exceed this magnitude. For the temperatures in the Venus atmosphere between 60 and 80 km, the calculated speed of sound is about 250 to 300 m sec^{-1}. Thus, the velocities estimated from the two averaged spectra appear to be well within realistic limits.

The velocity profile estimated from the Venus A spectrum shows a wide

variation in zonal velocities within an atmospheric layer only 10 km in depth. Such shears may not be unreasonable, however, since as Limaye (1977) has pointed out, the atmosphere is stably stratified in this region, and strong vertical mixing is unlikely. Also, the scale height in this region is relatively constant at 4 to 5 km. Near 60 km there appear to exist strong retrograde winds of about -75 m sec^{-1}, and there is slight evidence for a relative maximum in the profile of velocity magnitudes at that height. The retrograde winds decrease rapidly with height, becoming zero at roughly 64 km. Above this height the winds are apparently prograde in direction, with magnitudes steadily increasing with height to a maximum of about +68 m sec^{-1} near 70 km, where the estimated profile ends. The detection of prograde wind velocities with magnitudes of several tens of meters per second is indeed a remarkable result. The only other measurements of prograde winds are several single spectroscopic estimates by Traub and Carleton (1975) where the magnitudes of the prograde winds were only a few meters per second. Nevertheless, as noted in the discussion in Chapter III, some plausible dynamical regimes for the Venus atmospheric circulation, notably the model of Ramanathan and Cess (1975), do admit the possibility of prograde winds in the upper part of the Venus stratosphere.

The Venus 5 velocity profile appears to refer to a shallower layer in the atmosphere. In this region (about 65 to 70 km) all the estimated velocities are retrograde, having magnitudes from 90 to 131 m sec^{-1}. The Venus 5 velocities appear to increase in magnitude with height, showing considerably less vertical wind shear than in the Venus A profile.

Since the Venus A and Venus 5 velocity profiles, as well as the other estimates of wind velocities in the Venus atmosphere up to 80 km, refer to different local times of day, it is helpful to draw a cross section in

longitude and height of all available measured Venus equatorial zonal velocities. Figure 32 is such a cross section; the plotted data points include velocities from the profiles estimated from the Venus A and Venus 5 spectra, along with measurements from the Venera probes, and the velocities estimated by Limaye (1977) and Traub and Carleton (1975). Each velocity measurement is plotted at approximately the mean height and longitude (relative to the sub-solar point) to which it refers; error bars are not included for the sake of a clearer drawing. Velocity magnitudes are isoplethed using dashed lines, and the solid lines with arrows indicate possible streamlines for the mean flow.

It is important to remember that the zonal velocities plotted in the figure do not represent simultaneous observations, or, except for the Traub and Carleton results, averages over time periods longer than about a week. Thus this cross section may not necessarily represent the steady-state equatorial circulation of the Venus atmosphere. According to Dollfus (1975), in his review of photographs of the planet taken between 1927 and 1974, the general circulation of the Venus atmosphere as represented by the motions of large UV features has remained more or less the same within that 47-year time period. However, one cannot rule out the possibility of changes in the circulation occurring below the level of the UV-reflecting layer which may have time scales of the order of months or years. One short-term phenomenon detectable from Earth is the brightening of the polar regions which occurs on a time scale of several months and may be a "seasonal" effect. As Dollfus (1975) has noted, the brightening events occur almost exclusively when the planet is in the same half of its orbit around the sun. It is not yet known whether this brightening of the polar caps is related to some subtle change in the circulation of the Venus atmosphere.

Long-term changes in the Venus atmospheric circulation may be responsible for the inconsistency of the flow field due to the Venera 4 and Venera 8 velocity profiles in relation to the circulation derived from the other measurements. These two Venera profiles were measured prior to 1970, while the other results plotted in Figure 32 came from the period from 1971 to 1976. The large mass transports associated with the high zonal wind speeds near 40 km at the morning terminator require either excessively high zonal wind speeds (>1000 m sec^{-1}) in the stratosphere or meridional velocities several orders of magnitude larger than have been observed in order for the mass balance in the general circulation to be maintained. Because of this inconsistency and the lack of additional observations, we shall attempt no further discussion of the tropospheric circulation except to say that the zonal winds in the Venus troposphere appear to be consistently retrograde in direction.

Given the sparseness and relative uncertainty of the data points, as well as the weak mass transport in the stratosphere, some features of the circulation pattern can be resolved. In the layer roughly from 65 to 70 km, prograde velocities in the afternoon longitudes and retrograde winds in the morning region result in a zone of convergence at the sub-solar point and slightly westward, producing net upward vertical motions above this layer and downward motions below it. Above 75 km the flow appears to be uniformly retrograde in direction.

The stratospheric velocity field shown in Figure 32 is suggestive of a two-celled bipolar circulation schematically similar to that generated by the "moving flame" mechanism. However, more complex diurnal circulation patterns may show the same type of flow field in the sub-solar region. For example, in the three-dimensional model of Young and Pollack (1977), where

the stratospheric circulation is generated by the nonlinear interaction of planetary-scale eddies with the mean Hadley circulation of the troposphere, there also results net upward motions in the sub-solar region and consistently retrograde zonal winds at higher altitudes. It is not possible to determine from the sparse data in Figure 32 exactly what type of mechanism may be responsible for the stratospheric circulation.

Additional evidence for strong vertical motions in the sub-solar region was found in the Mariner 10 ultraviolet photographs of the equatorial regions. Belton et al. (1976b) have identified a region called the sub-solar disturbance (SSD) which contains cellular features having linear scales of 200 to 500 km, indicating the presence of convective motions in this region. The cellular features do not appear upwind or far downwind of the sub-solar point, where the UV features take the form of east-west streaks indicating retrograde zonal motion.

The retrograde velocities above 72 km in Figure 32 correspond with the pattern of UV features found in Mariner 10 photographs. However, none of the photographs shows obvious evidence for prograde zonal winds. The prograde velocities occurring at 65 to 70 km in the figure would lie below the height estimated by Limaye (1977) for the UV-reflecting layer and thus would not necessarily be detected in UV photographs.

In summary, it appears that the velocity profiles determined from HCl lines in the Venus A and Venus 5 spectra appear to be consistent with other estimates of zonal wind velocities and with the patterns of UV features photographed by Mariner 10. The composite stratospheric equatorial wind field appears to represent a diurnally-varying circulation induced by local heating in the sub-solar region. The exact mechanism responsible for this circulation cannot be determined from the currently available data.

CHAPTER V

CONCLUSION

The results presented in this study allow us to draw a number of conclusions; some of these have been stated in earlier chapters, but will be restated and summarized here.

(1) Pressure-induced lineshifts for HCl and HF absorption lines due to the CO_2 in the Venus atmosphere can be detected and measured in high-resolution infrared spectra of the planet. The lineshifts should be detectable in any infrared spectrum where the line positions can be determined within ± 0.001 cm^{-1}. Since spectra obtained in narrow frequency regions using tunable diode lasers, as well as spectra from Fourier-transform interferometers, can achieve such accuracies, the possibility exists for developing suitable monitoring instruments making use of pressure-induced lineshifts for hydrogen halides perturbed by CO_2 (for the Venus atmosphere) or by N_2 and O_2 for the earth's atmosphere) to measure wind velocities and pressures in planetary atmospheres. Since the lineshifts are linearly dependent on atmospheric pressure, they can be used to determine the pressure of line formation for the hydrogen halide lines in the planetary atmosphere, and Doppler shifts due to atmospheric motions at the pressure levels determined from the lineshifts can also be resolved and measured.

(2) For the Venus spectra used in this work, it was shown that asymmetries in line shapes in the HCl 2-0 band, caused by both pressure-induced shifts and Doppler shifts due to atmospheric motions at different levels in the upper atmosphere, can be used to estimate vertical profiles of the

average equatorial zonal wind velocity as a function of Venus atmospheric pressure. The R-branch of the HCℓ 2-0 band in the Venus spectra was chosen mainly because of the excellent quality of the spectral lines in this region. However, vertical profiles of velocities in planetary atmospheres can also be estimated using asymmetries of absorption lines belonging to other molecules, provided that atmospheric spectra of sufficient quality exist, and that there are available complete laboratory measurements of the pressure-induced lineshifts of interest.

In the case of Venus, the atmospheric pressures determined from the HCℓ line asymmetries are reasonably accurate, but the corresponding wind velocities show considerable uncertainty. A major portion of the uncertainty may be due to error in calculation of the translational and earth-rotational Doppler shifts. This error arises from the fact that the interferograms were not measured simultaneously; each one was integrated over a two- to three-hour period, and the final spectra, Venus A and Venus 5, are averages of several recordings.

An ideal experiment, focusing on the accurate measurement of line asymmetries in order to obtain Venus wind profiles, would involve the following: (i) very high-resolution measurements in the region of the HCℓ 2-0 band only, with as short a sampling time as possible; (ii) measurements made in pairs, one with the viewing aperture centered at the sub-earth point, where the earthward component of zonal velocity is zero, and the other made at approximately the same time with the viewing aperture centered on the point of interest on the planetary disk. This scheme is similar to that used by Traub and Carleton (1975) in their spectroscopic measurements of wind velocities on Venus. The instantaneous combined translational and earth-rotational Doppler shift could then be determined directly from the reference spectrum,

eliminating much of the averaging errors encountered in the present work.

(3) Venus zonal velocity profiles estimated from the infrared spectra show large vertical wind shears in the region 60 to 70 km above the surface of the planet, and the velocity profiles appear to vary greatly with location relative to the sub-solar point. The profiles obtained from the Venus A spectrum, which refers mainly to local afternoon regions on the planet, show a dramatic change from retrograde winds near 60 km to prograde velocities of the order of several tens of meters per second near 70 km. When these profiles are considered along with the few existing measurements of Venus wind velocities above 50 km, the composite stratospheric wind field appears to represent a diurnal circulation induced by strong local heating in the sub-solar region. Such a circulation pattern also appears to be consistent with the configuration of UV features photographed by Mariner 10 in the equatorial regions. A definite identification of the mechanism(s) responsible for the observed stratospheric circulation cannot be made at this time due to the uncertainties in existing measurements and the absence of wind data for the night side of Venus.

The results of this study, besides demonstrating how asymmetries in absorption lines can be used to estimate zonal velocity profiles in the Venus atmosphere, have provided some additional information regarding the vertical and longitudinal variation of zonal winds in the Venus stratosphere. It is hoped that Doppler tracking of the descent probes of the Pioneer Venus Mission in December 1978 will provide much more detailed information on the velocity distribution in the Venus atmosphere. The four probes are preprogrammed to impact the planet at four widely separated sites, including two on the night side, and are expected to provide a nearly simultaneous sample of Venus wind velocities between the surface and 70 km. Perhaps the additional information will verify the results obtained in the present work.

TABLE I

PHYSICAL CHARACTERISTICS OF VENUS AND EARTH

	Venus	Earth
Equatorial radius (km)		
(Radar)	6052 ± 5	6378.2
(Optical)	6115 ± 13	
Mean distance to Sun		
(million km)	108.6	149.5
(a.u.)	0.723332	1.000000
Mass relative to that of Earth	0.81427	1
Acceleration due to gravity (cm sec^{-1})	885.15	980.1
Solar constant (ly min^{-1})	3.8	2.0
Bond albedo	0.77 ± .07	0.3
Inclination of spin axis to orbital plane	3	23.5
Inclination of orbit to the ecliptic	3.394	0
Eccentricity of orbit	0.0068	0.0167
Length of year (days)	225	365.26
Period of rotation of solar planet (days)	243 (retrograde)	1
Tangential speed of solid planet due to rotation ($m\ sec^{-1}$)	1.8 cos ϕ	463.8 cos ϕ
Coriolis parameter (10^{-7} sec^{-1})	5.99 sin ϕ	1454 sin ϕ

TABLE 2

COMPOSITION OF THE VENUS ATMOSPHERE

(a) Molecules observed in the atmosphere of Venus above the clouds

Gas	Mixing Ratio	Total Amount ($cm\text{-}atm_{STP}$)	Pressure (mb)	Temperature (K)	Reference
CO	$4.5 \pm 1.0 \times 10^{-5}$	13	60	240	Connes et al. (1968)
	$5.1 \pm 0.1 \times 10^{-5}$	20	36	249 ± 3	L. Young (1972)
CO_2	0.97 ± 0.04	-	-	-	Vinogradov et al. (1970a,b)
	-	$3.3 \pm 0.3 \times 10^{5}$	100	240 ± 10	Connes et al. (1967)
	-	$2.8 \pm 0.4 \times 10^{5}$	60	240	Connes et al. (1968)
	-	$4.1 \pm 0.1 \times 10^{5}$	36	249 ± 3	L. Young (1972)
	-	$0.9 - 5.5 \times 10^{5}$	100	245	Fink et al. (1972)
HCℓ	6×10^{-7}	$1.9 \pm 0.4 \times 10^{-1}$	80	270 ± 30	Connes et al. (1967)
	$4.2 \pm 0.7 \times 10^{-7}$	$1.7 \pm 0.3 \times 10^{-1}$	160	240 ± 16	L. Young (1972)
HF	5×10^{-9}	-	100	240	Connes et al. (1967)
	7×10^{-9}	-	67	249 ± 3	L. Young (1972)

H_2O	10^{-4}	35	-	-	Dollfus (1963a,b)
	2.5×10^{-4}	100	90	-	Bottema et al. (1964a,b)
	8.7×10^{-6}	25	600	-	"
	10^{-4}	39	-	-	Belton & Hunten (1966)
	10^{-4}	30	-	-	Spinrad & Shawl (1966)
	1.1×10^{-2}	-	600	295	Vinogradov et al. (1968)
	2×10^{-6}	0.6	-	-	Kuiper (1969)
	2×10^{-5}	5	-	-	Schorn et al. (1969a,b)
	10^{-6}	-	10000	500	Vinogradov et al. (1970a,b)
	0.6×10^{-6}	0.2	-	-	Fink et.al. (1972)
	-	0.5	-	-	Gull et al. (1974)

TABLE 2—Continued

(b) Molecules not observed in the atmosphere of Venus above the clouds

Gas	Maximum Mixing Ratio	Maximum amount ($cm\text{-}atm_{STP}$)	References
CH_2O	10^{-6}	10^{-1}	Owen and Sagan (1972)
CH_3 and aldehydes	10^{-6}	10^{-1}	Owen and Sagan (1972)
CH_4	10^{-6}	3×10^{-1}	Connes et al. (1967)
$CH_3C\ell$	10^{-6}	3×10^{-1}	Connes et al. (1967)
CH_3F	10^{-6}	3×10^{-1}	Connes et al. (1967)
CH_3COCH_3 and ketones	10^{-6}	10^{-1}	Owen and Sagan (1972)
C_2H_2	10^{-6}	3×10^{-1}	Connes et al. (1967)
C_2H_4	10^{-5}	2	Kuiper (1952)
C_2H_6	10^{-5}	4	Kuiper (1952)
C_3O_2	10^{-7}	10^{-2}	Owen and Sagan (1972)

HCN	10^{-6}	3×10^{-1}	Connes et al. (1967)
H_2S	10^{-7}	10^{-2}	Owen and Sagan (1972)
N_2	2×10^{-2}	-	Vinogradov et al. (1970a,b)
NH_3	3×10^{-8}	10^{-2}	Kuiper (1962)
NO	10^{-6}	10^{-1}	Owen and Sagan (1972)
NO_2	10^{-8}	10^{-3}	Owen and Sagan (1972)
N_2O	6×10^{-4}	200	Kuiper (1952)
N_2O_4	4×10^{-8}	4×10^{-3}	Owen and Sagan (1972)
O_2	7×10^{-5}	24	Belton and Hunten (1968)
O_3	3×10^{-9}	3×10^{-4}	Owen and Sagan (1972)
SO_2	5×10^{-8}	5×10^{-3}	Cruikshank and Kuiper (1967)
	10^{-8}	10^{-3}	Owen and Sagan (1972)

TABLE 3

PARAMETERS FOR RECORDED SPECTRA OF VENUS

Spectrum	Date	Times (Local)		Illuminated Disk			Distance from Earth (a.u.)	Semidiameter (arc sec)
		Start	End	Phase Angle	Fraction Illum.	Stellar Mag.		
143	14 Oct 73	14:28	17:30	74.9°	0.631	-3.8	0.897 3169	9.37
149	15 Oct 73	14:12	16:26	75.3°	0.627	-3.8	0.889 8692	9.45
156	22 Oct 73	15:13	17:45	78.6°	0.599	-3.8	0.837 5038	10.04
161	25 Oct 73	14:49	17:50	80.0°	0.586	-3.9	0.814 9448	10.32
Venus A average				77.2°	0.611	-3.8	0.859 9087	9.80
226	12 Jun 74	4:48	7:27	57.4°	0.769	-3.5	1.201 0340	7.00
228	13 Jun 74	5:10	7:41	57.0°	0.772	-3.5	1.207 8121	6.96
230	14 Jun 74	4:29	7:37	56.6°	0.775	-3.5	1.214 5570	6.92
231	15 Jun 74	4:29	7:40	56.2°	0.778	-3.4	1.221 2683	6.89
234	16 Jun 74	4:30	7:38	55.8°	0.781	-3.4	1.227 9454	6.85
Venus 5 average				56.6°	0.775	-3.5	1.214 5234	6.92

TABLE 4

HYDROGEN HALIDE LINES OBSERVED IN THE VENUS SPECTRA

(a) HF 1-0 band

Line	Standard position (cm^{-1})	Venus A		Venus 5	
	($\pm 2.5 \times 10^{-4}$ cm^{-1})	Central Position (cm^{-1})	Quality Factor	Central Position (cm^{-1})	Quality Factor
R1	4038.9625	4039.135106	1	4038.807469	3
R2	4075.2936	4075.467221	0	4075.138583	1
R3	4109.9363	4110.111393	3	4109.776186	1
R4	4142.8460	4143.020316	1	4142.685340	2
R5	4173.9796	4174.155088	3	4173.818178	1
R6	4203.2960	4203.475137	0	4203.1315	0

(b) HF 2-0 band

	($\pm 15 \times 10^{-4}$ cm^{-1})				
P2	7665.5745	7665.908315	0	7665.285014	5
P1	7709.6839	7710.017692	0	7709.3928	0
R0	7788.8562	7789.190809	0	7788.5673	0
R1	7823.8212	7824.162003	5	7823.525966	5
R2	7855.6428	7855.983584	5	7855.343839	2
R3	7884.2790	7884.621637	0	-	-

TABLE 4—Continued

(c) $H^{35}Cl$ 2-0 band

Line	Standard Position (cm^{-1})	Venus A		Venus 5	
	($\pm 10^{-3}$ cm^{-1})	Central Position (cm^{-1})	Quality Factor	Central Position (cm^{-1})	Quality Factor
P6	5524.9996	5525.235831	4	5524.7990	0
P4	5577.3313	5577.571096	2	5577.118853	5
P3	5601.7659	5602.009737	0	5601.552334	2
P2	5625.0282	5625.268599	5	5624.812772	2
R0	5687.6504	5687.894402	4	5687.433641	3
R1	5706.0940	5706.338637	5	5705.877340	3
R2	5723.3020	5723.548570	1	5723.085991	2
R3	5739.2627	5739.508974	5	5739.043513	5
R4	5753.9647	5754.210921	4	5753.744724	5
R5	5767.3970	5767.643448	4	5767.176221	5
R6	5779.5488	5779.795288	5	5779.327061	5
R7	5790.4098	5790.656031	4	5790.187529	2
R8	5799.9700	5800.216745	4	5799.746375	1
R9	5808.2197	-	-	5807.9968	0

TABLE 4—Continued

(d) $H^{37}Cl$ 2-0 band

Line	Standard Position (cm^{-1})	Venus A		Venus 5	
	($\pm 10^{-3}$ cm^{-1})	Central Position (cm^{-1})	Quality Factor	Central Position (cm^{-1})	Quality Factor
P5	5547.8656	-	-	5547.6511	0
P4	5573,4171	5573.655490	2	-	-
P3	5597.8123	5598.053033	2	-	-
P2	5621.0379	5621.278192	1	-	-
P1	5643.0807	5643.322226	2	5642.866099	1
R0	5683.5662	5683.809110	4	5683.349254	4
R1	5701.9840	5702.222899	0	5701.759798	0
R2	5719.1689	5719.413631	2	5718.950232	2
R3	5735.1094	5735.354644	4	5734.890669	5
R4	5749.7940	5750.039806	5	5749.574644	5
R5	5763.2118	5763.457811	3	5762.991033	4
R6	5775.3521	5775.597533	3	5775.131670	4
R7	5786.2046	5786.448285	2	5785.9822	0
R8	5795.7594	5796.008412	0	-	-

TABLE 5

VENUS DOPPLER SHIFTS CALCULATED FROM EPHEMERIS DATA

		Doppler Shift Factor ($\times 10^{-5}$)		
Spectrum	Date	Planetary Motions	Earth Rotation	Total
143	14 Oct 73	+4.2986	-0.0155	+4.2831
149	15 Oct 73	+4.3035	+0.0090	+4.3125
156	22 Oct 73	+4.3359	-0.0268	+4.3091
161	25 Oct 73	+4.3488	-0.0205	+4.3283
Venus A average		+4.3217	-0.0134	+4.3083
226	13 Jun 74	-3.9204	+0.1105	-3.8099
228	13 Jun 74	-3.9013	+0.1056	-3.7957
230	14 Jun 74	-3.8823	+0.1119	-3.7704
231	15 Jun 74	-3.8627	+0.1112	-3.7515
234	16 Jun 74	-3.8426	+0.1103	-3.7323
Venus 5 average		-3.8819	+0.1099	-3.7720

TABLE 6

REFERENCE HEIGHTS OF CHORDS ACROSS LINES IN A-H(1) MODEL

Line	Height (km)				
	c_1	c_2	c_3	c_4	c_5
R0	71.7	71.4	70.2	67.4	67.8
R1	71.1	70.2	69.1	66.0	67.1
R2	71.1	69.9	69.0	65.9	67.1
R3	69.2	68.4	67.6	66.4	65.8
R4	68.7	68.6	68.1	67.2	65.2
R5	68.9	68.7	68.2	67.2	64.2
R6	68.8	68.6	68.1	67.4	63.6
R7	68.5	68.3	67.9	67.3	63.9
R8	68.3	68.0	67.8	67.1	63.9
Venus A Average	69.5±1.3	69.1±1.1	68.4±0.8	66.8±0.6	65.4±1.6
R0	71.3	70.6	69.5	66.3	67.3
R1	70.0	69.2	67.7	65.9	66.2
R2	66.3	66.0	65.9	65.5	65.3
R3	69.4	68.5	67.2	65.9	66.1
R4	69.4	68.7	67.8	66.3	65.9
R5	69.2	68.9	68.2	66.9	65.2
R6	69.0	68.7	68.3	67.4	63.7
R7	68.7	68.4	68.1	67.3	63.7
R8	68.4	68.1	67.9	67.2	63.8
Venus 5 Average	69.1±1.3	68.5±1.2	67.8±1.0	66.5±0.7	65.2±1.3
Overall Average	69.3±1.3	68.8±1.2	68.1±0.9	66.7±0.7	65.3±1.4

TABLE 7

VENUS WIND VELOCITIES CALCULATED FROM $C^{12}O^{16}$ 2-0 BAND

Spectrum	Number of Lines	Doppler Shift Factor ($\times 10^{-5}$)		Wind Velocity ($m\ sec^{-1}$)	
		CO band	Ephemeris	v_s	U_o
143	14	+4.2696	+4.2831	+ 40.5	+ 36.0
161	14	+4.2795	+4.3091	+146.3	+124.4
Venus A	14	+4.2726	+4.3083	+107.0	+ 93.2
226	16	-3.8601	-3.8099	+150.5	-169.1
234	16	-3.8171	-3.7323	+254.2	-293.9
Venus 5	16	-3.8406	-3.7720	+205.7	-234.3

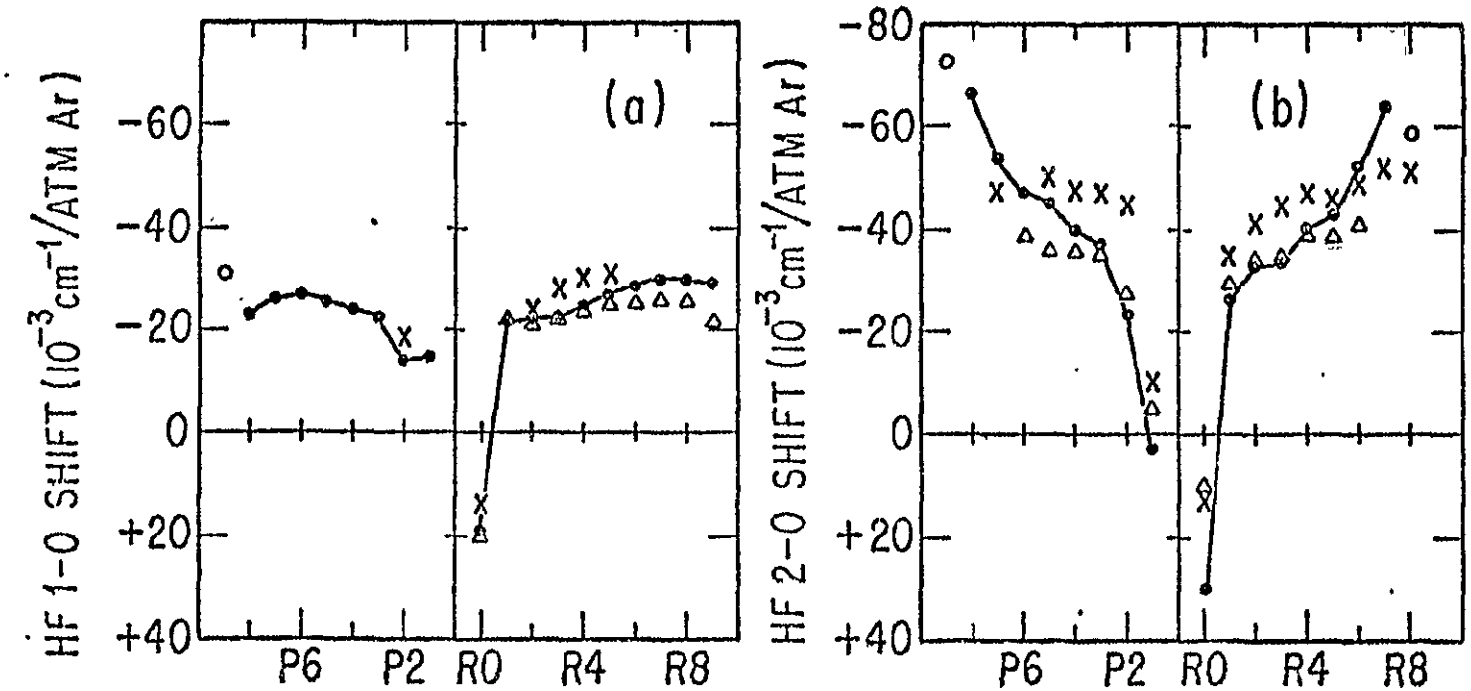

Fig. 1. -- Measured pressure-induced lineshifts for HF per atm Ar. (a) 1-0 band. Circles: Guelachvili and Smith (1978); Triangles: Jaffe et al. (1965); Crosses: Oksengorn (1963). (b) 2-0 band. Circles: Guelachvili and Smith (1978); Crosses: Wiggins et al. (1970.

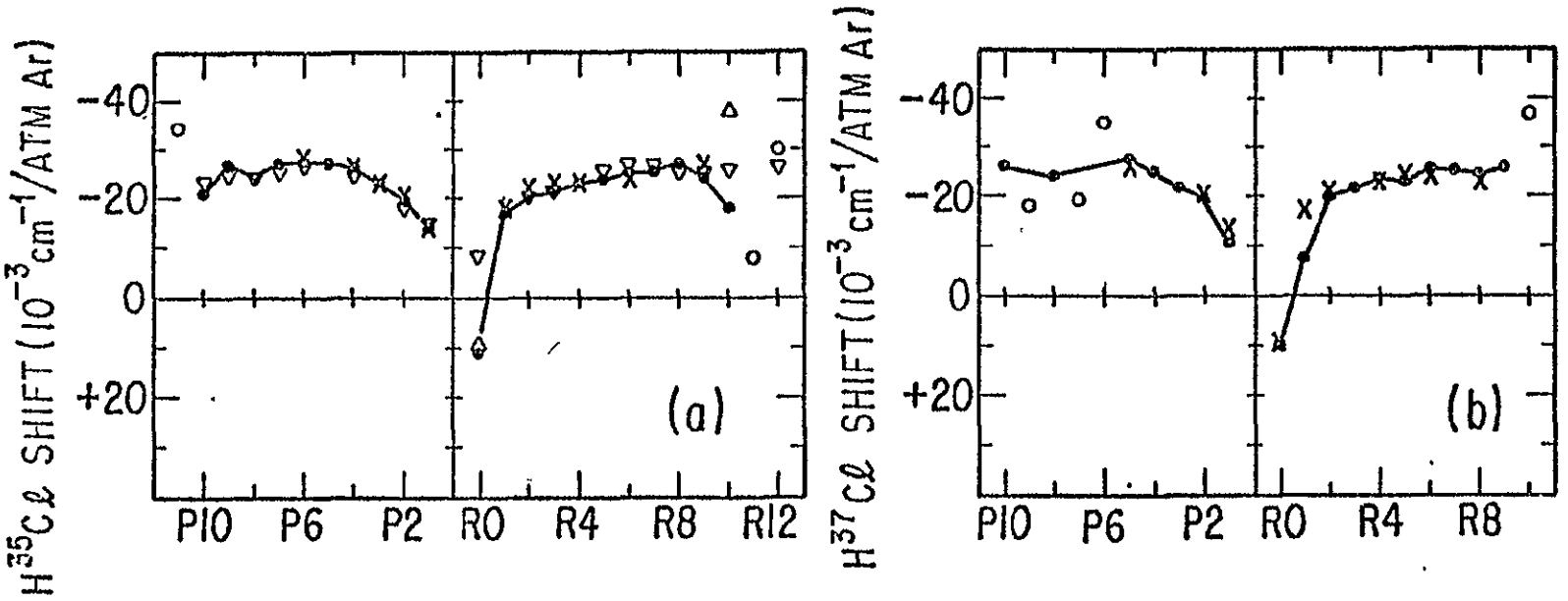

Fig. 2. -- Measured lineshifts per atm Ar in the HCℓ 2-0 band. (a) $H^{35}C\ell$. Circles: Guelachvili and Smith (1978); Triangles: Rank et al. (1960); Inverted triangles: Rank et al. (1964); Crosses: Hirshfeld et al. (1960). (b) $H^{37}C\ell$. Circles: Guelachvili and Smith (1978); Crosses: Hirshfeld et al. (1960).

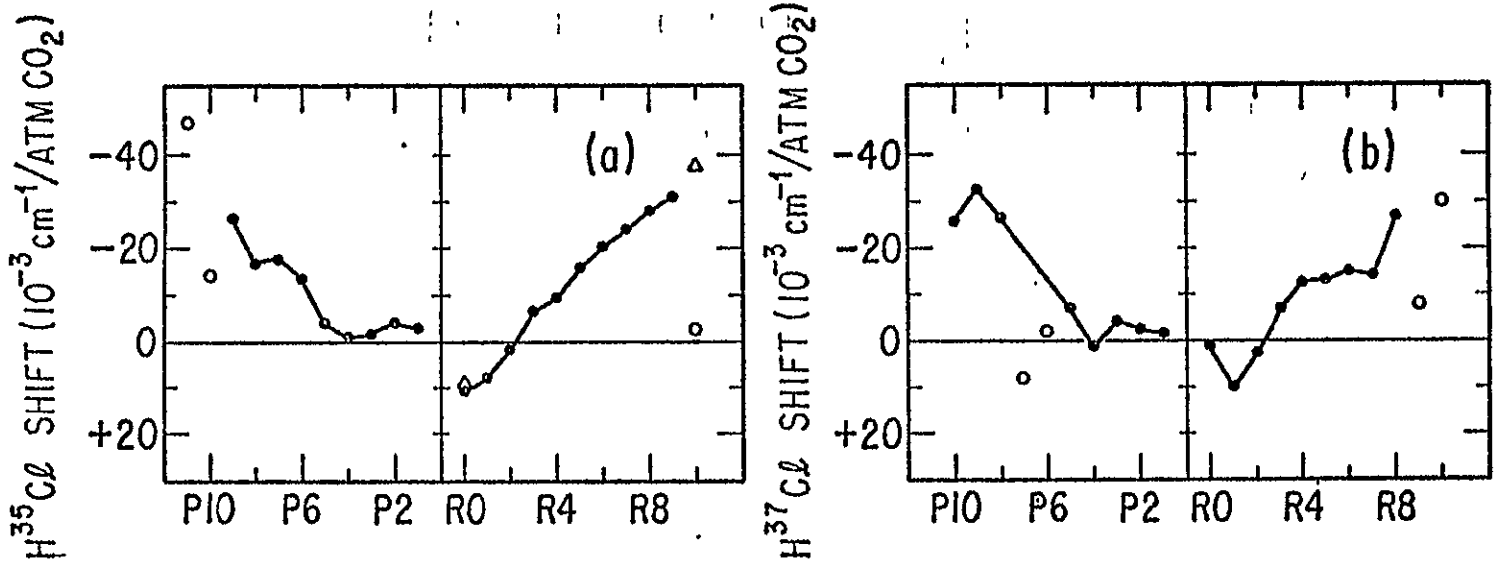

Fig. 3. -- Measured lineshifts per atm CO_2 in the HCℓ 2-0 band. (Guelachvili and Smith, 1978). (a) $H^{35}C\ell$. (b) $H^{37}C\ell$.

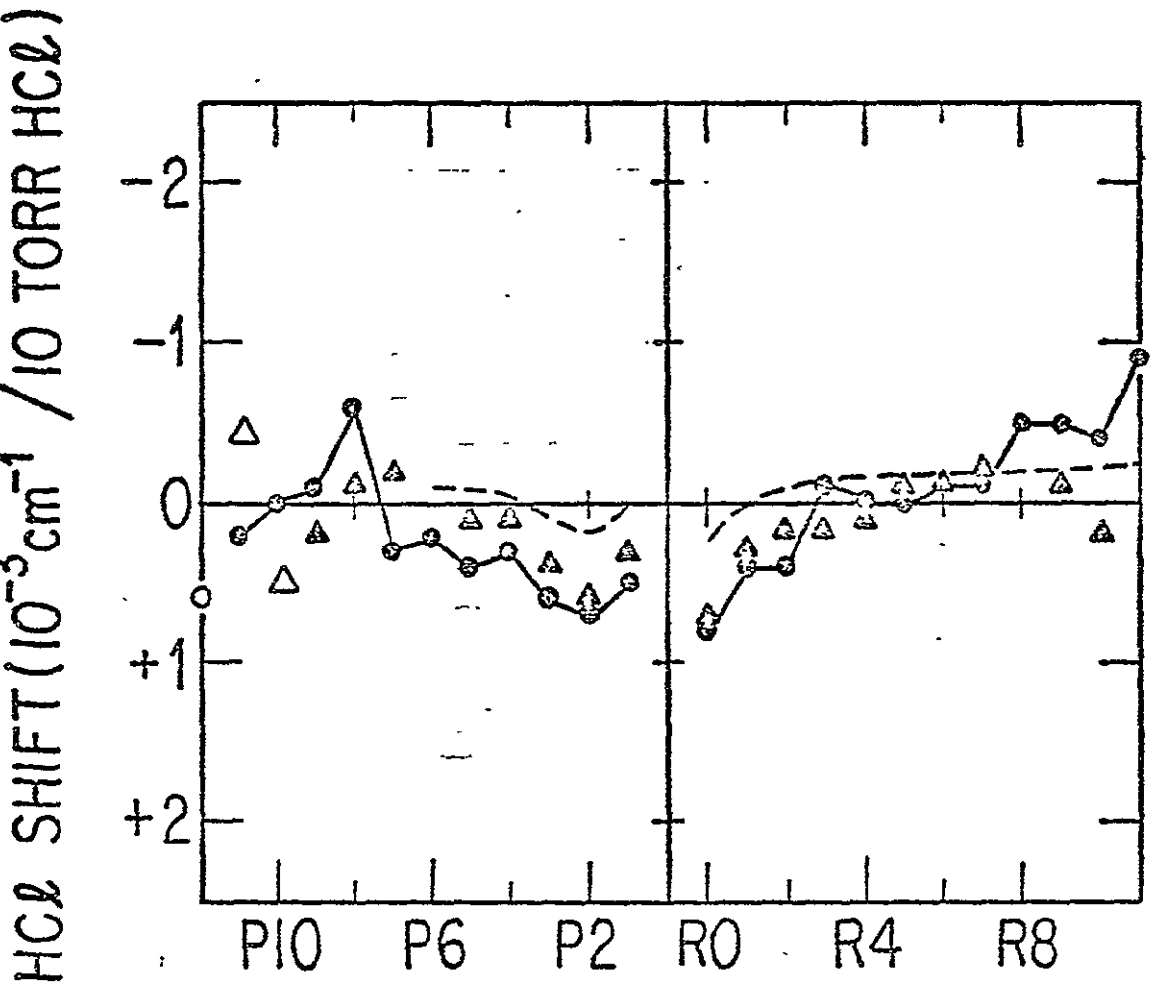

Fig. 4. -- Self-induced lineshifts in the HCl 2-0 band measured at low pressure. Circles: $H^{35}Cl$; Triangles: $H^{35}Cl$ (Guelachvili and Smith, 1978). Dashed line: Kimel et al. (1959).

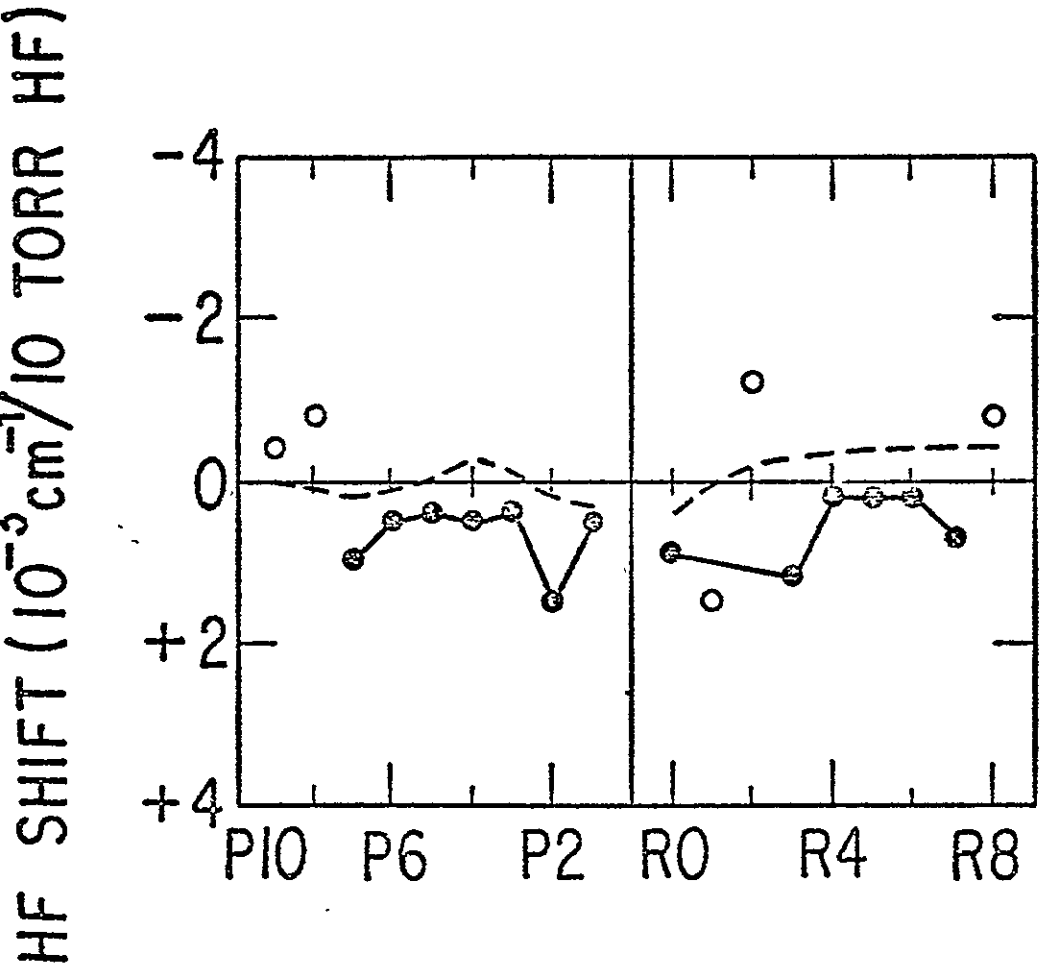

Fig. 5. -- Self-induced lineshifts in the HF 2-0 band measured at low pressure. Circles: 'Observed 'shifts (Guelachvili and Smith, 1978). Dashed lines: Shifts calculated by Boulet et al. (1976).

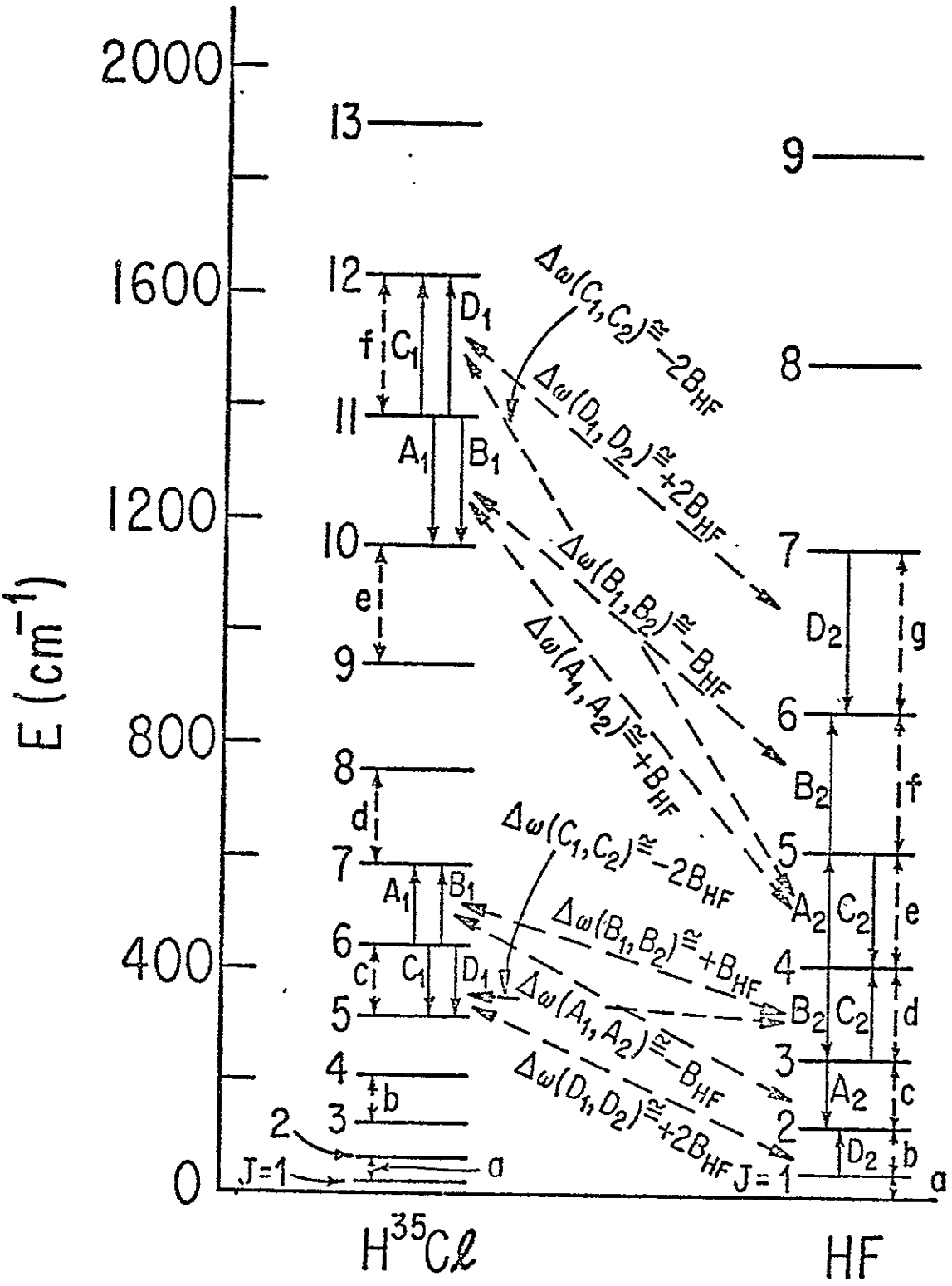

Fig. 6. -- Ground-state rotational energy levels and near-resonant transitions for $H^{35}Cl$ and HF (after Boulet et al. 1976).

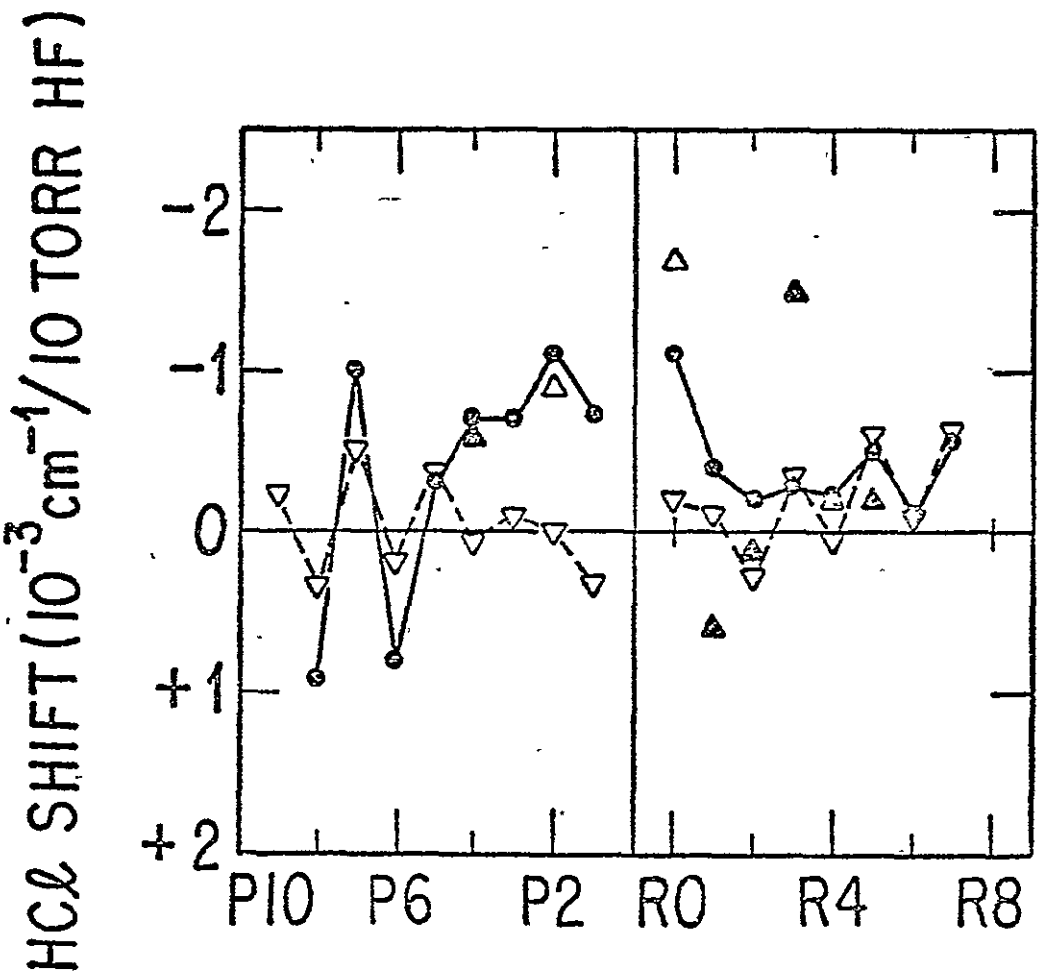

Fig. 7. -- Lineshifts in the HCℓ 2-0 band perturbed by 10 torr HF. Circles: $H^{35}Cℓ$ observed shifts; triangles: $H^{37}Cℓ$ observed shifts (Guelachvili and Smith, 1978); inverted triangles: calculated shifts (Boulet, 1977).

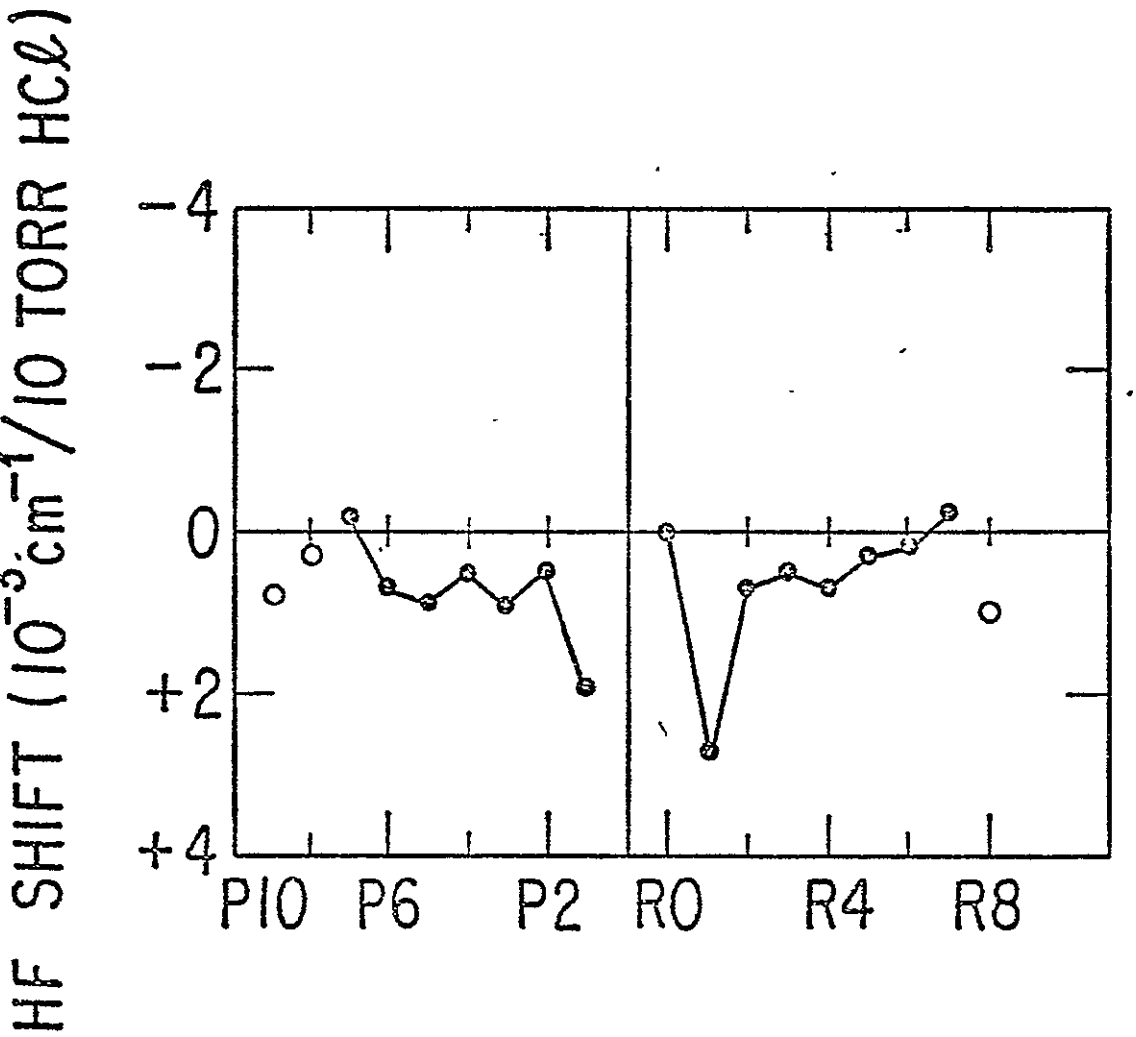

Fig. 8. -- Lineshifts in the HF 2-0 band perturbed by 10 torr HCℓ (Guelachvili and Smith, 1978).

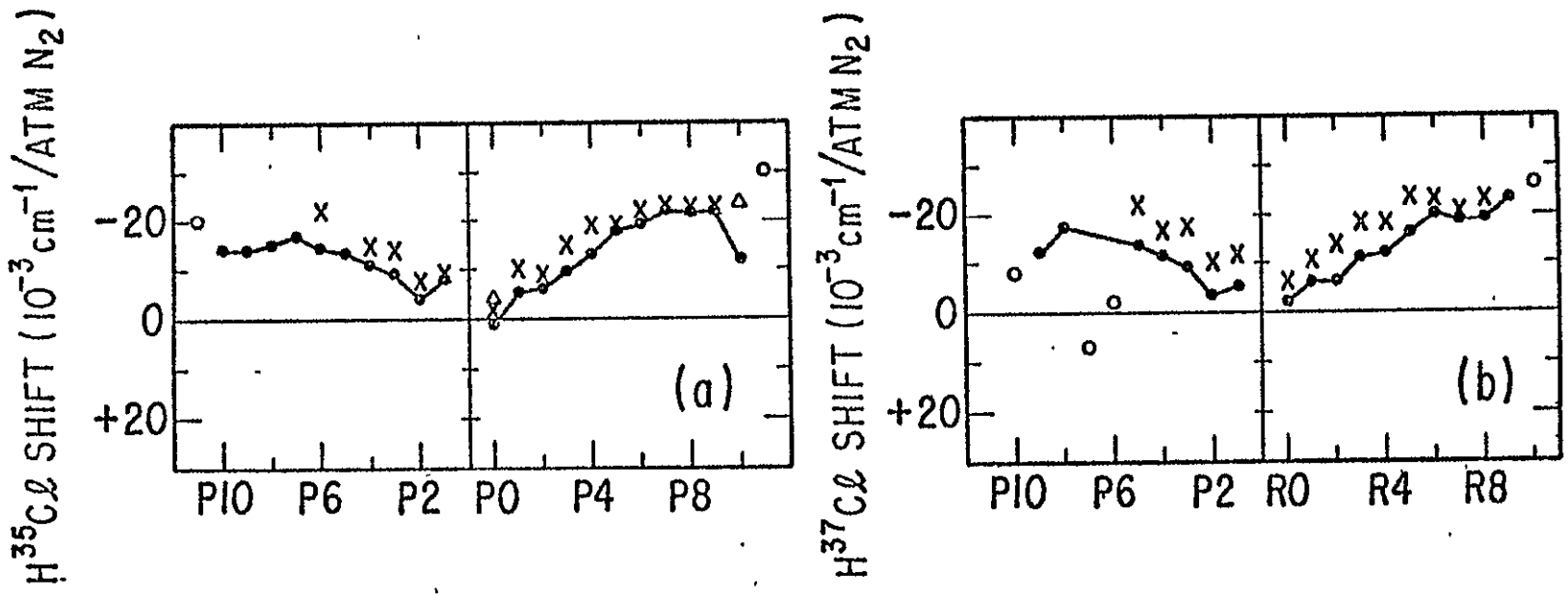

Fig. 9. -- Measured lineshifts per atm N2 in the HCℓ 2-0 band. Circles: Guelachvili and Smith (1978); triangles: Rank et al. (1960a); Crosses: Shifts measured by Kimel et al. (1959) for 1 atm dry air. (a) $H^{35}C\ell$. (b) $H^{37}C\ell$.

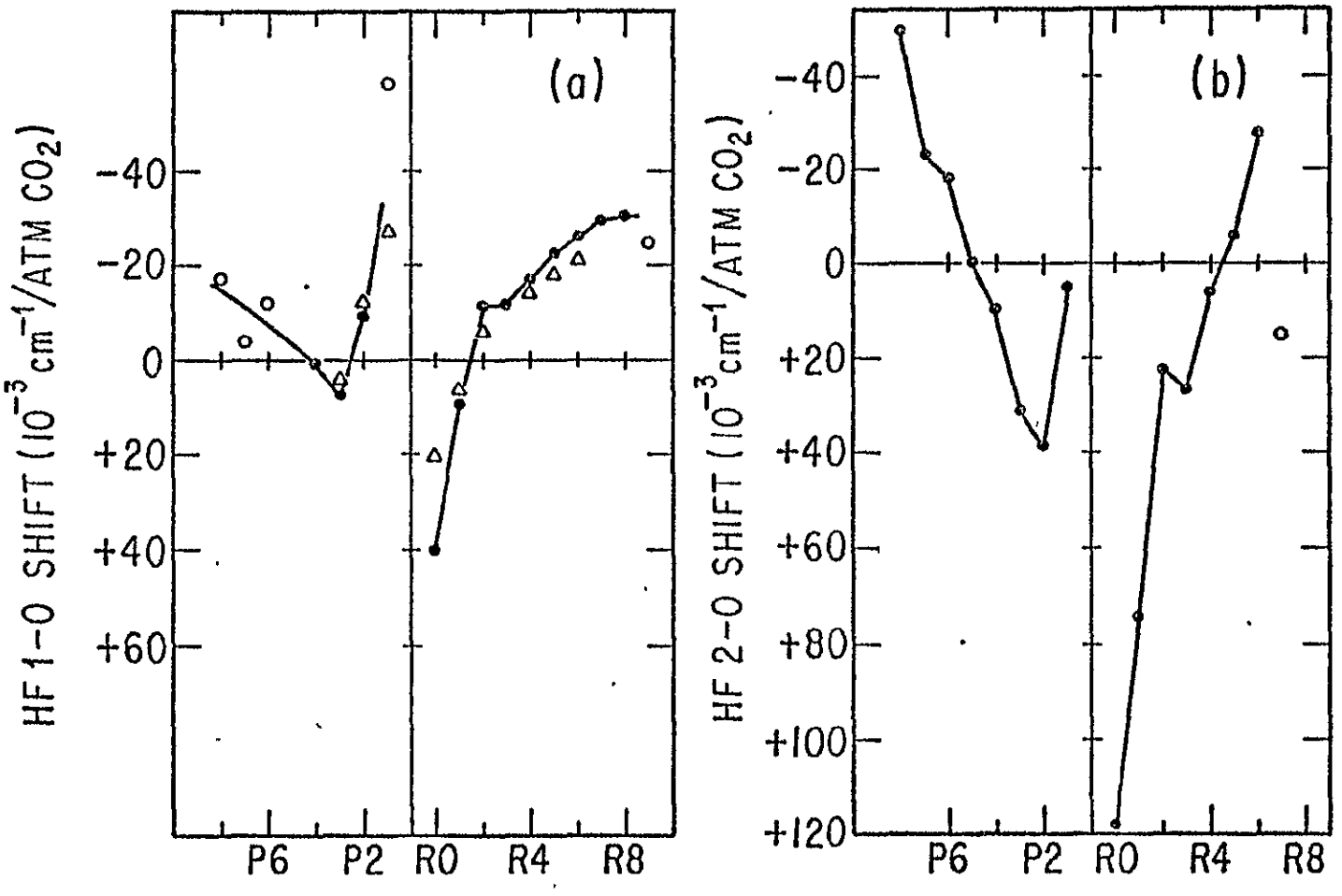

Fig. 10 -- Measured lineshifts for HF perturbed by CO_2. (a) 1-0 band. Circles: Guelachvili and Smith (1978); Triangles: Shaw and Lovell (1969). (b) 2-0 band. (Guelachvili and Smith, 1978).

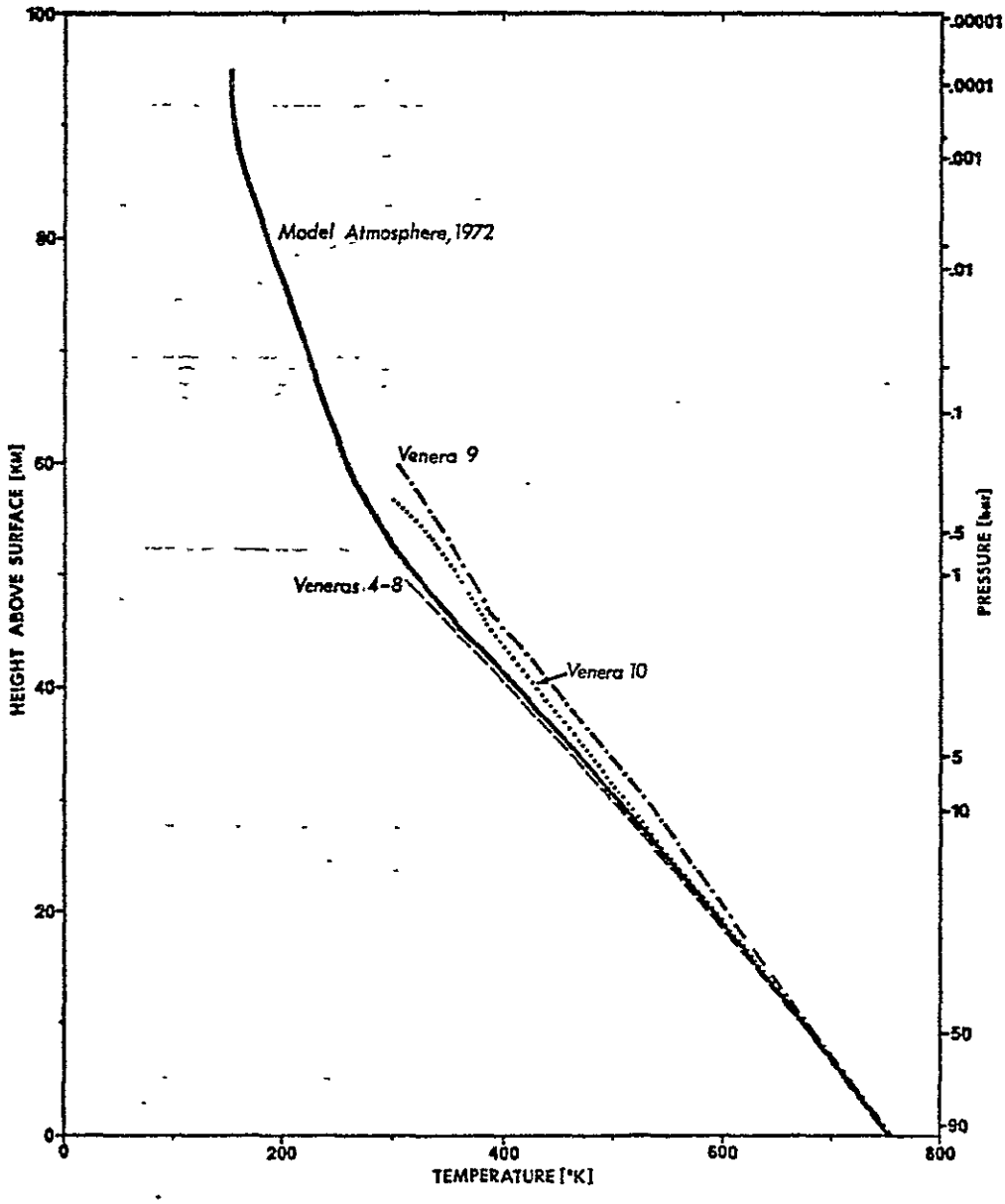

Fig. 11. -- Profile of temperatures in the Venus atmosphere.

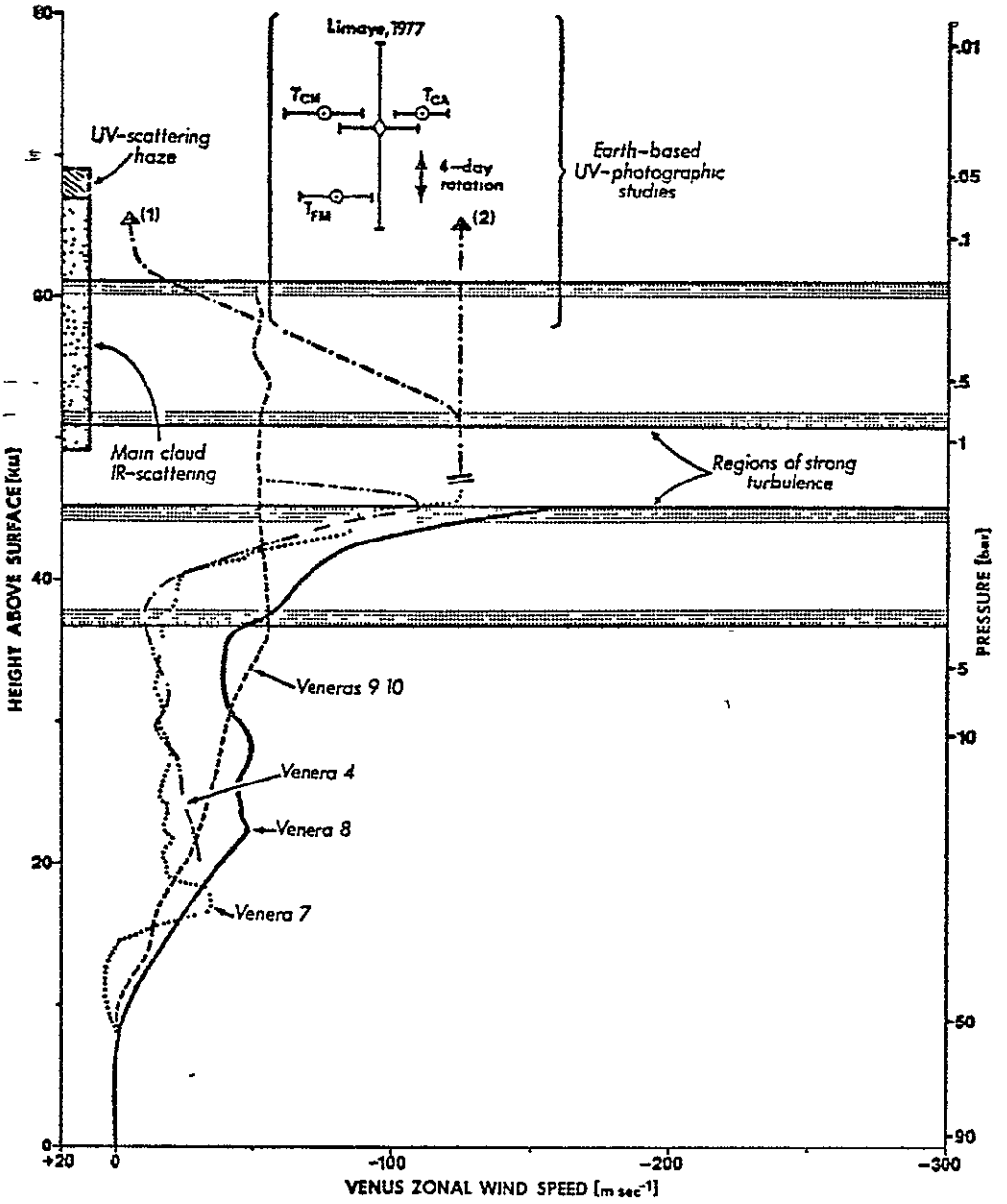

Fig. 12. -- Measurements of Venus zonal winds.

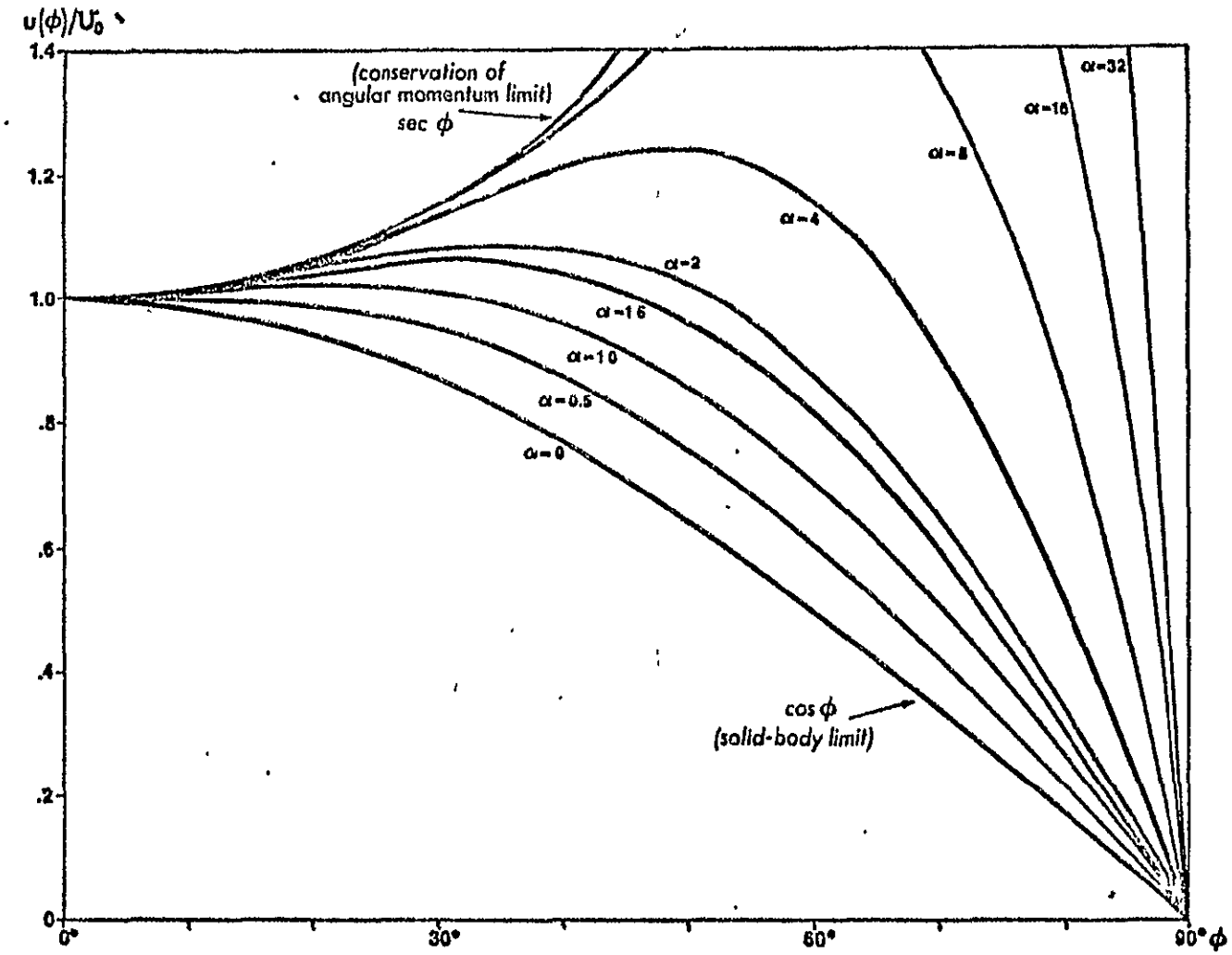

Fig. 13. -- Distribution with latitude of Venus zonal velocities.

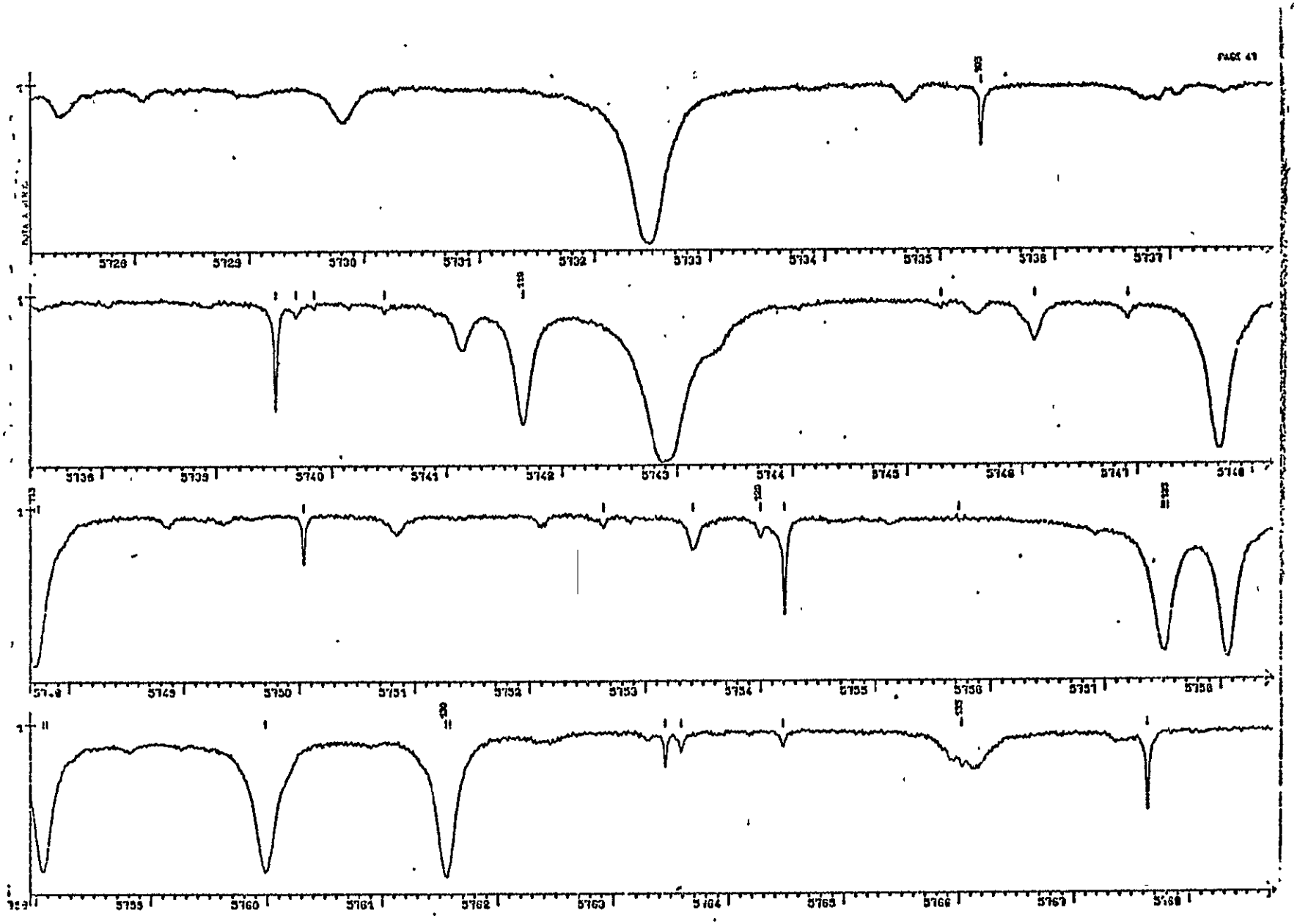

Fig. 14. -- Interferometric spectra of Venus near 5750 cm^{-1}.
(a) Venus A

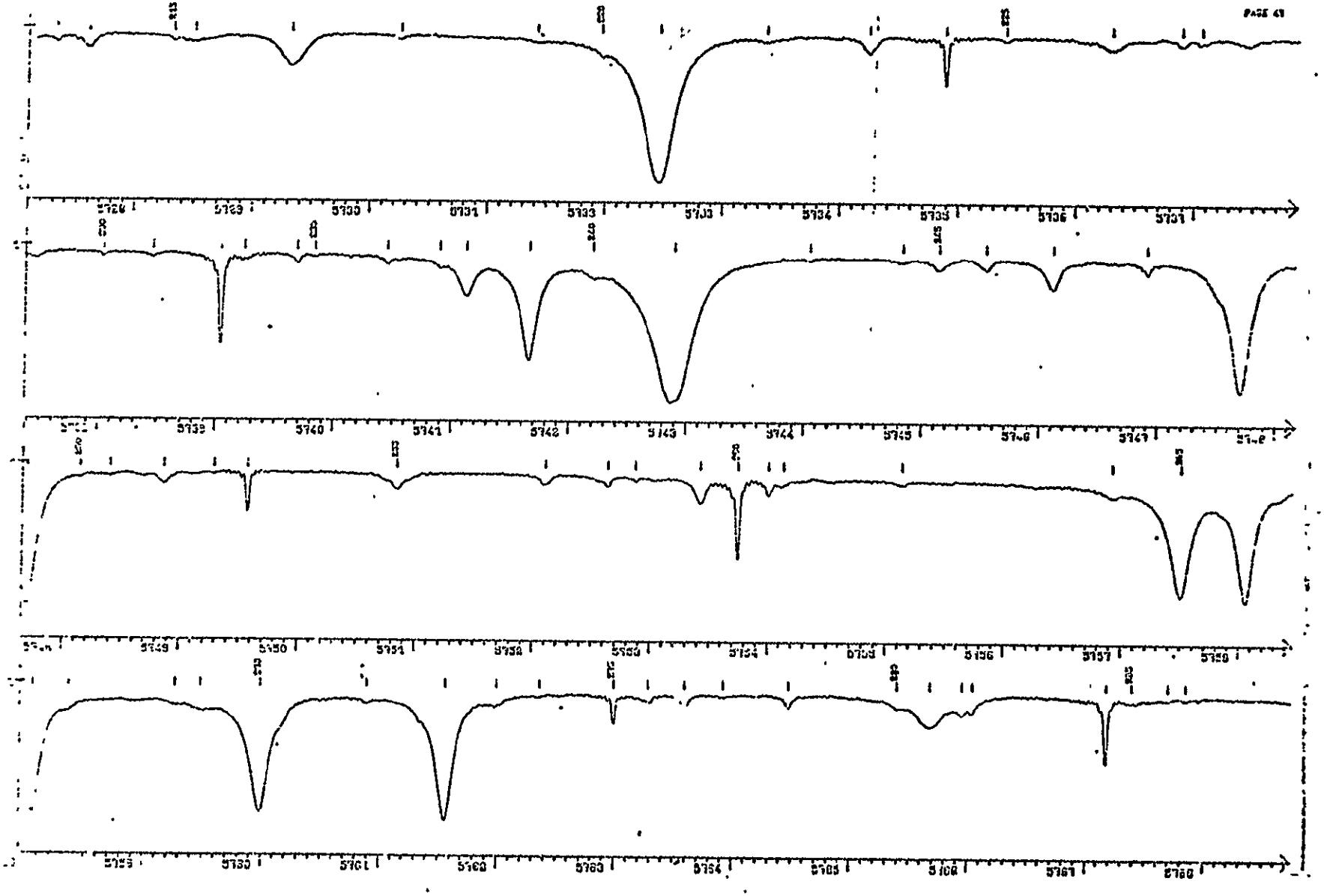

(b) Venus 5

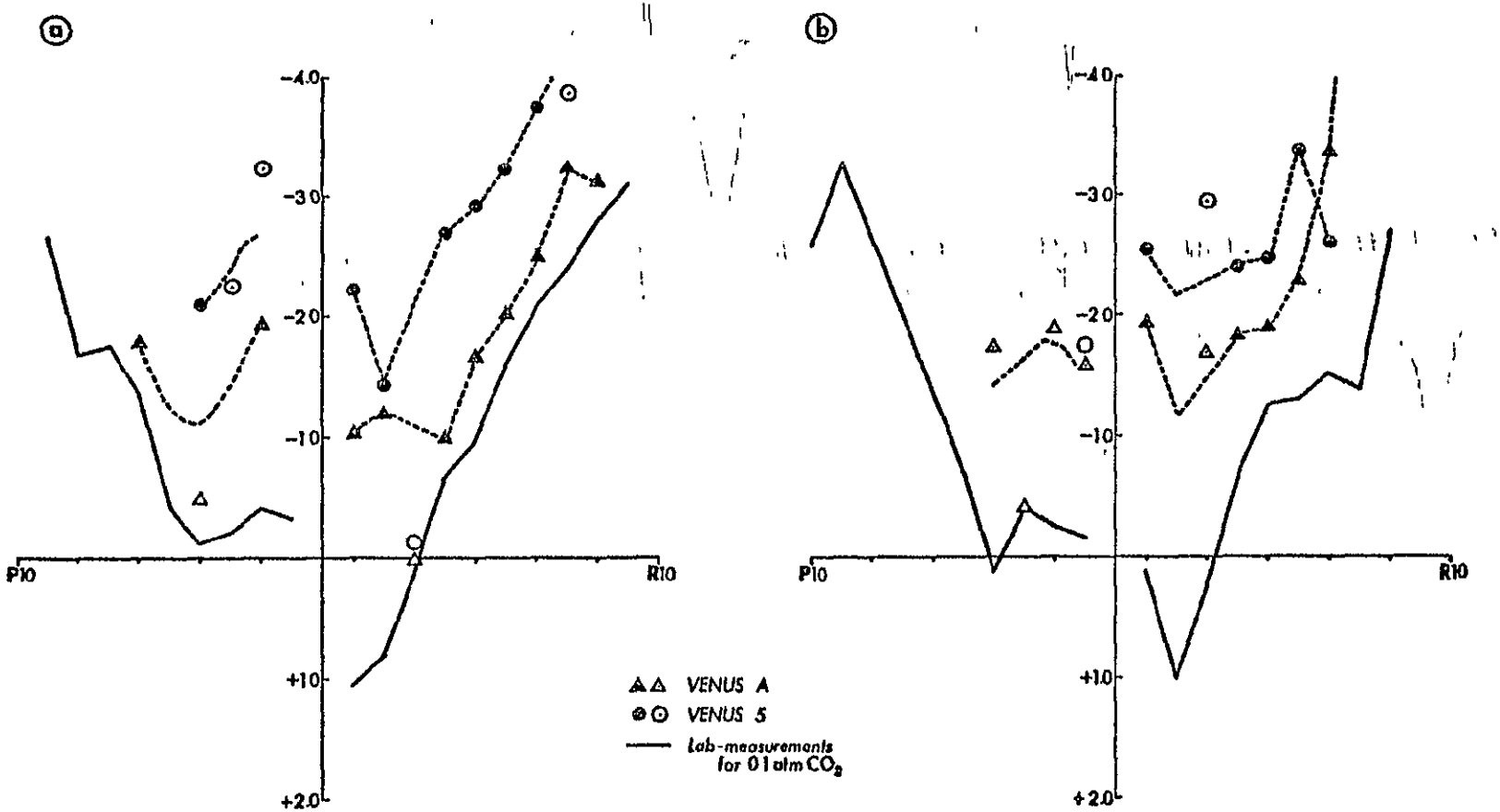

Fig. 15. -- Residual lineshifts from Venus spectra for the HCℓ 2-0 band. ($\times 10^{-3}$ cm^{-1}) (a) $H^{35}C\ell$. (b) $H^{37}C\ell$.

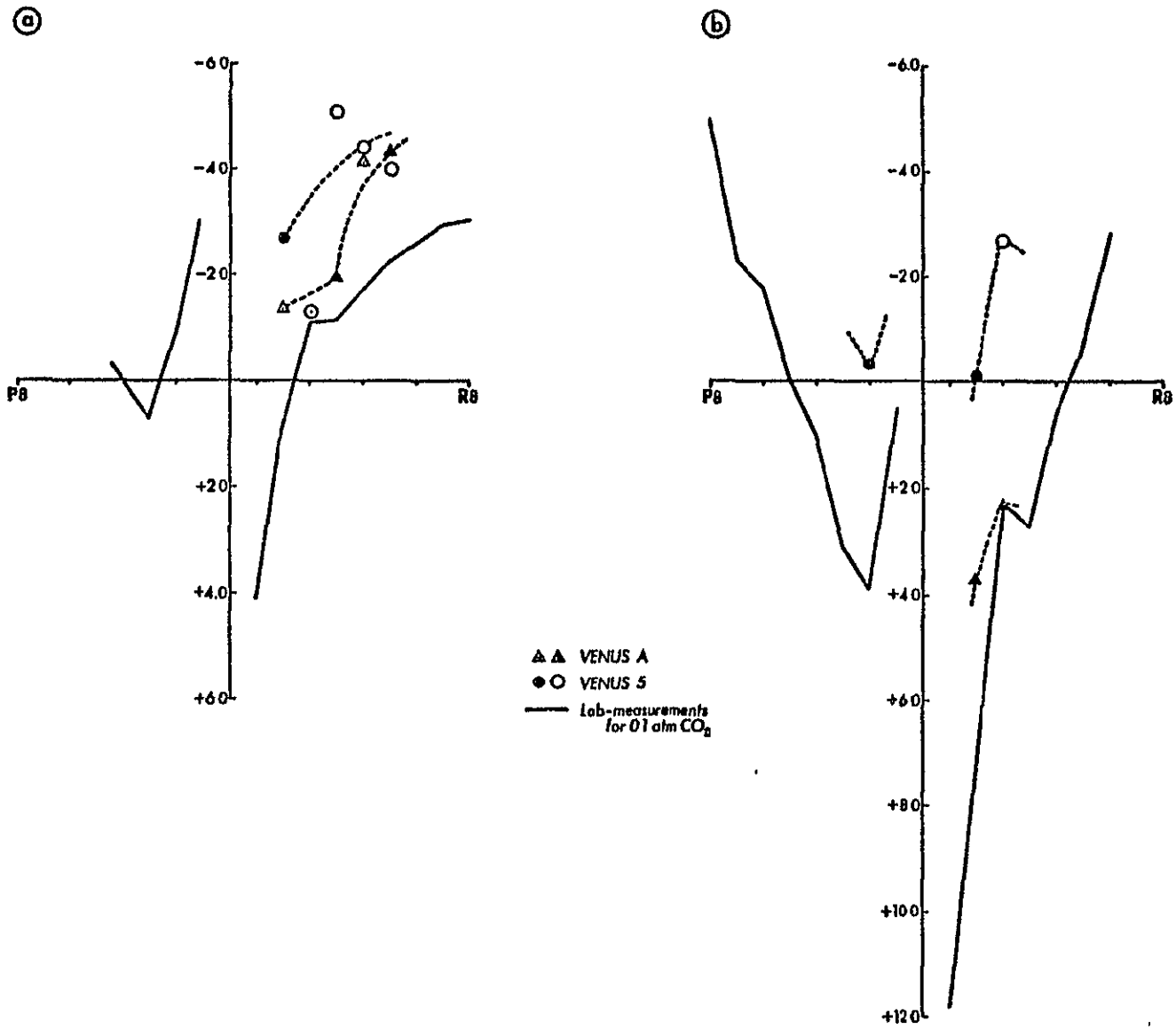

Fig. 16. -- Residual lineshifts for HF in the Venus spectra (x 10^{-3} cm^{-1}). (a) 1-0 band. (b) 2-0 band.

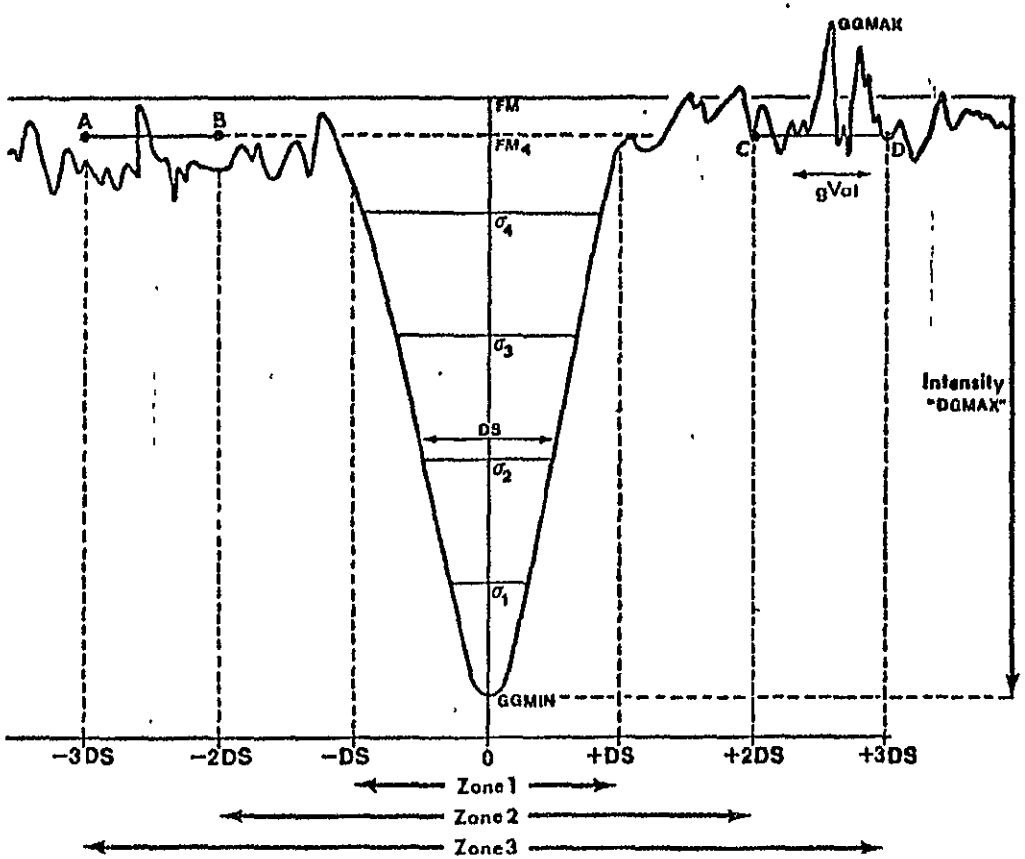

Fig. 17. -- Schematic drawing of calculation of the asymmetries in spectral lines by the DERPTH program.

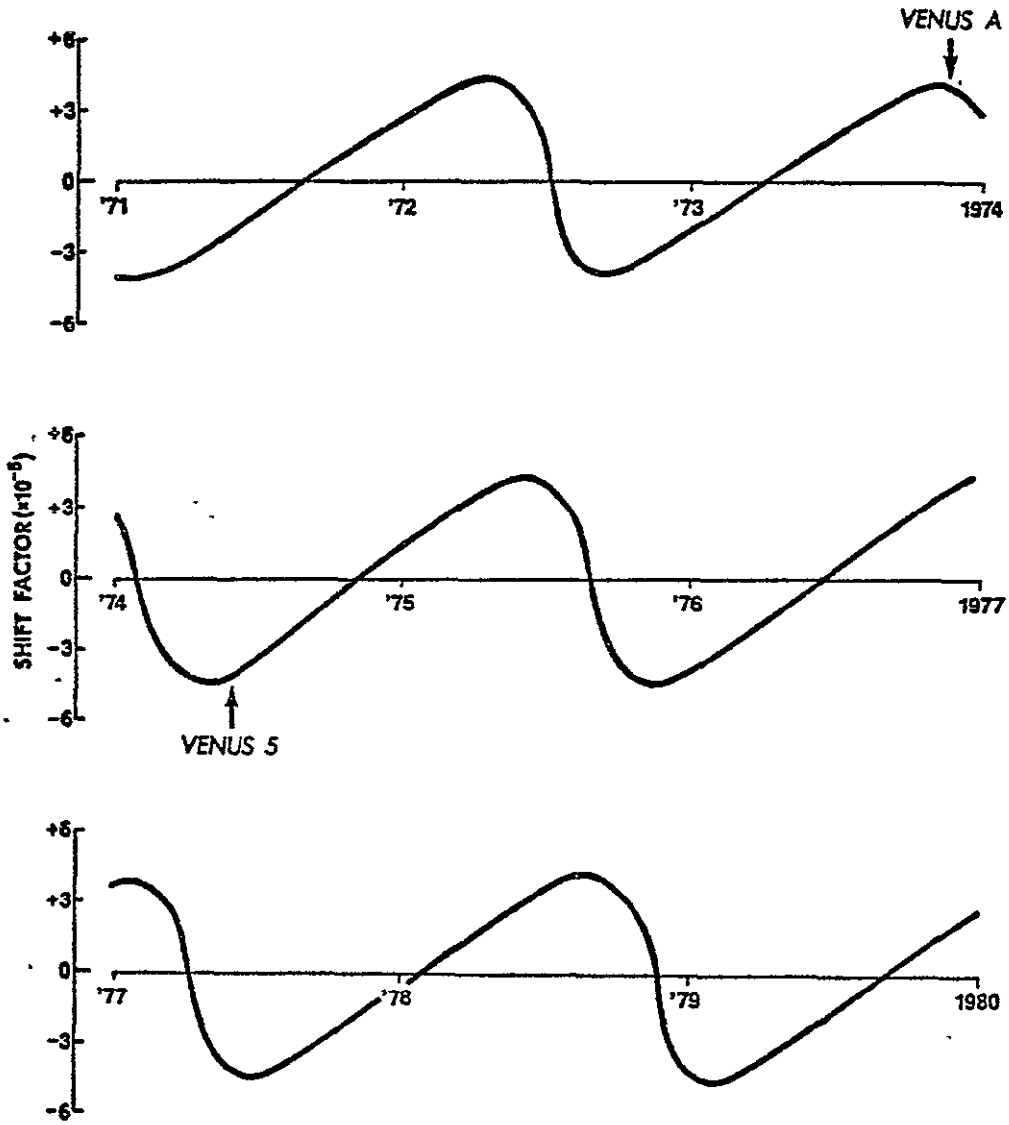

Fig. 18. -- Variation of translational Doppler shift factor from 1971 to 1980 (Niehaus and Petrie, 1961).

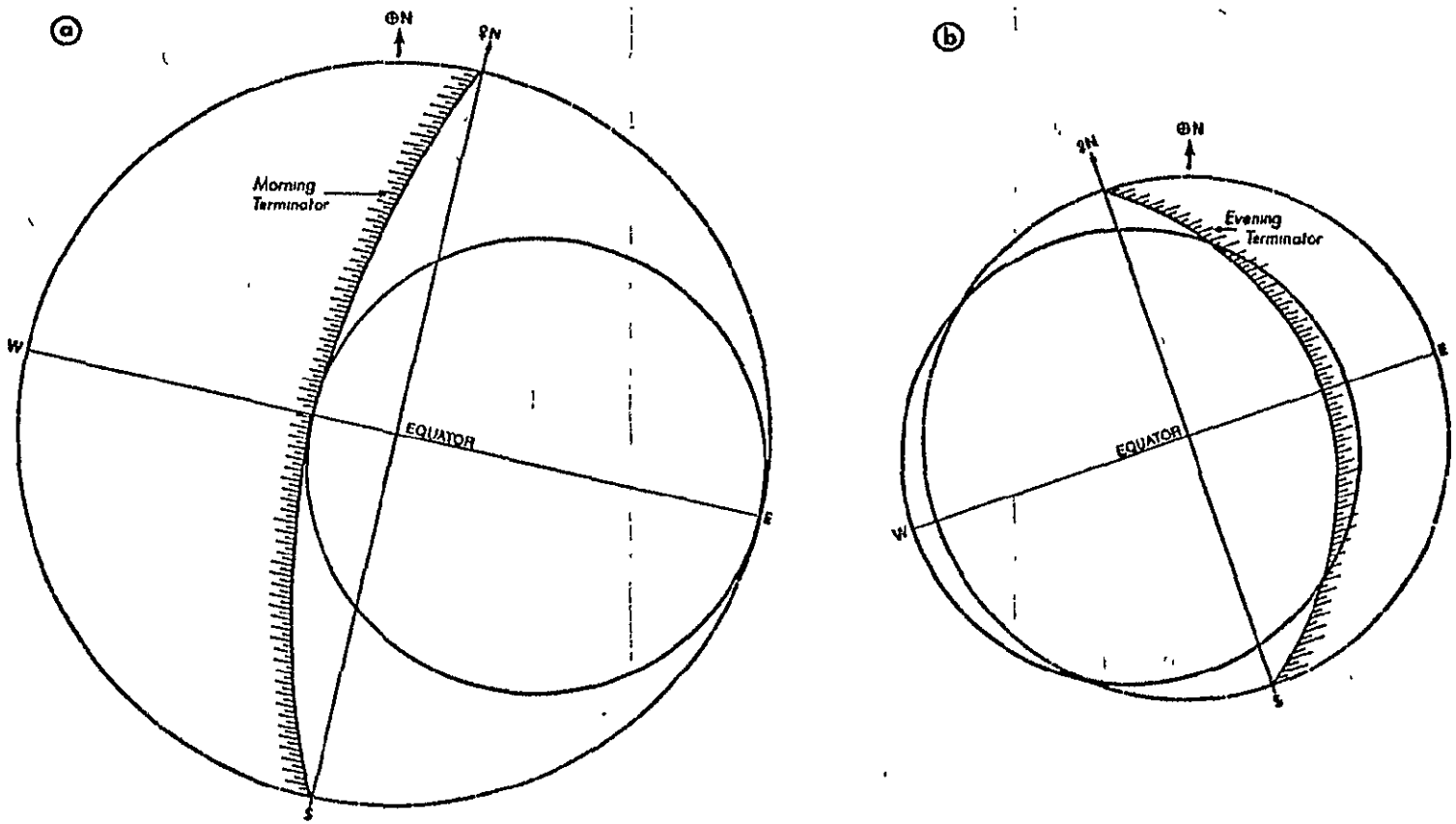

Fig. 19. -- Appearance of the Venus disk at the time of observations.
(a) Venus A. (b) Venus 5.

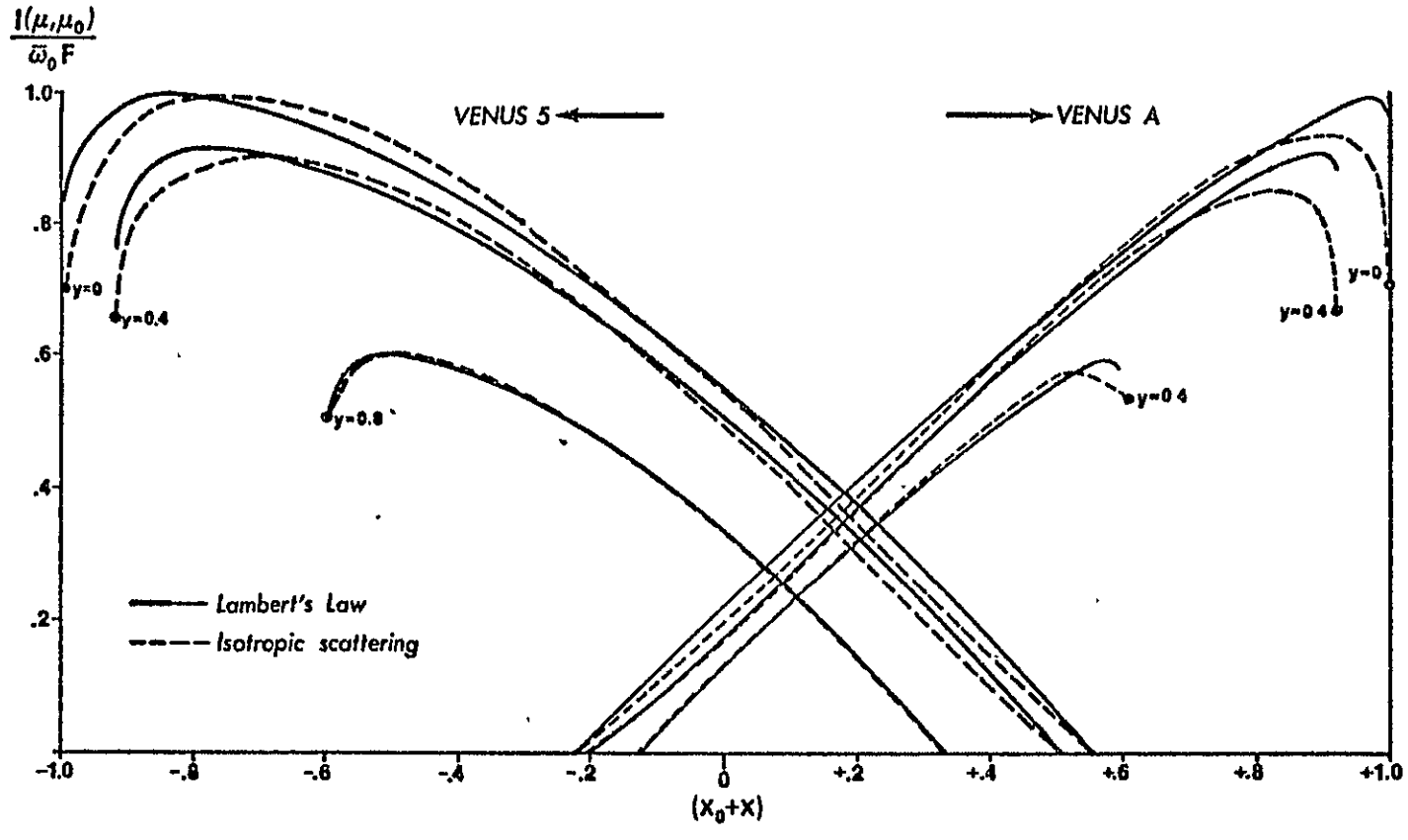

Fig. 20. -- Variation of brightness along parallels on the planetary disk. Solid curves: Lambert's Law reflection. Dashed curves: isotropic scattering.

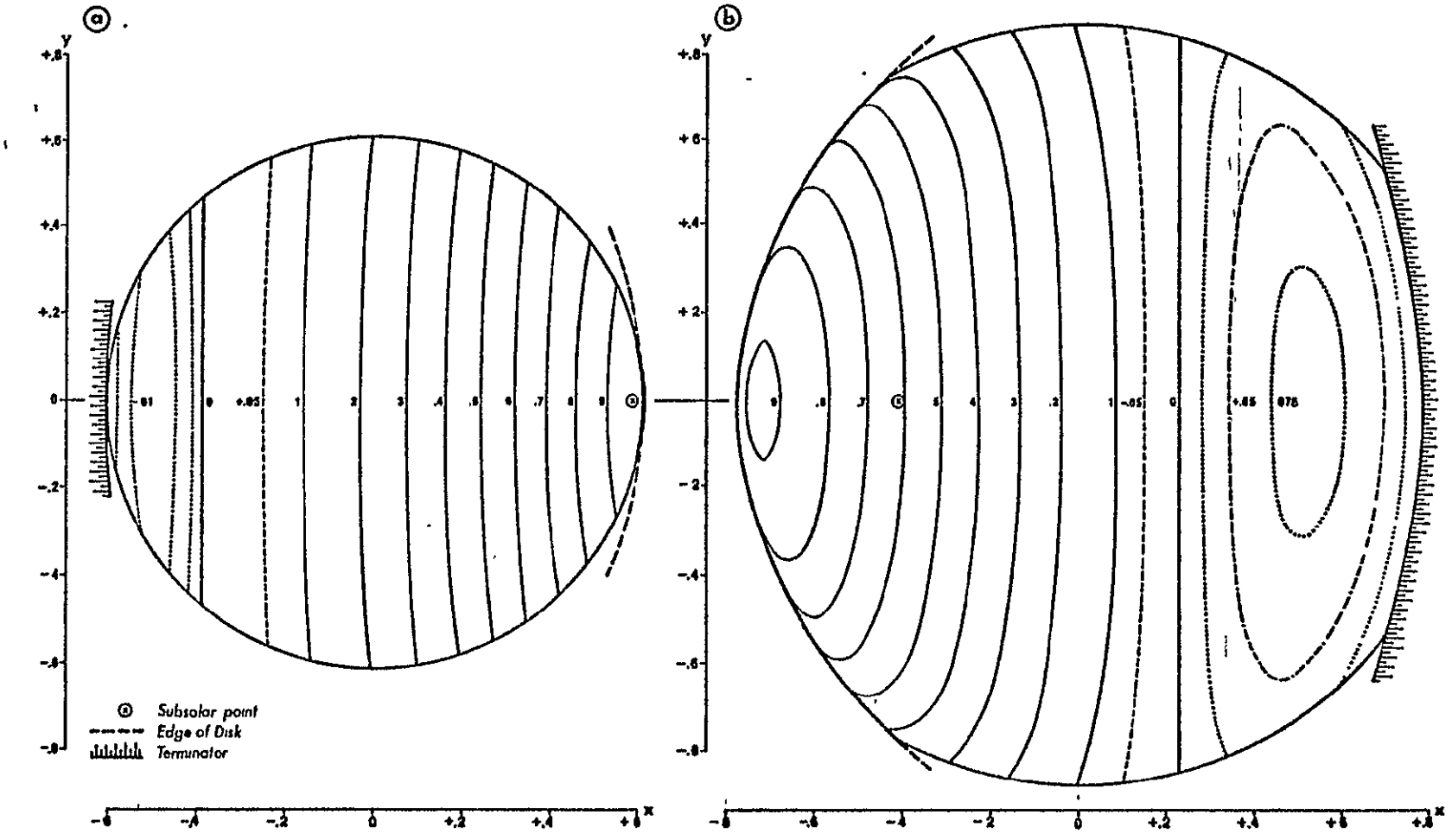

Fig. 21. -- Relative contribution to the earthward component of Venus zonal velocity.
(a) Venus A (b) Venus 5

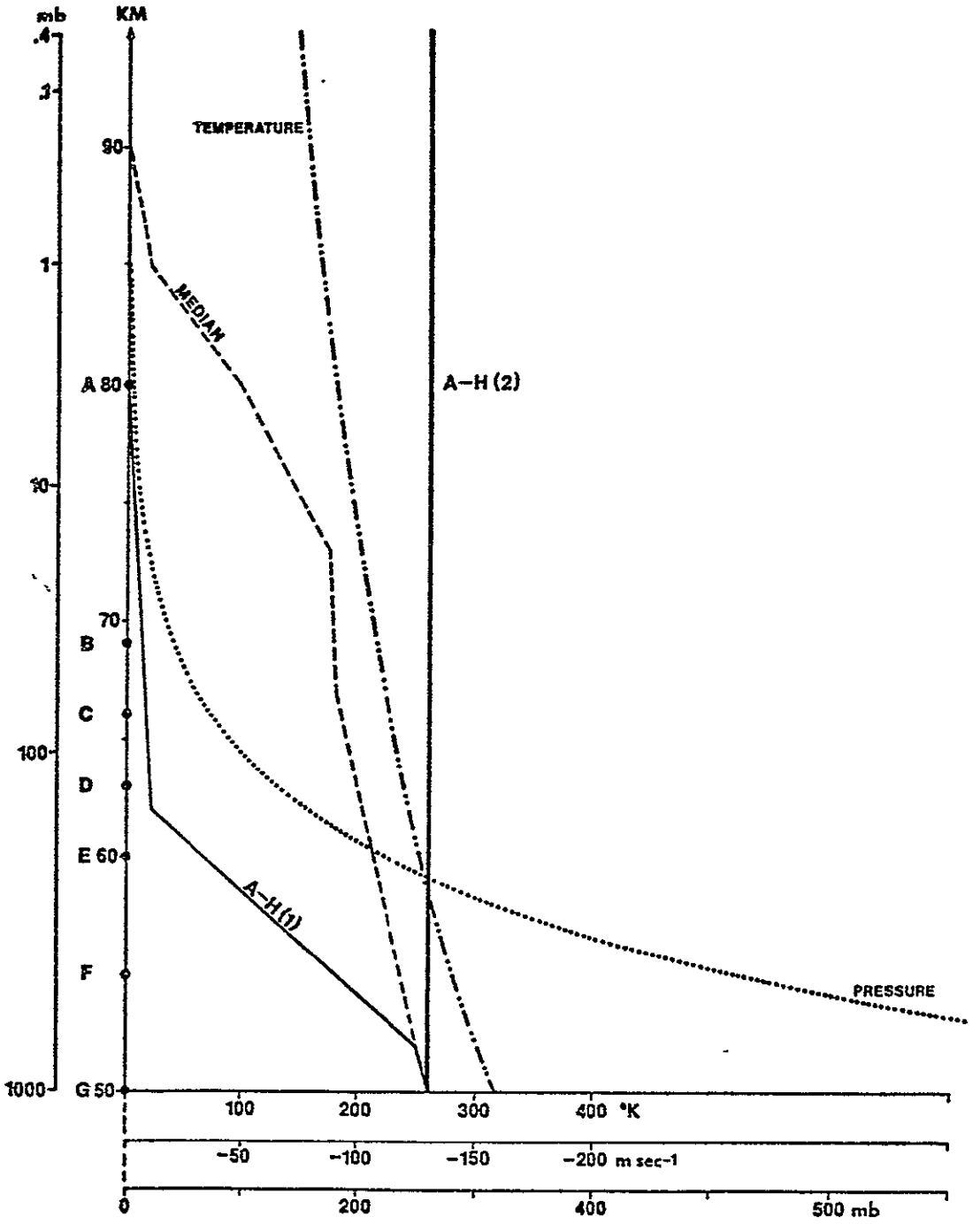

Fig. 22. -- Pressure, temperature and velocity profiles for Venus model atmospheres.

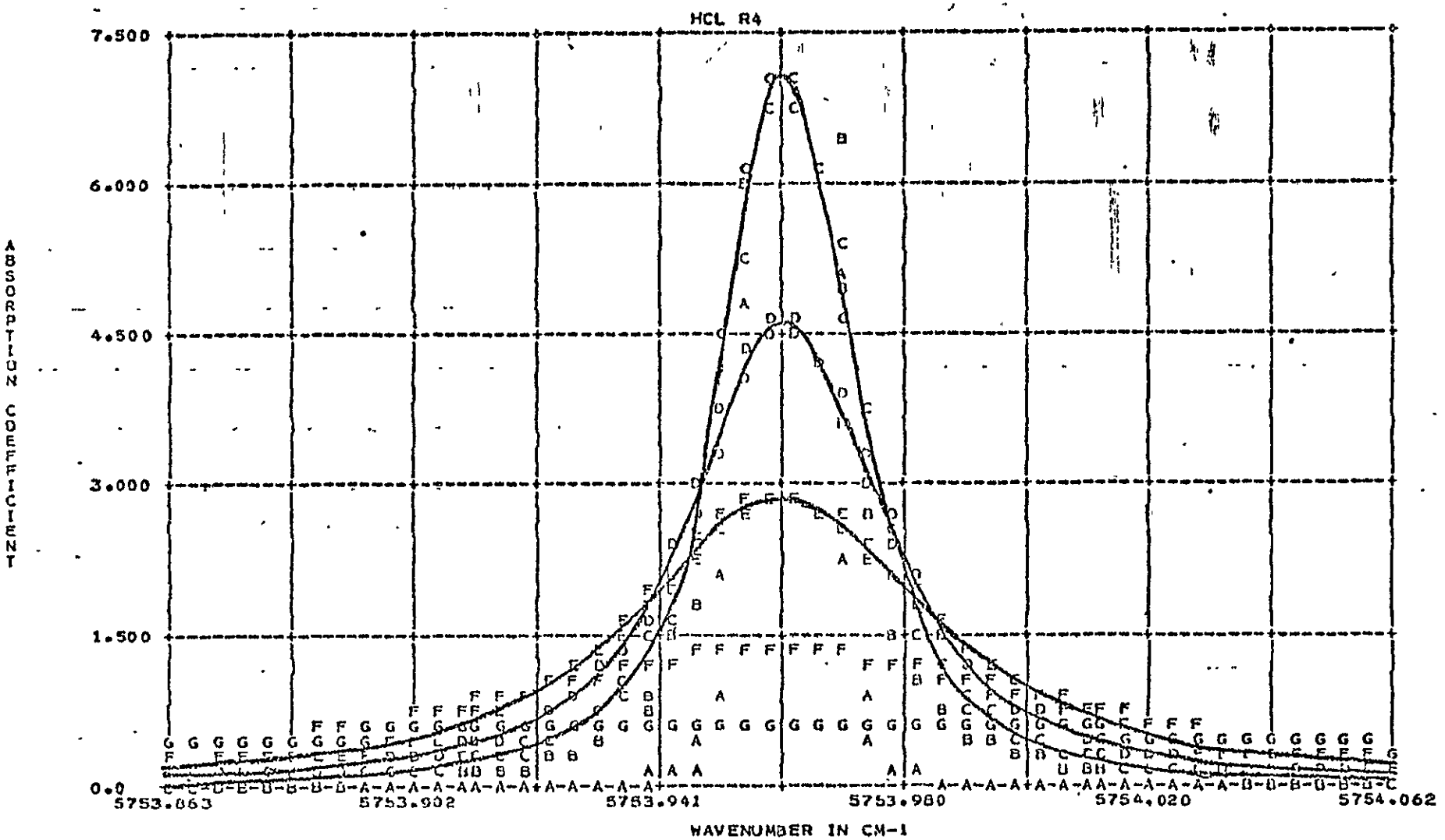

Fig. 23. -- Absorption coefficient for significant levels in the median model model atmosphere for the $H^{35}Cl$ R4 Line. (a) Venus A

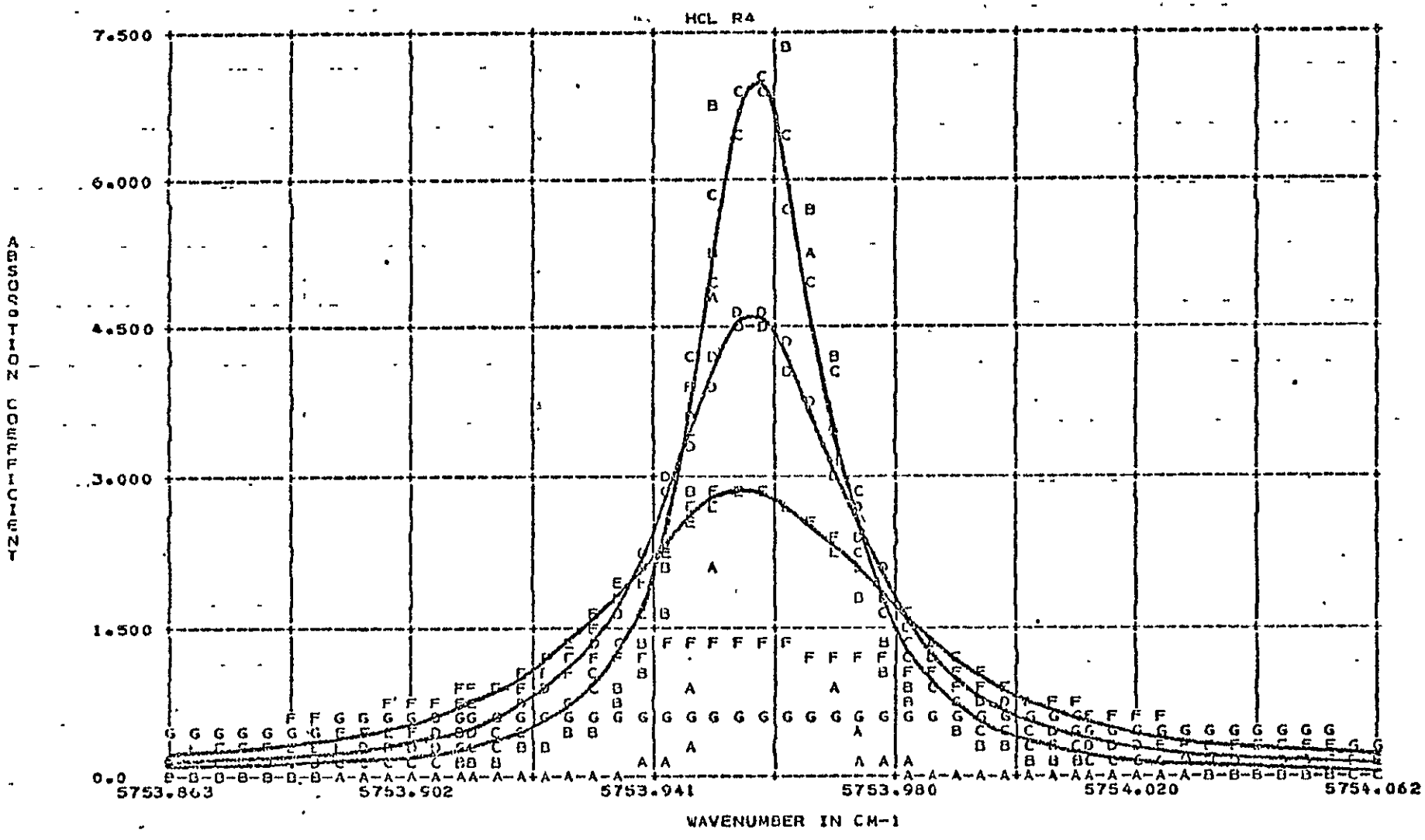
HCL R4
7.500
6.000
4.500
3.000
1.500
0.0
ABSORPTION COEFFICIENT
5753.863
5753.902
5753.941
5753.980
5754.020
5754.062
WAVENUMBER IN CM-1

(b) Venus 5

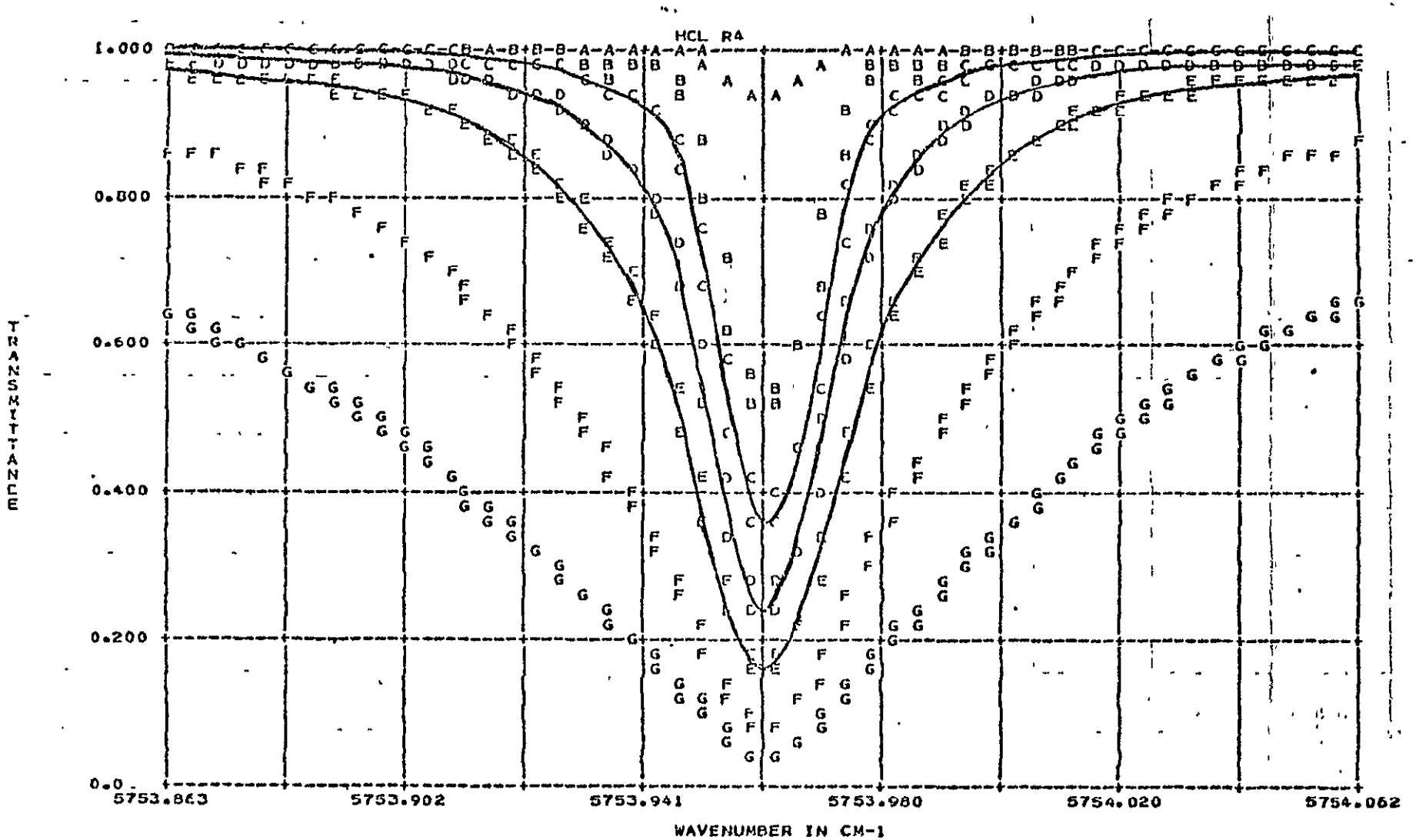

Fig. 24. -- Transmittance between 95 km and significant levels in the median model atmosphere for the $H^{35}Cl$ R4 line. (a) Venus A

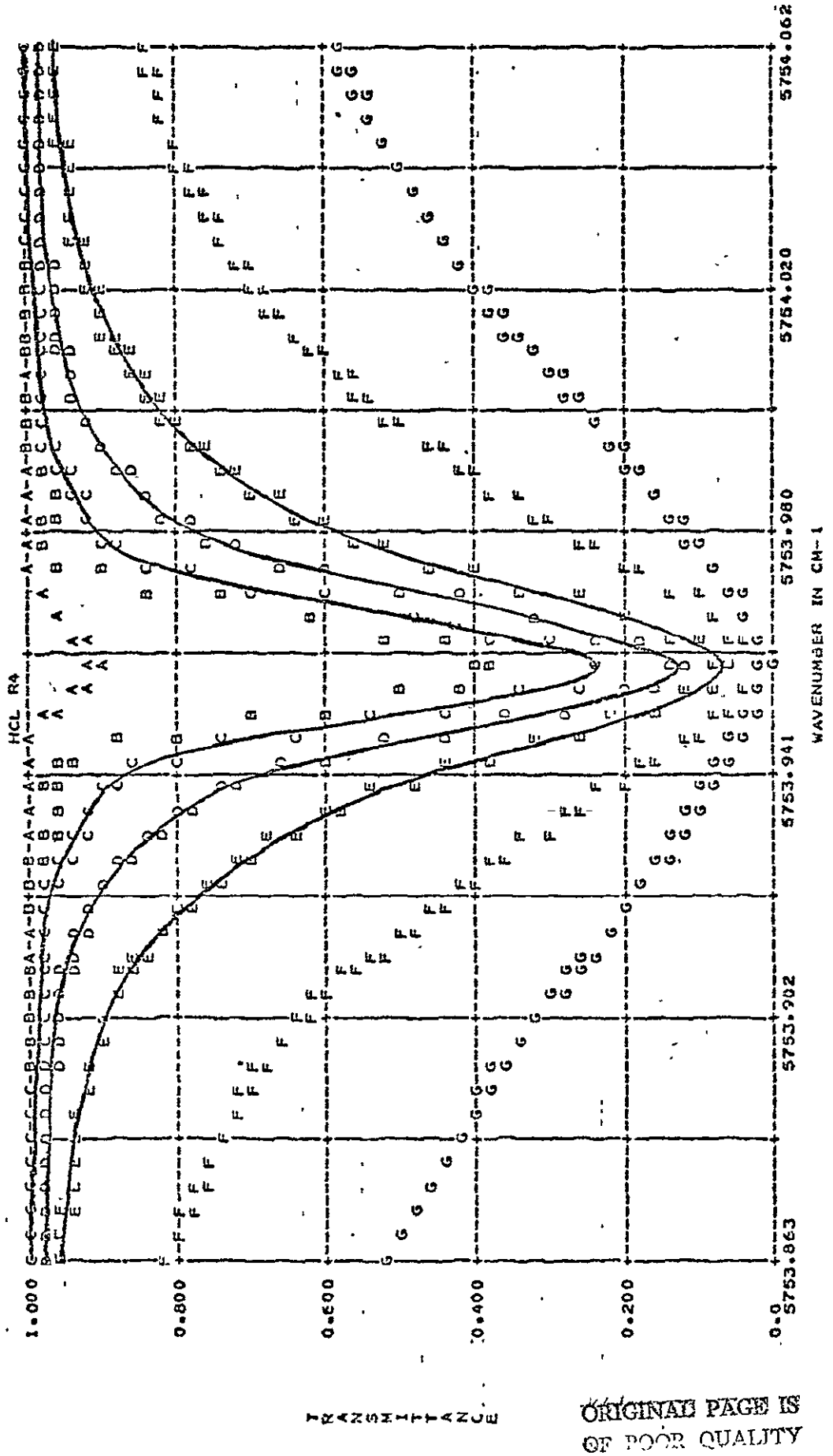

(b) Venus 5

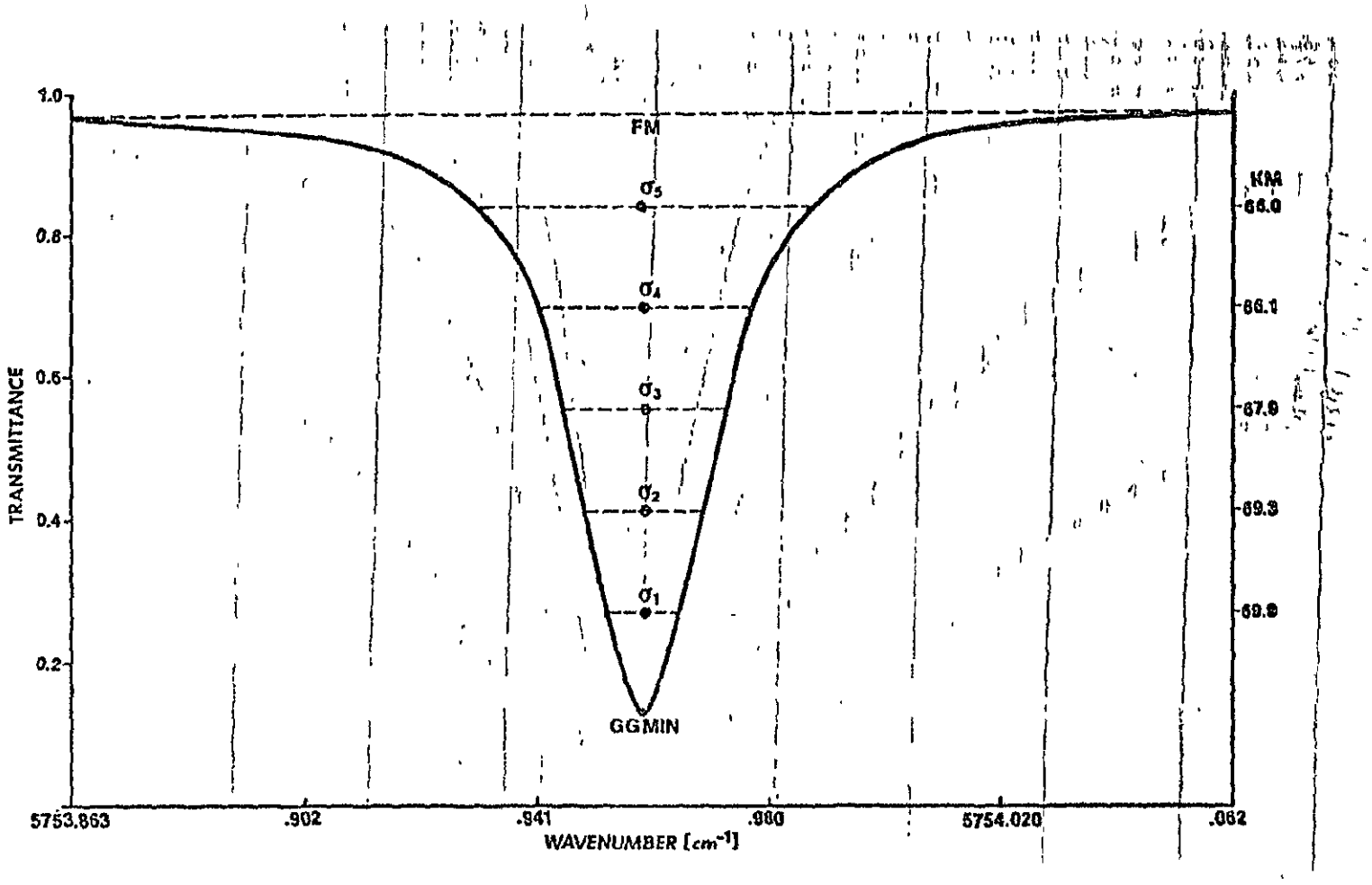

Fig. 25. -- Calculated asymmetric profile for the $H^{35}Cl$ R4 line in the median model atmosphere for Venus 5.

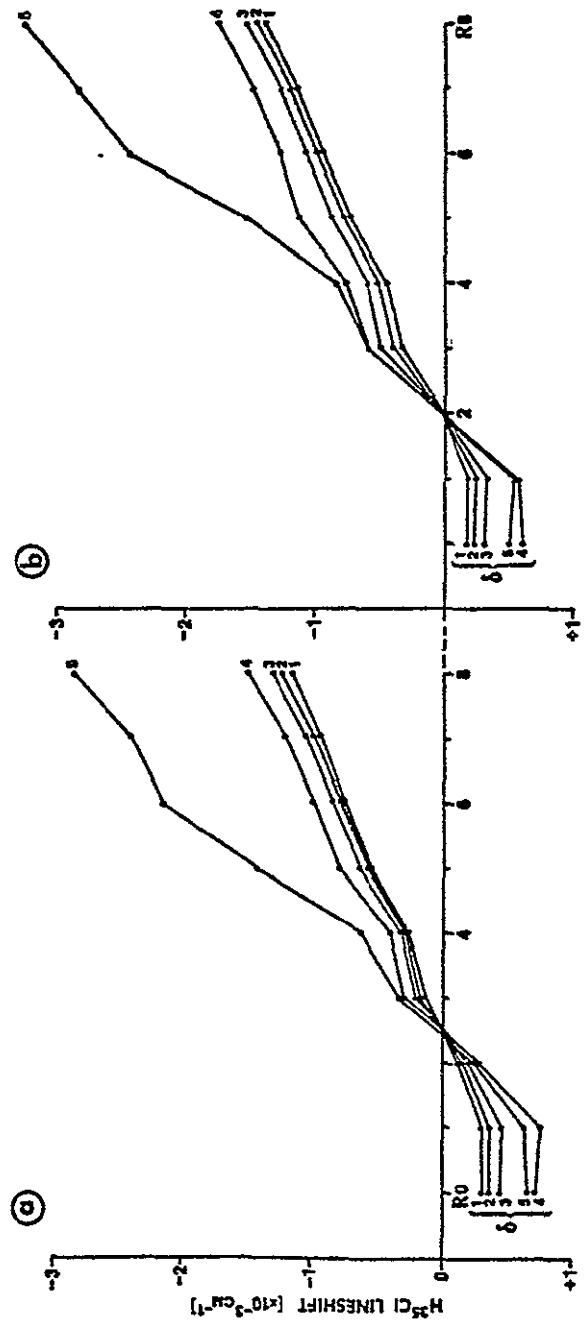

Fig. 26. -- Calculated lineshifts in the $H^{35}Cl$ R-branch for line profile "p" in the A-H(1) model atmosphere. (a) Venus A. (b) Venus 5.

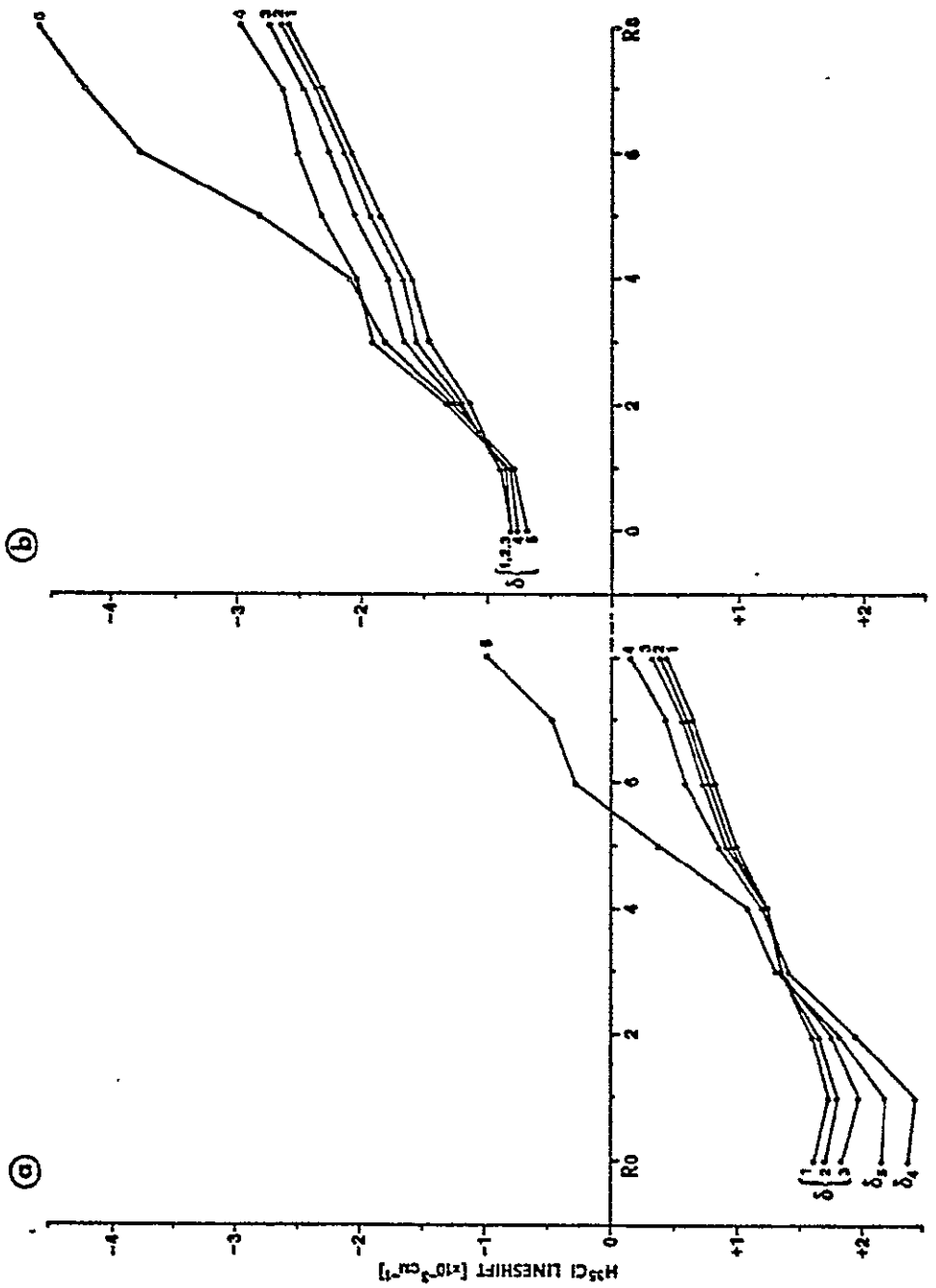

Fig. 27. -- Calculated lineshifts in the $H^{35}Cl$ R-branch for line profile "D" in the median model atmosphere. (a) Venus A. (b) Venus 5.

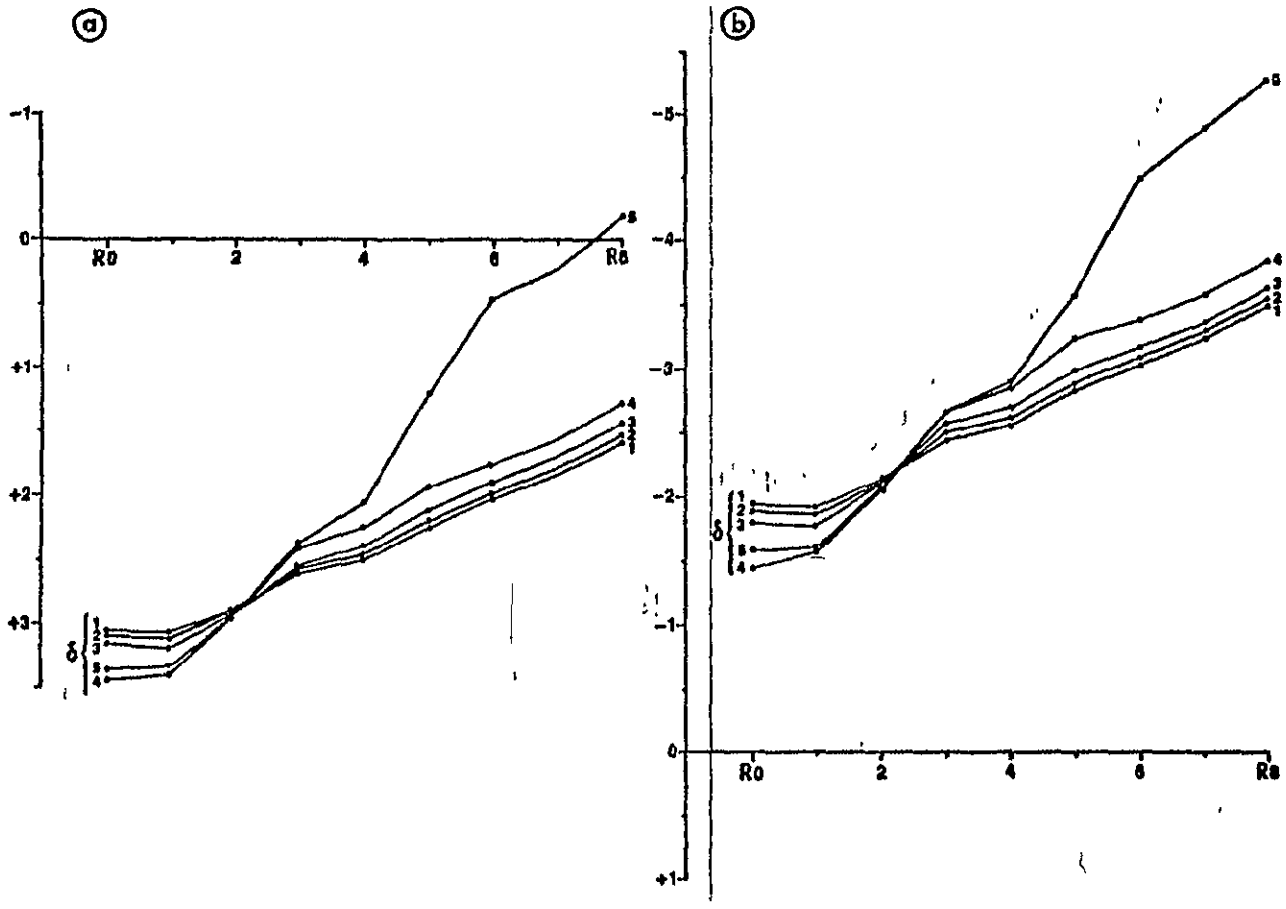

Fig. 28. -- Calculated lineshifts in the $H^{35}Cl$ R-branch for line profile "D" in the A-H(2) model atmosphere. (a) Venus A. (b) Venus 5.

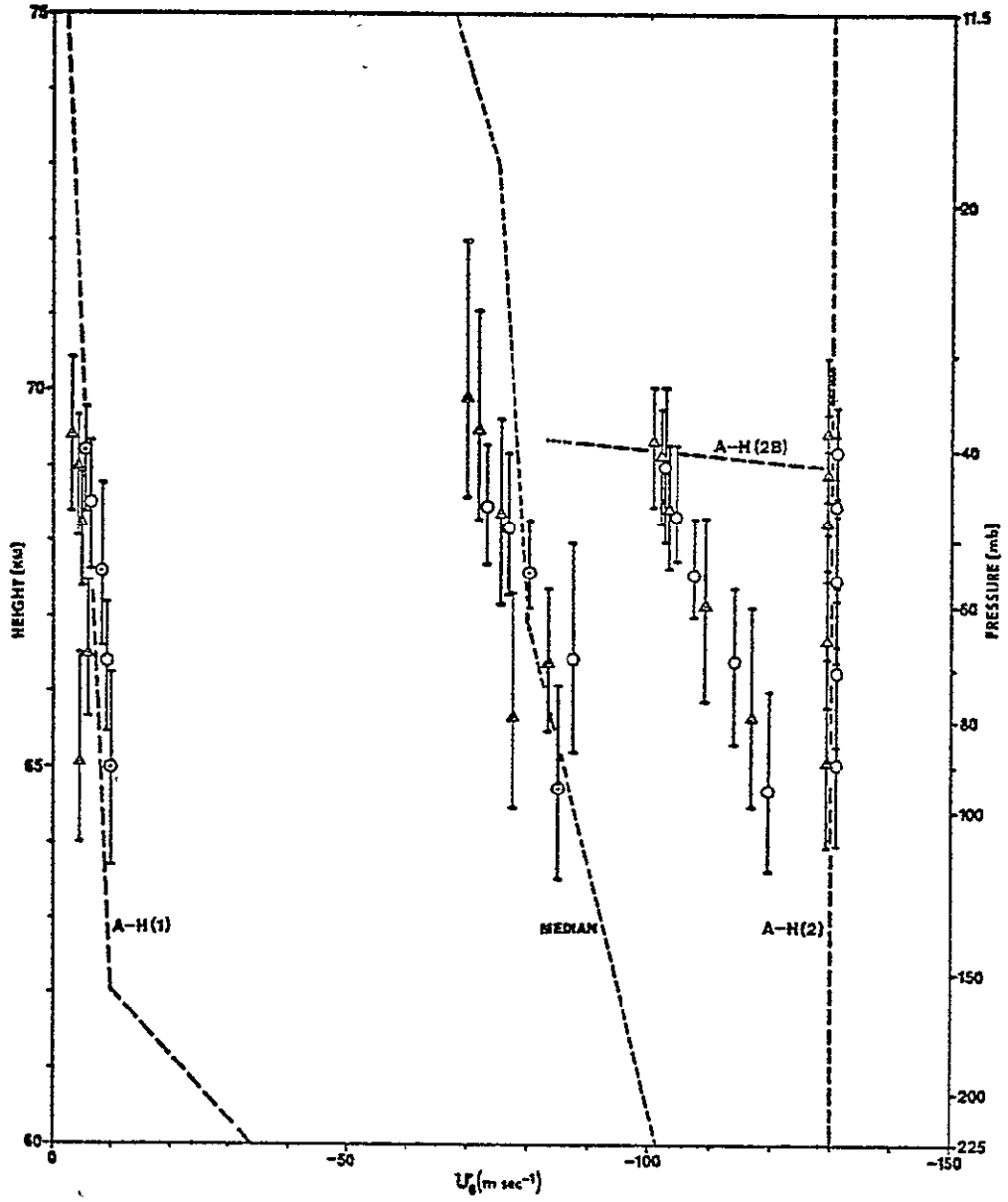

Fig. 29. -- Zonal velocity profiles retrieved from model results. Triangles: Venus A; Circles: Venus 5; Dashed lines: Original velocity profiles.

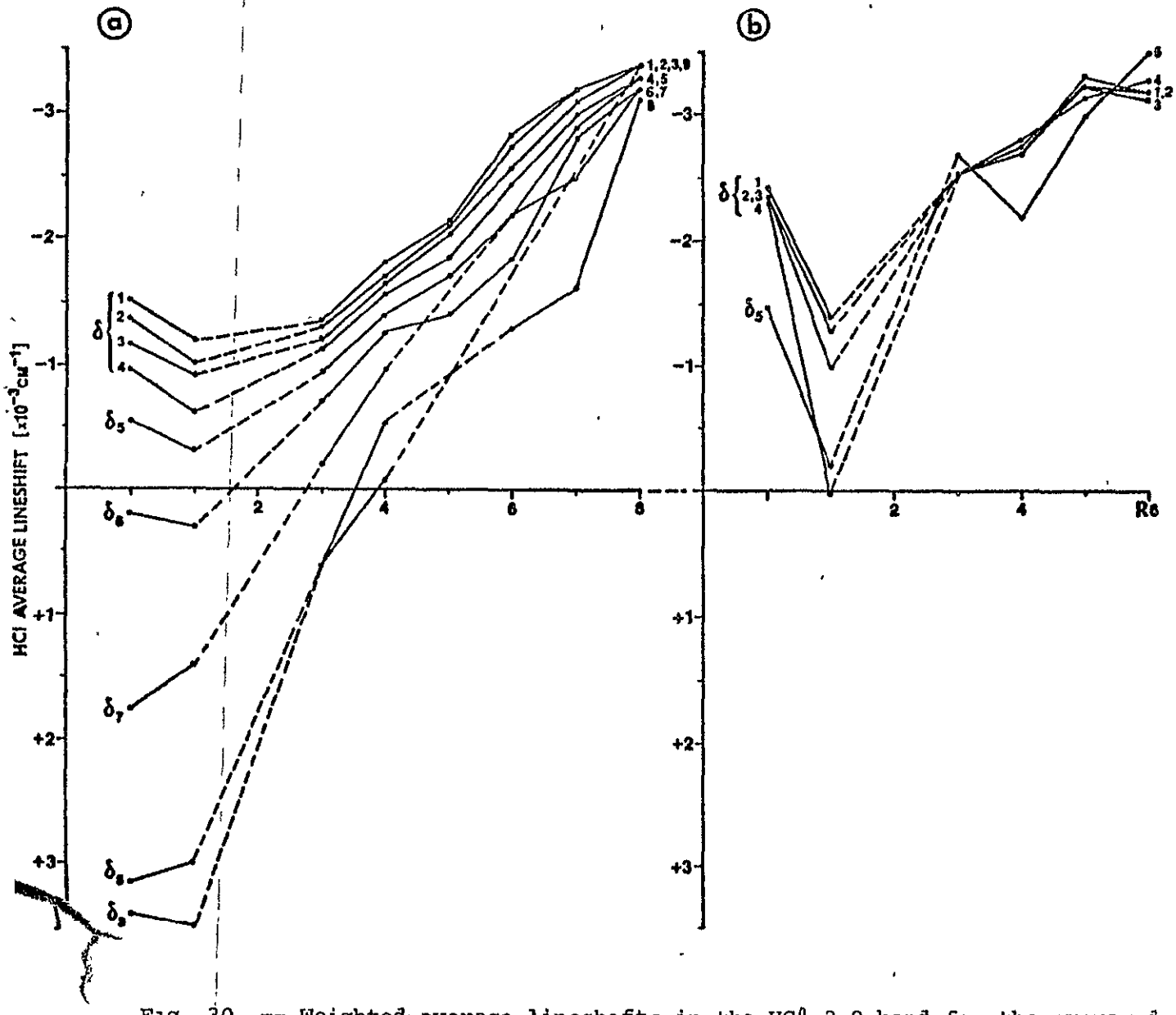

Fig. 30. -- Weighted-average lineshifts in the HCℓ 2-0 band for the averaged planetary spectra. (a) Venus A. (b) Venus 5.

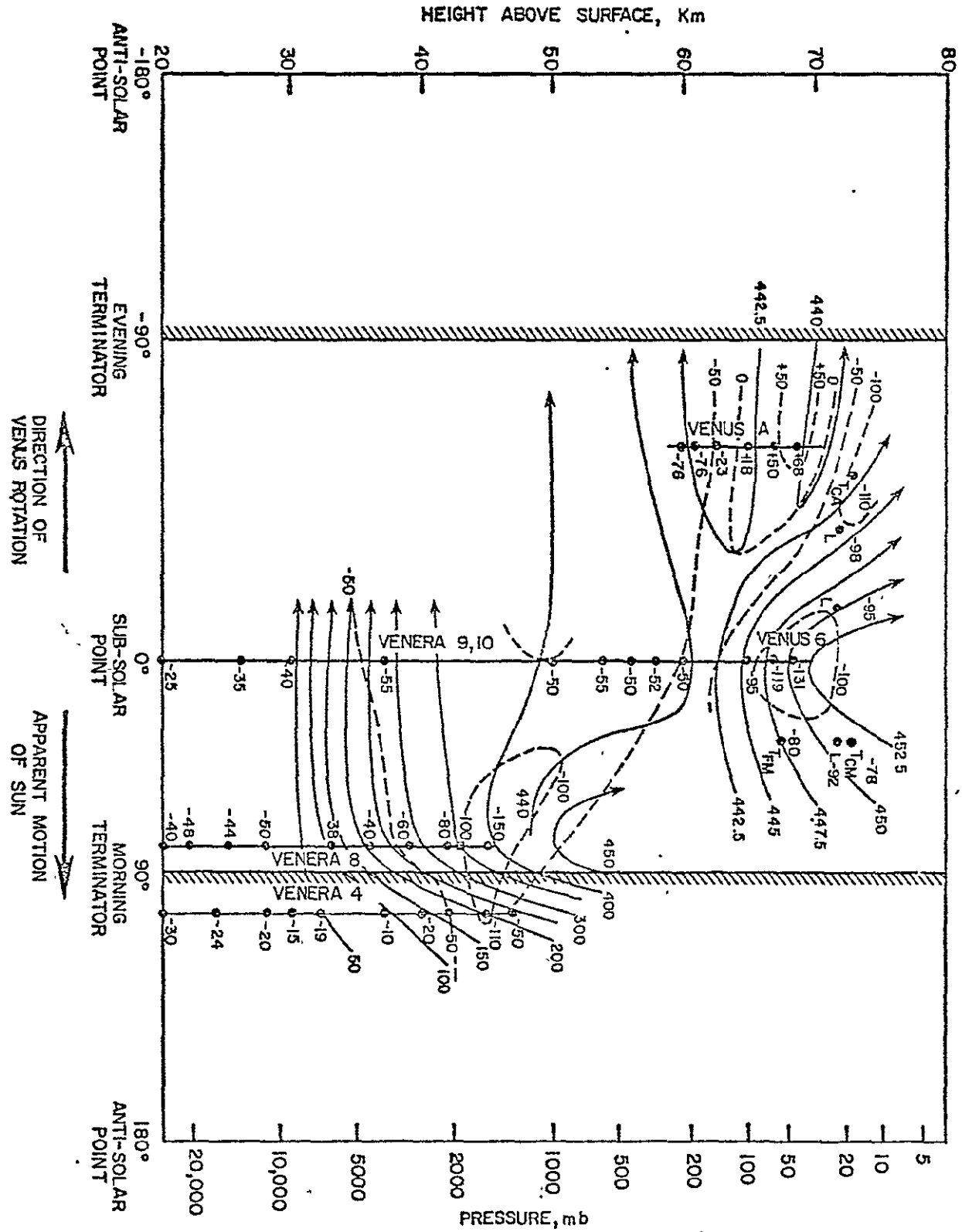

Fig. 32. -- Longitudinal cross section of Venus equatorial zonal velocities. Dashed lines: isotachs; contour interval is 50 m sec^{-1}. Solid lines: estimated streamfunction ψ in units of m sec^{-1} bar.

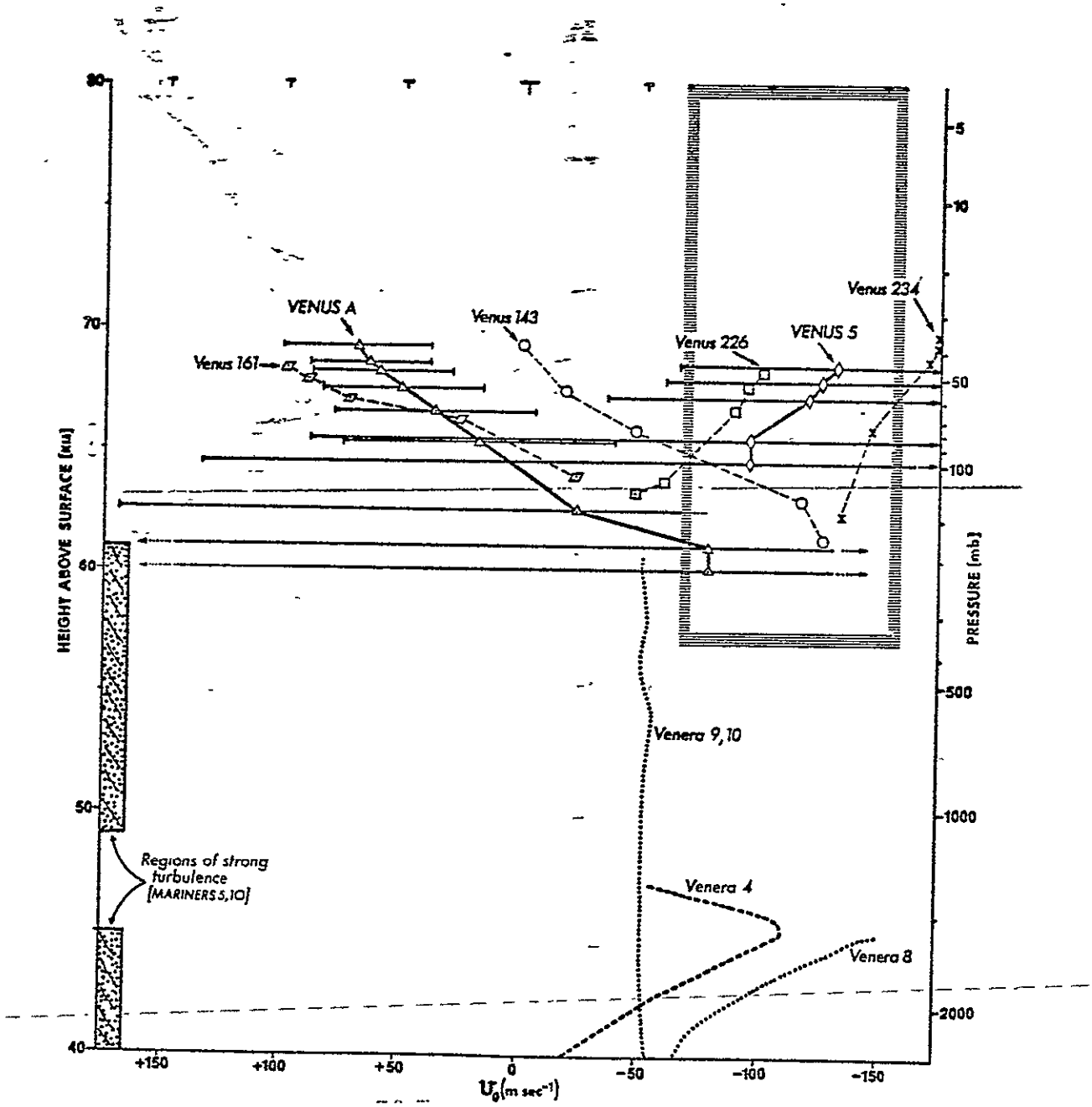

Fig. 31. -- Venus zonal velocity profiles estimated from interferometric spectra. Triangles: Venus A; Circles: Venus 143 (first day); Rhombi: Venus 161 (last day). Diamonds: Venus 5; Squares: Venus 226 (first day); Crosses: Venus 234 (last day).

REFERENCES

Ainsworth, J. E., and J. R. Herman, 1975: Venus wind and temperature structure: the Venera 8 data. J. Geophys. Res., 80, 173-179.

_____, and _____, 1977: On the reality of the Venus winds. Icarus, 30, 314-319.

Armstrong, B. H., 1967: Spectrum line profiles: the Voigt function. J. Quant. Spectrosc. Radiat. Transfer, 7, 61-88.

Belton, M. J. S., and D. M. Hunten, 1966: Astrophys. J., 146, 307.

_____, G. R. Smith, D. A. Elliot, K. Klaasen and G. E. Danielson, 1976a: Space-time relationships in the UV markings on Venus. J. Atmos. Sci., 33, 1383-1393.

_____, _____, G. Schubert and A. D. Del Genio, 1976b: Cloud patterns, waves and convection in the Venus atmosphere. J. Atmos. Sci., 33, 1394-1417.

Benedict, W. S., R. Herman, G. E. Moore and S. Silverman, 1956: The strengths, widths, and shapes of infrared lines. II. The HCl fundamental. Can. J. Phys., 34, 850-875.

Ben-Reuven, A., S. Kimel, M. A. Hirshfeld and J. H. Jaffe, 1961: Theory and measurement of pressure-induced shifts of HCl lines due to noble gases. J. Chem. Phys., 35, 955-962.

Bottema, M., W. Plummer and J. Strong, 1964a: Astrophys. J., 139, 1021.

_____, _____, _____ and R. Zander, 1964b: Astrophys. J., 140, 1640.

Bouanich, J. P. (1972): J. Quant. Spectrosc. Radiat. Transfer, 12, 1609.

Boulet, C., P. Isnard and A. Levy, 1973a: Noble-gas broadening of vibration-rotation lines belonging to diatomic molecules - II. Theoretical calculations of HCl lineshifts and widths. J. Quant. Spectrosc. Radiat. Transfer, 13, 897-909.

_____, P. Isnard and A. Levy, 1973b: Noble-gas broadening of vibration-rotation lines belonging to diatomic molecules - II. Theoretical calculations of CO lineshifts and widths. J. Quant. Spectrosc. Radiat. Transfer, 13, 911-921.

_____, D. Robert and L. Galatry, 1976: Shifts of the vibration-rotation absorption lines of diatomic molecules perturbed by diatomic polar molecules. A theoretical analysis. J. Chem. Phys., 65, 5302.

_____, 1977: Private communication.

Boyer, C., and H. Camichel, 1961: Observation photographique de la planete Venus. Ann. Astrophys., 24, 531-535.

_____, and P. Guerin, 1969: Etude de la rotation retrograde, en 4 jours, de la couche exterieure nuagese de Venus. Icarus, 11, 338-355.

Burangulov, N. I., S. S. Zlitenkevich, V. V. Kerzhanovich, A. S. Monin, M. K. Rozhdestvensky, A. S. Safray, V. G. Turikov and D. V. Chalikov, 1976: Dynamics of the atmosphere of Venus. NASA Technical Translation TT F-16809.

Chandrasekhar, S., 1960: Radiative Transfer. New York, Dover, 416 pp.

Connes, P., and J. Connes, 1966: Near-infrared planetary spectra by Fourier spectroscopy. I. Instruments and results. J. Opt. Soc. Am., 56, 896-910.

_____, _____, W. S. Benedict and L. D. Kaplan, 1967: Traces of HCl and HF in the atmosphere of Venus. Astrophys. J., 147, 1230-1237.

_____, _____, L. D. Kaplan and W. S. Benedict, 1968: Carbon monoxide in the Venus atmosphere. Astrophys. J., 152, 731-743.

Cruikshank, D. P., and G. P. Kuiper, 1967: Comm. Lunar Planet. Lab., No. 97.

Delouis, H., 1977: Les programmes de pointes automatiques de raies "DERPTE" et "DERPTH". Version 1.1, Centre Inter-Regional de Calcul Electronique, Orsay, France.

Devaux, C., M. Herman and J. Lenoble, 1975: Interpretation of the photometric measurements of Venus by Mariner 10. J. Atmos. Sci., 32, 1177-1189.

Dierenfeldt, K. E., U. Fink and H. P. Larson, 1977: Temperature and pressure determinations in the Venus atmosphere by means of high-resolution spectra from 1 to 2.5 μm. Icarus, 31, 11-24.

Dollfus, A., 1963a: Compt. Rend. Acad. Soc., 256, 1920.

_____, 1963b: Compt. Rend. Acad. Soc., 256, 3250.

_____, 1975: Venus: evolution of the upper atmospheric clouds. J. Atmos. Sci., 32, 1060-1070.

Fels, S. B., and R. S. Lindzen, 1974: The interaction of thermally excited gravity waves with mean flows. Geophys. Fluid Dyn., 6, 149-191.

Fink, U., H. P. Larson, G. P. Kuiper and R. F. Poppen, 1972: Icarus, 17, 617.

Foley, H. M., 1946: Phys. Rev., 69, 616.

Fultz, D., R. Long, G. Owens, W. Bohan, R. Kaylor and J. Weil, 1959: Studies of thermal convection in a rotating cylinder with some implications for large-scale atmospheric motions. Meteor. Monogr., 4, No. 21.

Gierasch, P. J., 1975: Meridional circulation and the maintenance of Venus atmospheric rotation. J. Atmos. Sci., 32, 1038-1044.

Goody, R. M., 1964: Atmospheric Radiation. Oxford, Clarendon Press, 436 pp.

Guelachvili, G., 1973: New infrared wavenumber standards (2-0 band of $^{12}C^{16}O$) by high-resolution Fourier spectroscopy in vacuum. Optics Comm., 8, 171-175.

_____, 1976: Absolute wavenumber measurements of 1-0, 2-0, HF and 2-0, $H^{35}Cl$, $H^{37}Cl$ absorption bands. Optics Comm., 19, 150-154.

_____, and M. A. H. Smith, 1978: Measurements of pressure-induced shifts in the 1-0 and 2-0 bands of HF and in the 2-0 bands of $H^{35}Cl$ and $H^{37}Cl$. J. Quant. Spectrosc. Radiat. Transfer , in press.

Gull, T. R., C. R. O'Dell and R. A. R. Parker, 1974: Water vapor in Venus determined by airborne observations of the 8200 Å band. Icarus, 21, 213, 218.

Hansen, J. E., and J. W. Hovenier, 1974: Interpretation of the polarization of Venus. J. Atmos. Sci., 31, 1137-1160.

Hapke, B., 1976: Photometry of Venus from Mariner 10. J. Atmos. Sci., 33, 1803-1815.

H. M. Nautical Almanac Office, 1961: Explanatory supplement to the Astronomical Ephemeris and the American Ephemeris and Nautical Almanac. London, Her Majesty's Stationery Office, 505 pp.

Herget, W. F., W. E. Deeds, N. M. Gailar, R. J. Lovell and A. H. Nielsen, 1962: Infrared spectrum of hydrogen fluoride;Line positions and line shapes. Part II. Treatment of data and results. J. Opt. Soc. Am., 52, 1113-1119.

Herman, R. M., and R. H. Tipping, 1970: Impact theory for the noble gas pressure-induced HCl vibration-rotation and pure rotation line shifts--II. J. Quant. Spectrosc. Radiat. Transfer, 10, 897-908.

Herzberg, G., 1950: Spectra of Diatomic Molecules. 2nd ed., New York, Van Nostrand Reinhold, 658 pp.

Hirchfelder, J. O., C. F. Curtis and R. Byrd, 1954: Molecular Theory of Gases and Liquids. New York, Wiley, 1110 pp.

Hirshfeld, M. A., J. H. Jaffe and S. Kimel, 1960: Pressure-induced shifts of HCl lines due to foreign gases. J. Chem. Phys., 32, 297-298.

Jaffe, J. H., M. A. Hirshfeld and A. Ben-Reuven, 1964: Pressure-induced shifts of DCl lines due to HCl: Shift oscillation. J. Chem. Phys., 38, 1705-1706.

_____, A. Rosenberg, M. A. Hirshfeld and N. M. Gailar, 1965: Pressure-induced shifts of hydrogen fluoride lines due to noble gases. J. Chem. Phys., 43, 1525-1528.

Jarecki, J., and R. M. Herman, 1975: Widths and shifts of HF vibration-rotation lines induced by pressure of rare gases. J. Quant. Spectrosc. Radiat. Transfer, 15, 707-726.

Kalnay de Rivas, E., 1975: Further numerical calculations of the circulation of the atmosphere of Venus. J. Atmos. Sci., 32, 1017-1024.

Kaplan, L. D., J. Connes and P. Connes, 1969: Carbon monoxide in the Martian atmosphere. Astrophys. J., 157, L187-192.

_____, P. Connes, J. Connes and M. A. H. Smith, 1975: The spectroscopic evidence for argon on Mars. Paper presented at the 56th Annual Meeting of the American Geophysical Union, and at the XVI General Assembly of the International Union of Geodesy and Geophysics.

Keldysh, M. V., 1977: Venus exploration with the Venera 9 and Venera 10 spacecraft. Icarus, 30, 605-625.

Kerzhanovich, V. V., and M. Ya. Marov, 1977: On the wind-velocity measurements from Venera spacefraft data. Icarus, 30, 320-325.

Kimel, S., M. A. Hirshfeld and J. H. Jaffe, 1959: Pressure-induced shifts of HCl absorption lines in the infrared. J. Chem. Phys., 31, 81-84.

Kuiper, G. P., 1952: in G. P. Kuiper (ed.), The Atmospheres of the Earth and Planets. Chicago, University of Chicago Press, p. 371.

_____, 1969: Comm. Lunar Planet. Lab., No. 101.

Kuipers, G. A., 1958: The spectrum of monomeric hydrogen fluoride: Line shapes, intensities and breadths. J. Molec. Spectrosc., 2, 75-98.

Leovy, C. B., 1973: Rotation of the upper atmosphere of Venus. J. Atmos. Sci., 30, 1218-1220.

Limaye, S. S., 1977: Venus Stratospheric Circulation: a diagnostic study. Ph.D. Dissertation, University of Wisconsin-Madison, 104 pp.

_____, and V. Suomi, 1977: A normalized view of Venus. J. Atmos. Sci., 34, 205-215.

Marov, M. Ya., and O. L. Ryabov, 1972: Model' atmosfery Venery [Model of the atmosphere of Venus]. Institute of Applied Mathematics, AN SSSR. Preprint No. 23.

_____, V. S. Avduevsky, V. V. Kerzhanovich, M. K. Rozhdestvensky, N. F. Borodin and O. L. Ryabov, 1973: Venera 8: Measurements of temperature, pressure and wind velocity on the illuminated side of Venus. J. Atmos. Sci., 30, 1210-1214.

Moroz, V. I., 1967: Physics of Planets. NASA Technical Translation TT F-515.

Nautical Almanac Office, U.S. Naval Observatory, 1973: The American Ephemeris and Nautical Almanac for the year 1973. Washington, U.S. Government Printing Office, 584 pp.

_____, 1974: The American Ephemeris and Nautical Almanac for the year 1974. Washington, U.S. Government Printing Office, 562 pp.

Niehaus, W. C., and T. W. Petrie, 1961: Tables of stellar and planetary Doppler shifts from 1962 to 1982. Standard Oil Co. of Ohio.

Norton, R. H., and R. Beer, 1976: New apodizing functions for Fourier spectrometry. J. Opt. Soc. Am., 66, 259-264.

Oksengorn, B., 1963: Etude experimentale des deplacements et elargissements des raies du spectre de vibration-rotation de l'acide fluorhydrique perturbe par l'argon sous haute pression. Spectrochimica Acta, 19, 541-548.

Owen, T., and C. Sagan, 1972: Minor constituents in planetary atmospheres: ultraviolet spectroscopy from the Orbiting Astronomical Observatory. Icarus, 16, 557-568.

Ramanathan, V., and R. D. Cess, 1975: An analysis of the strong zonal circulation within the stratosphere of Venus. Icarus 25, 89-103.

Rank, D. H., W. B. Birtley, D. P. Eastman and T. A. Wiggins, 1960a: Pressure-induced shifts of HCl lines due to foreign gases. J. Chem. Phys., 32, 296-297.

_____, _____, _____, and _____, 1960b: Pressure shifting of spectrum lines: Some empirical generalizations. J. Chem. Phys., 32, 298-299.

_____, D. P. Eastman, B. S. Rao and T. A. Wiggins, 1963: Breadths and shifts of molecular band lines due to perturbation by foreign gases. J. Molec. Spectrosc., 10, 34-50.

Sasamori, T., 1971: A numerical study of the atmospheric circulation on Venus. J. Atmos. Sci., 28, 1045-1057.

Schorn, R. A., E. S. Barker, L. D. Gray and R. C. Moore, 1969: Icarus, 10, 98.

_____, L. D. Gray and E. S. Barker, 1969b: Icarus, 10, 241.

_____, and A. T. Young, 1977: Spectroscopic determination of the rotation period of Venus. Bull. Am. Astron. Soc., 4, 467.

Shaw, B. M., and R. J. Lovell, 1969: Foreign-gas broadening of HF by CO_2. J. Opt. Soc. Am., 59, 1598-1601.

Smart, W. M., 1947: Spherical Astronomy. Oxford, Cambridge University Press, 430 pp.

Spinrad, H., and S. J. Shawl, 1966: Astrophys. J., 146, 328.

Stone, P. H., 1975: The dynamics of the atmosphere of Venus. J. Atmos. Sci., 32, 1005-1016.

Taylor, F. W., 1975: Interpretation of Mariner 10 infrared observations of Venus. J. Atmos. Sci., 32, 1101-1106.

Toth, R. A., R. H. Hunt and E. K. Plyler, 1970: Line strengths, line widths, and dipole moment function for HCℓ. J. Molec. Spectrosc., 35, 110-126.

Traub, W. A., and N. P. Carleton, 1975: Spectroscopic observations of winds on Venus. J. Atmos. Sci., 32, 1045-1059.

Varanasi, P., S. K. Sarangi and G. D. T. Tejwani, 1972: Line shape parameters for HCℓ and HF in a CO_2 atmosphere. J. Quant. Spectrosc. Radiat. Transfer, 12, 857-872.

Vinogradov, A. P., Yu. A. Surkov and B. M. Andreichikov, 1970a: Research in the composition of the atmosphere of Venus aboard the automatic stations Venera 5 and Venera 6. Soviet. Phys. Dokl., 15, 4-6.

_____, _____, _____, O. M. Kalinka and I. M. Grechishcheva, 1970b: Cosmic Res., 8, 533.

Wiggins, T. A., N. C. Griffen, E. M. Arlin and D. L. Kerstetter, 1970: Broadening and shifting of HF lines due to noble gases. J. Molec. Spectrosc., 36, 77-83.

Woo, R., 1975: Observations of turbulence in the atmosphere of Venus using Mariner 10 radio occultation measurements. J. Atmos. Sci., 32, 1084-1090.

Young, A. T., 1975a: The clouds of Venus. J. Atmos. Sci., 32, 1125-1132.

_____, 1975b: Is the four-day "rotation" of Venus illusory? Icarus, 24, 1-10.

Young, L. D. G., 1972: High-resolution spectra of Venus--a review. Icarus, 17, 632-658.

_____, 1974: Infrared spectra of Venus. In Woszczyk and Iwaniszewska (eds.), Exploration of the Planetary System, Dordrecht, Holland, Reidel, pp. 77-160.

Young, R., and G. Schubert, 1973: Dynamical aspects of the Venus 4-day circulation. Planet. Space Sci., 21, 1563-1580.

_____, and J. B. Pollack, 1977: A three-dimensional model of dynamical processes in the Venus atmosphere. J. Atmos. Sci., 34, 1315-1351.